Deltares

Comparison Hydrodynamics and Salinity of Tide Estuaries; Elbe, Humber, Schelde and Weser

Interreg North Sea Programme
European Union Regional Development Fund

TIDE
Tidal River Development

European Union The European Regional Development Fund
The Interreg IVB North Sea Region Programme
Investing in the future by working together for a sustainable and competitive region

1203583-000

Deltares

Title
Comparison Hydrodynamics and Salinity of Tide Estuaries; Elbe, Humber, Schelde and Weser

Project	Reference	Pages
1203583-000	1203583-000-ZKS-0005	97

Keywords
Tidal intrusion; Salinity intrusion; Scheldt, Humber, Elbe, Weser

Summary
The present report deals with the simulation of tidal wave propagation and salinity intrusion in four major (TIDE) estuaries in north-west Europe:

- Scheldt (Netherlands-Belgium),
- Humber (United Kingdom),
- Elbe (Germany) and
- Weser (Germany).

Simulation results have been compared with measured data of the four estuaries. The simulation results are based on relatively simple analytical models for tidal wave propagation and salinity intrusion in exponentially converging channels of constant depth. The exponentially converging width is represented as $b= b_o e^{-x/Lb}$ with L_b= converging width scale derived from known cross-sections along the estuary and b_o= effective width at mouth.
In all cases the measured tidal range values can be simulated reasonable well by the analytical model, particularly in the mouth region of the estuary. The prediction of the salinity intrusion by the analytical model was less good for the Scheldt and Weser Estuaries (overprediction).

References
Assignment RWS-WD No. 31046101/4500168390; SPA-TIDE (INTERREG)

Version	Date	Author	Initials	Review	Initials	Approval	Initials
Preliminary	April 2011	L.C. van Rijn		K. Kuijper		T. Schilperoort	
Final	Sep 2011	L.C. van Rijn		K. Kuijper		T. Schilperoort	

State
Final

Contents

List of symbols

A = Area of cross-section (m^2)
b= width (m)
b_o= width at mouth (x=0), (m)
C= Chézy-coefficient ($m^{0.5}/s$)
c= width-averaged tidal wave speed (m/s)
d_{50}= median sediment diameter (m)
g= acceleration of gravity (m/s^2)
H= tidal range or tidal wave height (m)
H_o= tidal range or tidal wave height at mouth (m)
h= width-averaged water depth to mean sea level (MSL), (m)
h_o= width-averaged water depth to mean sea level (MSL) at mouth (m)
k_s= bed roughness of Nikuradse (m)
L_b= converging length scale of planform of estuary (m)
R= hydraulic radius (m)
Q= discharge (m^3/s)
Q_r= river discharge (m^3/s)
$\hat{Q}$ = peak tidal discharge (m^3/s)
$\hat{Q}_o$= peak tidal discharge at mouth (m^3/s)
S= width and depth-averaged salinity (promille)
S_o= width and depth-averaged salinity at mouth (promille)
T= tidal period (s)
$\overline{u}$ = width and depth-averaged tidal velocity (=Q/A), (m/s)
$\hat{\overline{u}}$ = width and depth-averaged peak tidal velocity (m/s)
$\hat{\overline{u}}_o$= width and depth-averaged peak tidal velocity at mouth (m/s)
$\overline{u}_r$= width and depth-averaged river velocity (=Q_r/A), (m/s)
$\overline{u}_s$= width and depth-averaged Stokes velocity (m/s)
u_{sa}= width-averaged velocity near the bed due to salinity-induced flow (m/s)
V= volume (m^3)
x= horizontal coordinate (m)
η= tidal elevation to mean sea level (m)
$\hat{\eta}$ = tidal amplitude to mean sea level (m)
$\hat{\eta}_o$= tidal amplitude to mean sea level at mouth (m)
ρ_o= fluid density of fresh water (kg/m^3)
ρ_{sa}= fluid density of saline water (kg/m^3)
$\Delta\hat{\overline{u}}$ = difference of peak tidal velocities during flood and ebb (m/s)
φ= phase difference (lead) between vertical and horizontal tide (hours, degrees)

Abbreviations

NAP=	Dutch ordnance level (about equal to MSL)
MSL=	mean sea level
HW, LW=	high water, low water
HWS,LWS=	high water slack, low water slack
LAT=	lowest astronomical tide
MHWS, MLWS=	mean high water spring, mean low water spring

1 Introduction

The TIDE-project (2010-2012) is a partnership of port authorities, universities, environmental and public agencies covering four major estuaries in north-western Europe:

- Elbe in Germany,
- Weser in Germany,
- Scheldt in The Netherlands and Belgium,
- Humber in United Kingdom.

The Scheldt is the longest of the four TIDE estuaries, but it has the smallest river catchment. The catchment area of the Elbe is by far the largest and is about 3 times larger than that of the Weser.
Each estuary hosts at least one major port: Hamburg (Elbe), Vlissingen and Antwerpen (Scheldt), Bremen and Bremerhaven (Weser) and Hull (Humber).

These estuaries have been selected because they all have strong tidal wave propagation and massive sediment transport along the (shipping) channels. Furthermore, they are all designated as NATURA 2000 sites.
Large and important cities are located along these estuaries. As societies and human welfare developed, the demand for more trade, grew accordingly. Deeper fairways were then needed, which resulted in tidal amplification and the increased import of fine sediments causing deposition of channels and docks. The issue of increasing tidal range has become a global cause for concern and need for safety against flooding.
Estuaries are also marine and fresh water habitats. However, the natural habitats show a long history of degradation due to land reclamation, fairway deepening, and increased emissions.

The basic objectives of the TIDE-Project are:

- to identify knowledge gaps in hydrology, morphology and ecology, and
- to integrate planning in local policy while ensuring that NATURA 2000 and Water Framework Directive requirements are met.
- to produce a range of good practices.

The present report is focussed on tidal wave propagation and salinity intrusion in the four TIDE-estuaries based on simple analytical methods and crude estimates of the parameters involved. Bulk geometrical parameters will be crudely estimated based on available charts and maps to see whether the analytical method yields meaningful values or not for the TIDE estuaries. Basic tidal parameters will be determined, compared and discussed. The theoretical background, parameters and applied models are explained in the Annexes.
More detailed modelling can only be done using numerical models, which is beyond the scope of this study.

Tidal data have been compiled by:

Humber	K. Gardiner	Institute of Estuarine and Coastal Studies (IECS), University of Hull, Hull, UK.
Elbe	M. Fickert	Hamburg Port Authority (HPA), Hamburg, Ggermany.
Weser	S. Saathoff	Flussgebietsmanagement,Übergangs-/Küstengewässer, NLWKN Betriebsstelle Brake-Oldenburg, Oldenburg, Germany.
Scheldt	C. Kuijper	Deltares, The Netherlands.

The report has been composed by L.C. van Rijn of Deltares and reviewed by C.Kuijper of Deltares.

Stefaan Ides from the Port of Antwerp is gratefully acknowledged for his detailed comments on the draft report.

2 Estuaries of Tide Project

2.1 Tide Estuaries

Measured and simulated data of tidal wave propagation and salinity intrusion in four major (TIDE) estuaries in northwestern Europe are presented.

The four TIDE estuaries are:

- Scheldt (Netherlands-Belgium),
- Humber (United Kingdom),
- Elbe (Germany) and
- Weser (Germany).

The simulation results are based on relatively simple analytical models for tidal wave propagation and salinity intrusion in exponentially converging channels of constant depth. The exponentially converging width is represented as $b= b_o e^{-x/Lb}$ with L_b= converging width scale derived from known the decreasing width of the planform of the estuary and b_o= effective width at mouth.
The basic equations are given in Appendices A to F.

2.2 Scheldt estuary

2.2.1 Physical parameters

The Scheldt estuary is a meso-tidal estuary in the south-west part of the Netherlands and in the north-west part of Belgium (see **Figure 2.2.1**) and is connected to the Scheldt river, which originates in the north-west of France. The total length of the Scheldt river including the estuary is about 350 km; the tide penetrates up to the city of Gent in Belgium (about 160 km from the mouth). The length of the relatively wide portion of the estuary is about 60 km (up to Bath). The cross-sections of the estuary show two to three deeper channels with shoals in between and tidal flats close to the banks. The width of the mouth at Westkapelle (The Netherlands) is about 25 km and gradually decreases to about 0.8 km at Antwerp, see **Table 2.2.1**. The width-averaged water depth (h_o) to MSL between Vlissingen and Hansweert is about 12 m. The width-averaged water depth (h_o) to MSL between Hansweert and Bath is about 11 m. The width-averaged bottom is almost horizontal up to x = 80 km from the mouth.
Since 1900, the main shipping channel has been deepened (by dredging and dumping activities) various times affecting the tidal range along the estuary. Dredging works started at the end of the 19th century. Initially, the volumes were very small, mainly to maintain depth on the sills. Since World War II, the volumes of dredging increased steadily. In the 1970's a first intensive deepening was carried out. Between 1997-1999 and 2009-2010 two other deepenings were carried out.
The tidal range at the mouth (Westkapelle and Vlissingen) has been approximately constant over the last century (slight increase of 4% per century), but the tidal range inside the estuary has gone up by about 0.5 to 1 m due to various channel deepenings and other factors (**Pieters, 2002**). Particularly, the high water levels have gone up considerably. The low water levels have gone down slightly at some locations (about 0.2 m at Antwerp) despite sea level rise of about 0.2 m per century. A detailed description of the historical developments is given by **Pieters (2002)**.

Table 2.2.1 *Tidal data (spring tide) of Scheldt estuary around year 2000*

Stations	Distance x (km)	Width b (km)	Tidal range H (m)	H/H_o (measured)
Westkapelle (mouth)	0	25	4.2 (= H_o)	1
Vlissingen	12	6	4.5	1.07
Terneuzen	30	6	4.8	1.14
Hansweert	45	6	5.0	1.19
Bath	63	3	5.5	1.31
Antwerpen	95	0.8	5.85	1.39
Rupelmonde	110	<0.5	5.95	1.42
Temse	115	<0.5	5.85	1.39
Dendermonde	130	<0.5	4.2	1.0
Gent	160	<0.5	2.34	0.55

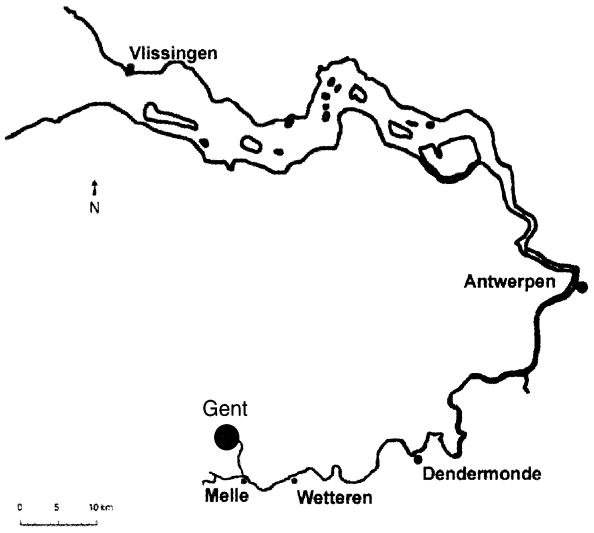

Figure 2.2.1 *Scheldt estuary, The Netherlands*

The tide is semi-diurnal with a tidal range (H_o) at the mouth (Westkapelle) varying in the range of 2.4 m at neap tide to 4.2 m at spring tide. The maximum peak tidal velocity (averaged over width) at mouth ($\hat{\bar{u}}_o$) varies in the range of 0.8 to 1.2 m/s. The two most important tidal constituents are the M_2 and the S_2-components. The tidal curve at the mouth (Westkapelle) has a very regular (almost sinusoidal) pattern. The tidal range increases in landward direction up to Rupelmunde (upstream of Antwerp), see **Table 2.2.1,** and decreases from there in landward direction.
The discharge of the Scheldt river varies in the range of 50 to 200 m^3/s. The mean annual value is about 120 m^3/s. Given the relatively small river discharge, the estuary is a well-mixed flow system with a constant fluid density over the water depth.
Measured tidal data during spring tide at various stations in the Scheldt estuary are shown in **Table 2.2.1** (based on **De Kramer, 2002)**.

The relative contribution of the flow above the tidal flats within the estuary can be obtained from hypsometric curves, which express the horizontal area as a function of depth in a certain channel section (**Deltares, 2010**).

Figure 2.2.2 shows the hypsometric curve for the section Vlissingen to Bath. The vertical axis shows the depth contour below NAP (about mean sea level, MSL) and the horizontal axis shows the horizontal area at the depth contour. For example, the horizontal area at the –10 m depth contour is 1.1 10^8 m^2 between Vlissingen and Bath. The blue area above the curve expresses the total conveyance volume and is about 25 10^8 m^3 below NAP. Thus, the total water volume below NAP is about 2500 million m^3 for this section. Given a section length of about 50 km and a mean section width of about 4 km, the mean section depth is about 12.5 m. The total volume above the –2 m depth contour and above the tidal flats represents the tidal storage volume ($V_{storage}$; see yellow area of **Figure 2.2.2**) and is relatively small compared to the total volume in the channels ($V_{channel}$) below the –2 m NAP depth contour.

Figure 2.2.3 shows the ratio $V_{storage}$ and $V_{channel}$ as a function of time for three channel sections: Vlissingen-Terneuzen, Terneuzen-Hansweert and Hansweert-Bath. The storage volume is about 5% to 10% of the total channel volume and decreases slightly in time between 1955 and 2005.

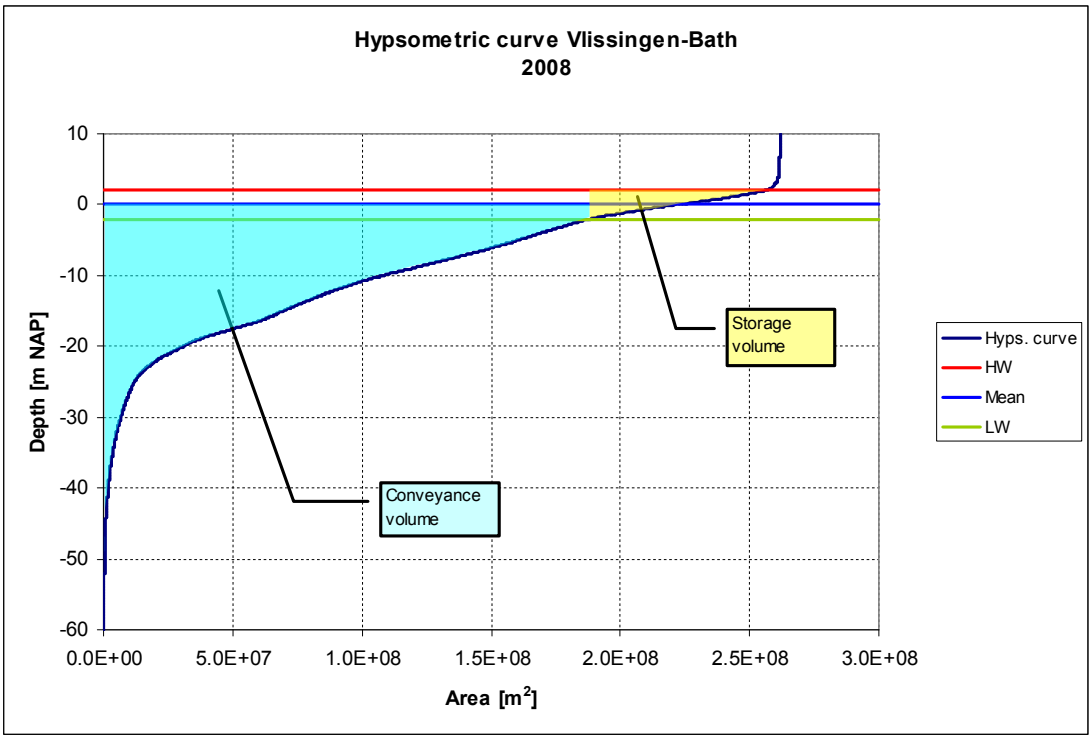

Figure 2.2.2 *Hypsometry for the section Vlissingen-Bath in the year 2008 (Deltares, 2010).*
Blue: water volume in channel.
Yellow: water volume on flats with upper and lower bounds of NAP+2m and NAP-2m.

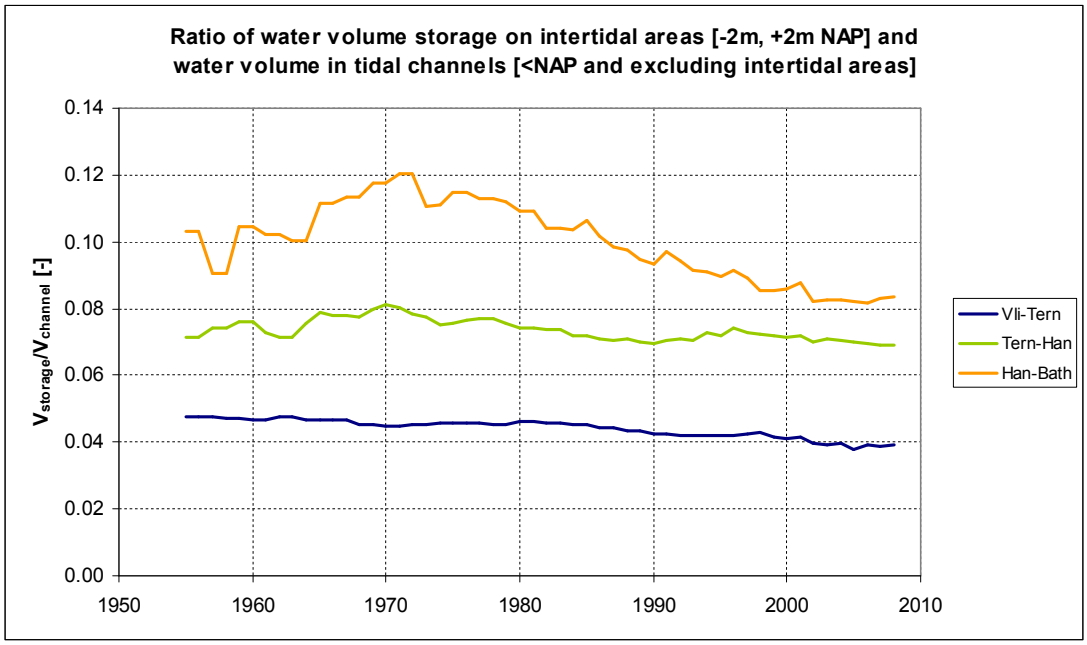

Figure 2.2.3 *Ratio of water volume on the intertidal flats and in the channels for the sections Vlissingen-Terneuzen, Terneuzen-Hansweert and Hansweert-Bath (Deltares, 2010).*

2.2.2 Simulation results

Input data

The linearized analytical model (spreadsheet tidalmotion.xls; Van Rijn, 2011) has been used to compute the tidal range values along the Scheldt estuary, The Netherlands/Belgium.
The basic input data are:

- tidal amplitude and tidal period at mouth ($\hat{\eta}_o = 0.5H_o$ and T);
- effective width (b_o);
- effective width-averaged water depth to MSL (h_o);
- converging length scale (L_b);
- effective bed roughness of Nikuradse (k_s)

The cross-section is schematized to a rectangular profile with an effective water depth (to MSL) which is constant along the estuary. The effective width at the mouth between Westkapelle and Zeebrugge is estimated to be about 20 to 25 km. Herein, a value of 25 km has been used. The width is assumed to vary exponentially along the estuary. The convergence length scale parameter of the width ($b= b_o \exp(-x/L_b)$) is of the order of $L_b \cong 25$ km (giving widths of 2 km at Bath and 0.55 km at Antwerp). Other estimates of the converging length scale in the range of 20 to 30 km are also possible, see **Figure 2.2.4**.

The tidal amplitude ($\hat{\eta}_o$) at the mouth is set to 2.1 m with T= 45000 s (springtide).

Assuming that small-scale bed forms (mini and mega ripples) are dominant, the bed roughness is varied in the range of k_s = 0.03 to 0.1 m.
The mean or width-averaged water depth (h_o) below MSL at the mouth is assumed to be about 10 m.

Tidal range along estuary

Figure 2.2.4 shows the tidal range along the estuary based on the linearized solution for an exponentially decreasing width (converging estuary channel with water depth of h_o= 10 m). The tidal range values vary in the range of 5.5 to 6.3 m due to variations of the bed roughness value in the range of 0.03 to 0.1 m and the converging length scale in the range of 20 to 30 km. Numerical values (1D-Delft model) are also shown (**Van Rijn, 2011**).

The analytical results show that the computed tidal amplification is in close agreement (within 10%) with the observed values for a roughness value of k_s = 0.03 and 0.05 m, see also **Table 2.2.2**. The computed wave speed (averaged value for the traject mout-Antwerp) is about 19 m/s to 17 m/s for these roughness values, which is somewhat larger than the measured data of 15 m/s (mouth) to 11 m/s (landward end), (**Van Rijn, 2011, Savenije, 2005**). The analytical solution yields a phase lead of about 2.7 hours, which is somewhat larger than the observed value of about 2 hours. The peak tidal velocities at the mouth are in the range of −0.75 m/s to −0.85 m/s. The tidal amplification is somewhat too small for larger k_s-values.

Stations	**Distance x (km)**	**Width b (m)**	**Observed Tidal range H (m)**	**Computed Tidal range H (m)** k_s = 0.03 m C = 65 $m^{0.5}$/s L_b= 25 km	**Computed Tidal range H (m)** k_s = 0.05 m C = 61 $m^{0.5}$/s L_b= 25 km	**Computed Tidal range H (m)** k_s = 0.1 m C = 55 $m^{0.5}$/s L_b= 25 km
Westkapelle (mouth)	0	25000	4.2 (= H_o)	4.20	4.20	4.20
Vlissingen	12	15500	4.5	4.40	4.38	4.36
Terneuzen	30	7500	4.8	4.75	4.70	4.64
Hansweert	45	4100	5.0	5.04	4.96	4.88
Bath	63	2000	5.5	5.50	5.32	5.19
Antwerpen	95	550	5.85	6.20	6.00	5.76
				c= 19.6 m/s (wave speed)	c= 17.7 m/s	c= 16.1 m/s
				φ = 2.74 hrs (phase lead)	φ = 2.70 hrs	φ = 2.66 hrs

Table 2.2.2 *Measured and computed tidal data (spring tide) of Scheldt estuary based on analytical linearized method for a converging channel (k_s= bed roughness value; C= Chézy coefficient)*

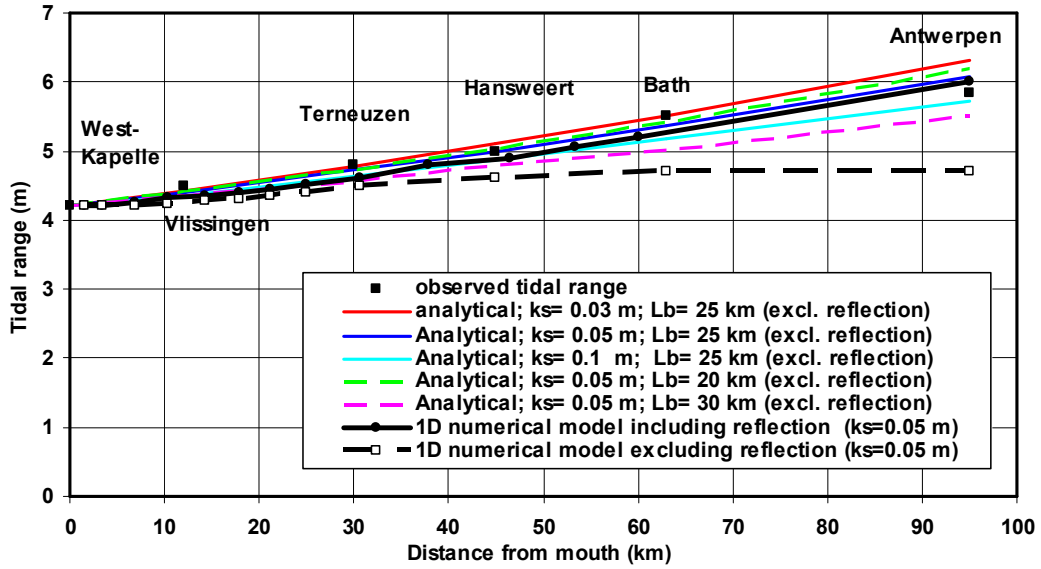

Figure 2.2.4 *Tidal range along estuary for different k_s- and L_b-values, Scheldt estuary*

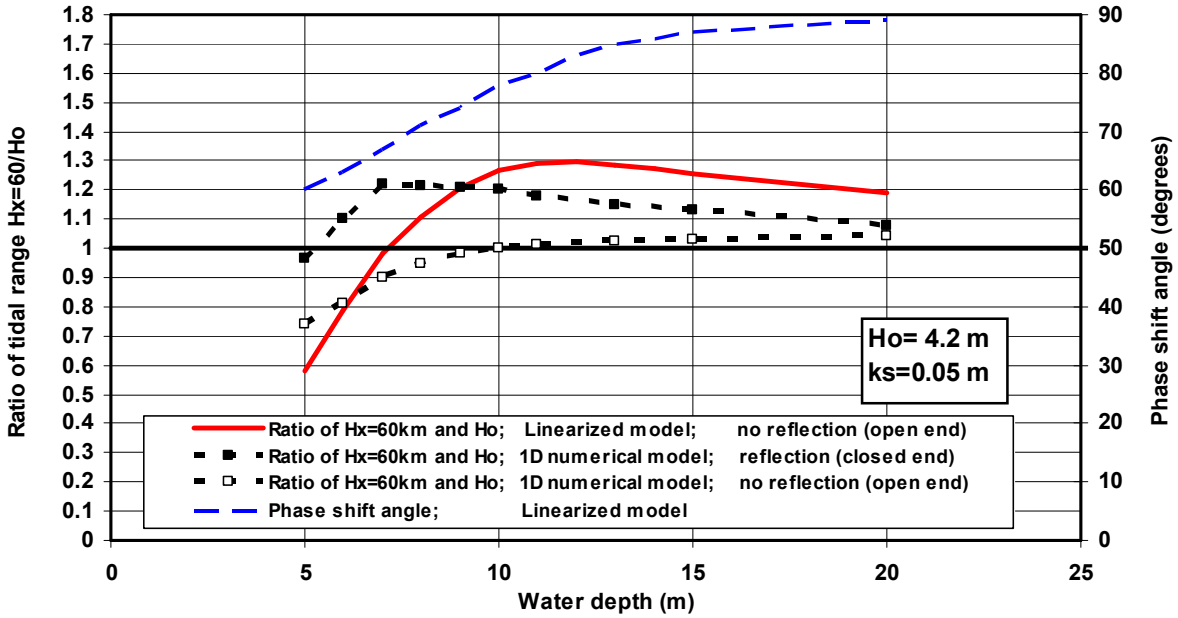

Figure 2.2.5 *Amplification between mouth and Bath (60 km from Mouth), Scheldt estuary*

Figure 2.2.5 shows the ratio of the tidal range ($H_{x=60km}/H_o$) at x = 60 km and at the entrance x = 0 as a function of the water depth (in the range of 5 to 20 m) based on the analytical model. The phase shift angle between the horizontal and vertical tide is also shown. Tidal damping due to bottom friction (k_s = 0.05 m) dominates for water depths smaller than about 7 m resulting in a ratio ($H_{x=60km}/H_o$) smaller than 1. The ratio of the tidal range ($H_{x=60km}/H_o$) shows amplification (>1) for water depths larger than about 7 m. Thus, increasing the water depth by engineering works (dredging of channels, poldering of intertidal areas, etc) leads to a larger tidal range ratio along the estuary. The maximum amplification based on the analytical solution of the linearized momentum eqution is about 1.3 at a water depth of about 11 m. A further increase of the depth does not lead to larger amplification values.

The results of the numerical DELFT1D-model (see **Figure 2.2.5**) taking all terms into account are also shown, both for a channel with a closed end (with reflection) and an open end (no reflection). The numerical results with reflection are based on a closed channel at Antwerp (x=95 km). The numerical results without reflection are based on an open end at Antwerp by extending the channel (from Antwerp) to about 180 km (**Van Rijn, 2011**). The results of the numerical model show a significant effect of reflection at the channel end. The tidal range ratio is somewhat smaller (about 20%) for a channel with an open end and water depths smaller than 15 m. The linearized model shows systematic overprediction for water depths larger than about 7 m.

Salinity intrusion along the estuary

The volume ratio number of the Scheldt estuary is R= V_{river}/V_{tide}= $\pi Q_r T/\hat{Q}T$= $\pi Q_r/\hat{Q} \cong 0.002$ (<0.1) resulting in well-mixed conditions with V= volume, Q_r= river discharge, $\hat{Q}$= peak tidal discharge, $\hat{Q}_o$= peak tidal discharge at mouth (x= 0).

The linearized analytical model has been used to estimate the salinity intrusion length (Kuijper and Van Rijn, 2011).

The model computes the cross-section-averaged salinity distribution along the estuary at high water slack (HWS).

Additional input data are:

- salinity at mouth (S_o);
- freshwater river discharge (Q_r).

Figure 2.2.6 shows the cross section-averaged salinity along the Scheldt estuary at HWS for k_s= 0.01 and 0.05 m. The salinity at the mouth is set to 30 promille (somewhat smaller than measured values of 32 promille). The river discharge is set to Q_r= 150 m^3/s, which somewhat larger than the annual average value of 120 m^3/s. The salinity model has been calibrated to give a salt intrusion length of 120 km as observed. The salt intrusion length increases for decreasing bed roughness.

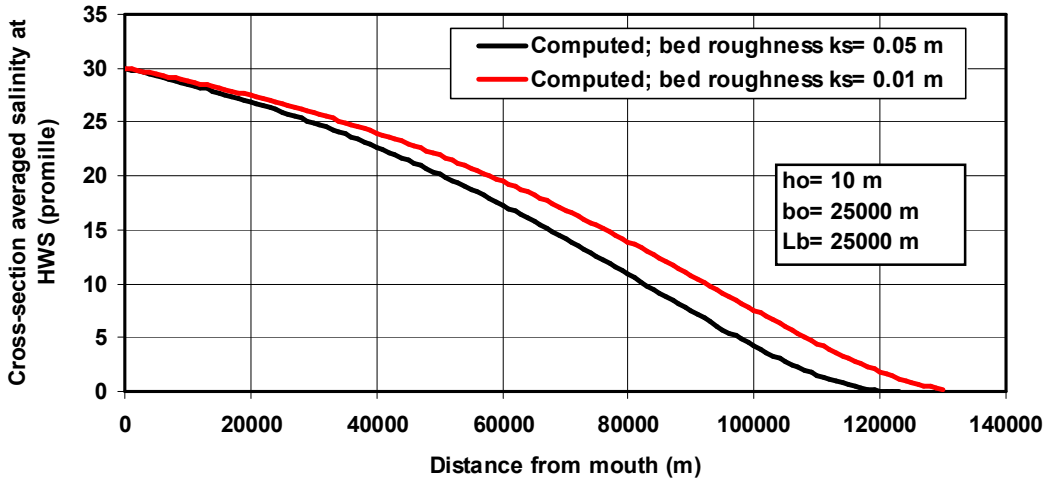

Figure 2.2.6 *Tide- and cross-section averaged salinity along Scheldt estuary*

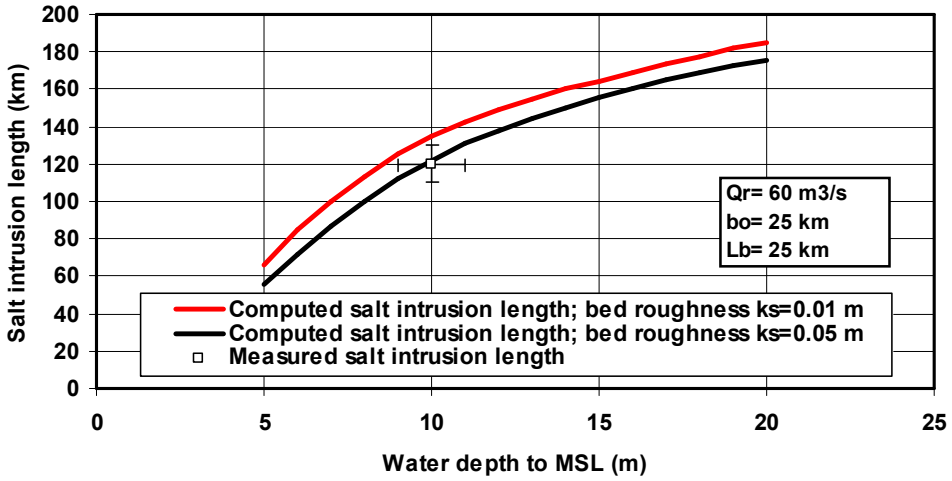

Figure 2.2.7 *Maximum salt intrusion length as function of water depth and bed roughness, Scheldt estuary*

Figure 2.2.7 shows measured and computed salt intrusion lengths for a river discharge of 60 m^3/s. The computed salt intrusion length is about 60 km for a small water depth of 5 m and about 180 km for a water depth of 20 m. The salt intrusion length increases for increasing water depths and decreasing bed roughness. The measured salt intrusion length is assumed to vary between 110 and 130 km (about 10% variation). The water depth is assumed to vary between9 and 11 m (10% variation).

Tide-averaged net velocities

Sediment import and export are related to net tide-averaged velocities consisting of (Annex A3 and B2):

1. River velocity $u_r = Q_r/A$ with Q_r = river discharge and A = area of cross-section;
2. Stokes drift velocity $\overline{u}_s = -0.25\,(H/h_o)\cos\varphi$ with H = tidal range, h_o= water depth to MSL, φ = phase shift between horizontal and vertical tide (+ = seaward and − = landward);
3. Net maximum velocity near the bed related to salinity-gradient in well-mixed conditions is $u_{sa} = -0.035\,Mh^2$ with $M = g^{0.5}\,[C/\{\gamma\,(|\hat{\overline{u}}|+|\overline{u}_r|)\,h\}]\,(h/\rho_o)\,(\partial\rho_{sa}/\partial x)$, $\hat{\overline{u}}$ = peal tidal velocity, h= water depth to MSL, C= Chézy coefficient, $\rho_{sa} = \rho_o + 0.77\,S$, S= salinity (promille); ρ_o= fluid density of fresh water;
4. Net velocity related to tidal asymmetry $\Delta\hat{\overline{u}} = |\hat{\overline{u}}_{flood} - \hat{\overline{u}}_{ebb}|$ in landward or in seaward direction; $\hat{\overline{u}}_{flood}$= peak tidal velocity during flood, $\hat{\overline{u}}_{ebb}$= peak tidal velocity during ebb.

Figure 2.2.8 shows net velocities along the entrance section (about 40 km) of the Scheldt estuary for h_o= 10 m, k_s= 0.05 m and Q_r= 150 m^3/s. The river velocity is amost zero.
The landward-directed Stokes drift is almost constant (about 0.02 m/s) along the Scheldt. It increases slightly in landward direction.
The net velocity near the bed related to the salinity gradient is about 0.01 m/s in landward direction. It increases slightly in landward direction up to x= 85 km. Beyond that location it decreases gradually to zero at x= 120 km.

The net velocity related to the tidal asymmetry is approximately $\Delta\hat{\overline{u}} = 0.2\,\hat{\overline{u}}$ (based on measured values) resulting in a value of about 0.2 m/s along the Scheldt. This compoment

(blue lines) can be in landward and seaward direction depending on geometrical parameters (channel configuration).
Sediment import or export in the Scheldt estuary is largely determined by the net asymmetry-related velocity, as the other net velocity components are quite small (almost zero).

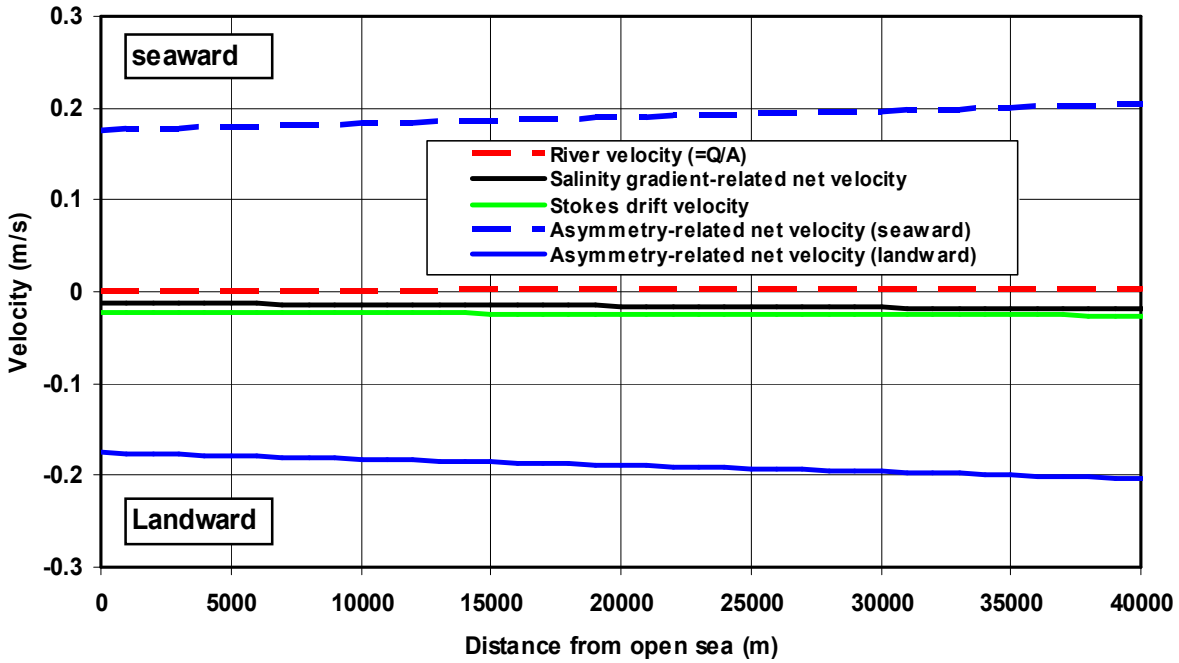

Figure 2.2.8 *Net velocities along entrance section (40 km) of Scheldt estuary*

2.3 Humber estuary

2.3.1 Physical parameters

The Humber estuary is a macro-tidal system located on the north-east coast of England, bordering the North Sea. Major tributaries flowing into the estuary include the rivers Ouse, Wharfe, Aire, Don, Trent and Hull, see **Figure 2.3.1**.

The total length of tidal waters is about 300 km.. The greatest distance of tidal penetration is 147 km from the outer estuary at Spurn Head to Cromwell Weir on the Trent.

The tidal range of springtide varies between 6 and 7 m. The mean spring tidal range (MHWS-MLWS) at the mouth is about 6 m, based on the Admiralty Chart 109. HW at Kingston Dock Hull is about one hour later than that at Grimsby. The measured maximum tidal velocity is about 1.5 m/s.

The total input of fresh water of all rivers is about 250 m^3/s.

The salinity intrusion lengths are about 80 km in River Ouse, about 78 km in River Trent, about 84 km in River Don and about 50 km in River Hull, see **Figure 2.3.1**.

The geometrical and tidal parameters are given in **Table 2.3.1.** These values are crude estimates based on Admiralty Chart No. 109 (River Humber, River Ouse and Trent) and data supplied by University of Hull, and from internet sites www.humber.com and www.tidetimes.org.uk.

Table 2.3.1 *Basic data of Humber estuary (Admiralty Chart 109; 1993)*

Location	Distance from mouth (km)	Effective width at LAT (m)	Maximum depth to LAT (m)	Tidal range at springtide (MHWS-MLWS) (m)	Maximum flood current (m/s)
Spurn Head (x=0)	0	6000	25	6	1.5
Grimsby	7	5000	15	6.1	1.5
Immingham	13	3000	17	6.4	1.5
Hull (Kingston Dock)	28	2000	15	6.7	2.0
Humber bridge	37	1200	9	6.8	1.5
Blacktoft (River Ouse)	55	300	6	5.7	1.0

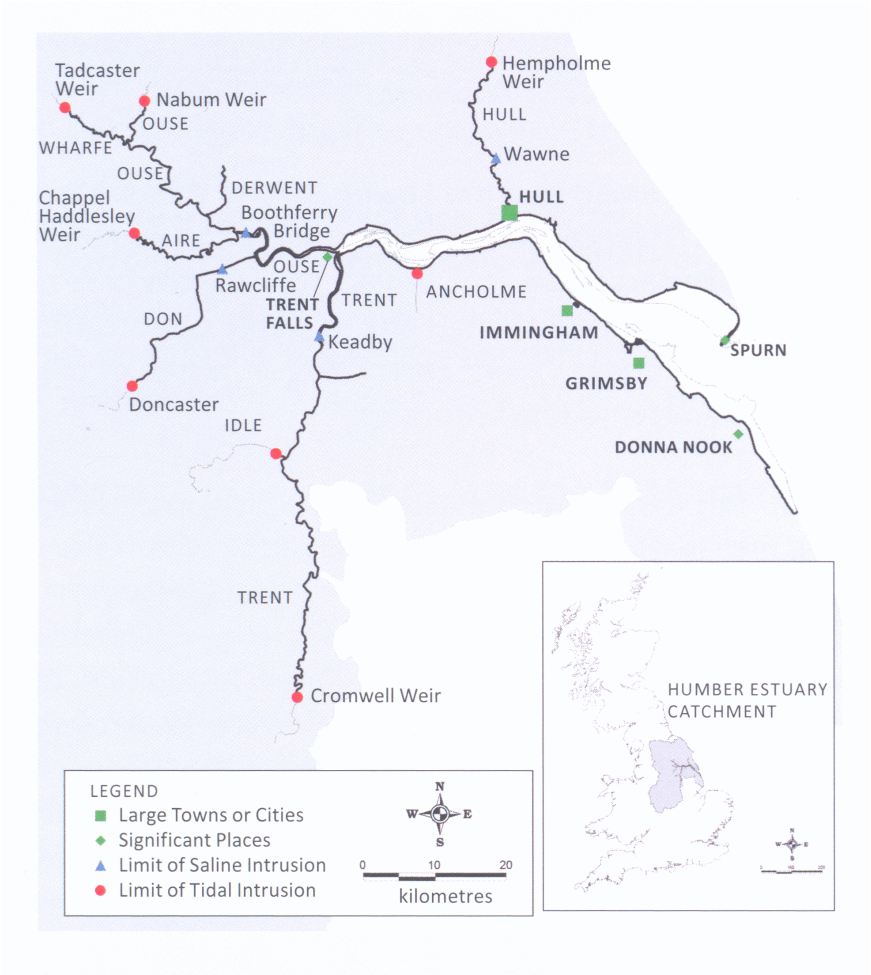

Figure 2.3.1 *Humber estuary*

2.3.2 Simulation results

Input data

The linearized analytical model (spreadsheet tidalmotion.xls; Van Rijn, 2011) has been used to compute the tidal range values along the Humber estuary and River Ouse on the East Coast of England.

The cross-section is schematized to a rectangular profile with an effective water depth (to MSL).

The basic input data are:

- tidal amplitude and tidal period at mouth ($\hat{\eta}_o = 0.5H_o$ and T);
- effective width at the mouth (b_o);
- effective width-averaged water depth to MSL (h_o);
- converging length scale (L_b);
- effective bed roughness of Nikuradse (k_s)

Assuming that the tidal penetration is more importantly affected by the width of the deeper tidal channels than by the width of the tidal flats, the effective width at the mouth (Spurn Head) is set to the width of the main tidal channels characterized by the width at LAT, which is about b_o= 6000 m.

The convergence length scale parameter of the width ($b=b_o \exp(-x/L_b)$) is of the order of $L_b \cong$ 25 km giving widths of 4.5 km, 3.5 km, 2 km and 1.4 km at Grimsby, Immingham, Hull, and Humber Bridge.

The tidal amplitude ($\hat{\eta}_o$) at the mouth is set to 3 m with T= 45000 s (springtide).

Assuming the presence of small-scale ripples along the fine sediment bottom of the Humber Estuary, the bed roughness is estimated to be in the range of k_s= 0.01 to 0.1 m.

The measured maximum water depth (to MSL) varies in the range of 25 m to 9 m between the mouth and Humber Bridge.
The mean width-averaged water depth (h_o) below MSL at the mouth is crudely estimated to vary in the range of 10 to 15 m.

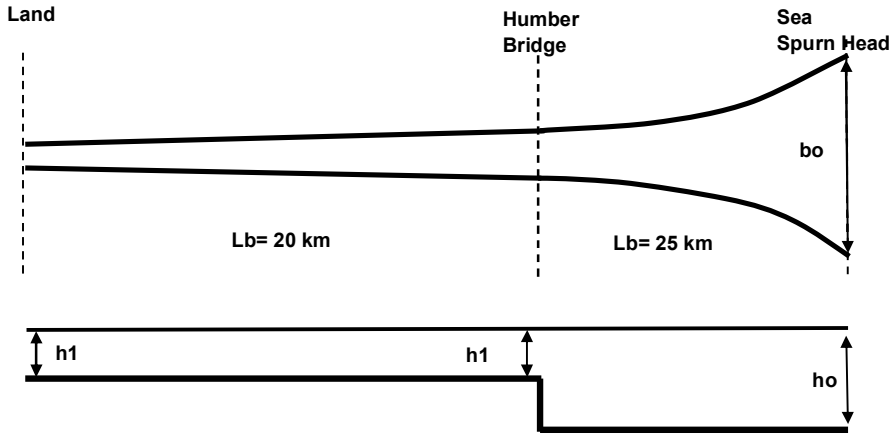

Figure 2.3.2 *Schematization of Humber estuary, East coast of England*

To model the decreasing depth in landward direction, a schematization with two channel sections (each with constant depth h_o and h_1, see **Figure 2.3.2**) has been used, as follows:

- converging channel section seaward of Humber Bridge (at 37 km from mouth) with L_b= 25 km and water depth h_o, the width varies between b_o= 6000 m and b_{37}=1300 m;
- converging channel section landward of Humber Bridge with L_b= 20 km and depth h_1= 0.5h_o, the width landward of Humber Bridge varies between b_{37}= 1300 m and b_{100}= 55 m.

Based on available data, the depth of the river section is estimated to be roughly equal to half the depth of the entrance section.

Tidal range along the estuary

Analysis of measured data shows that the tidal range is maximum at Humber Bridge (HB) at about 37 km from the mouth (Spurn Head). The measured ratio of the tidal range at 37 km and that at the mouth is about H_{37}/H_o= 1.14. The observed amplification between Humber

Bridge and the mouth has been used to estimate the effective water depth and bed roughness involved.

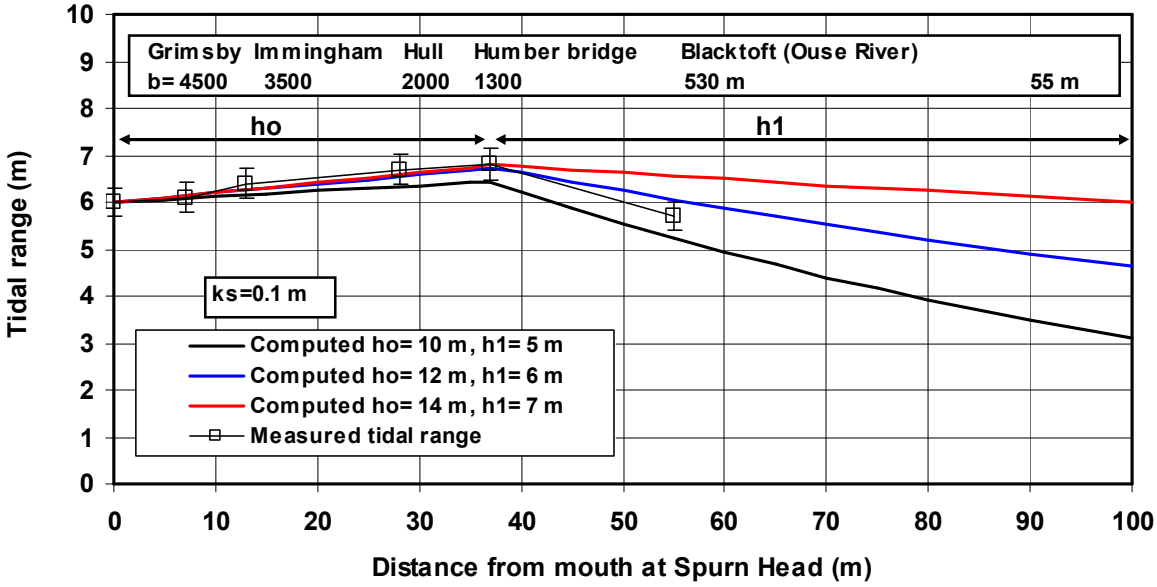

Figure 2.3.3 *Tidal range along Humber estuary and River Ouse, East Coast of England*

Figure 2.3.3 shows measured and computed tidal range values during springtide up to Blacktoft at 55km from the mouth. Landward of Humber Bridge the tidal range gradually decreases along the River Ouse due to the decreasing depth (k_s = 0.1 m). The variation range of the measured tidal range values is assumed to be 5%.
Based on a schematization with two channel sections (see **Figure 2.3.2**), the computed tidal range values are increasing (amplification) up to Humber Bridge and are decreasing (damping) landward of Humber Bridge for h_o in the range of 10 to 14 m (and thus h_1 in the range of 5 to 7 m), see **Figure 2.3.3**. The best results are obtained for h_o=12 m and thus h_1= 6 m (with k_s= 0.1 m).

Figure 2.3.4 shows the ratio (H_{37}/H_o) of the tidal range at Humber bridge (37 km from mouth) and at the mouth Spurn Head as function of the water depth and bed roughness. The water depth was varied in the range of 7 to 20 m. The bed roughness was varied in the range of 0.01 to 0.3 m. Using a small bed roughness of k_s= 0.01 m, the tide is amplified for all water depths between 7 and 20 m. The maximum amplification occurs for a water depth of about 12 m. Increasing the water depth yields a slight reduction of the amplification. The tide is damped for bed roughness values larger than 0.1 m and water depths smaller than about 8 m. The predicted values of H_{37}/H_o are in good agreement with measured data for a water depth of about h_o= 12 to 14 m and k_s= 0.1 m (Chézy coefficient of 58 $m^{0.5}/s$).

Figure 2.3.5 shows the phase difference between the horizontal and vertical tide as function of the water depth and the bed roughness. The computed values show a phase lead of the flow velocity in the range of 2.1 to 3.1 hours. The phase lead increases with increasing depth and with decreasing bed roughness. The measured phase lead is about 2.5 hours.

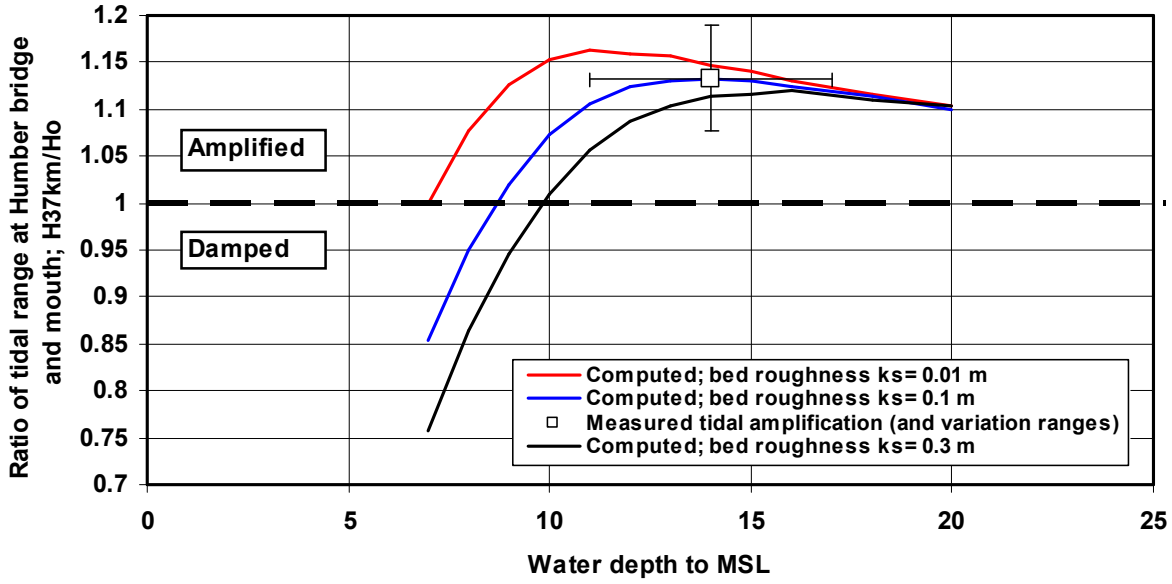

Figure 2.3.4 *Ratio of H_{37} and H_o as function of water depth and bed roughness, Humber estuary*

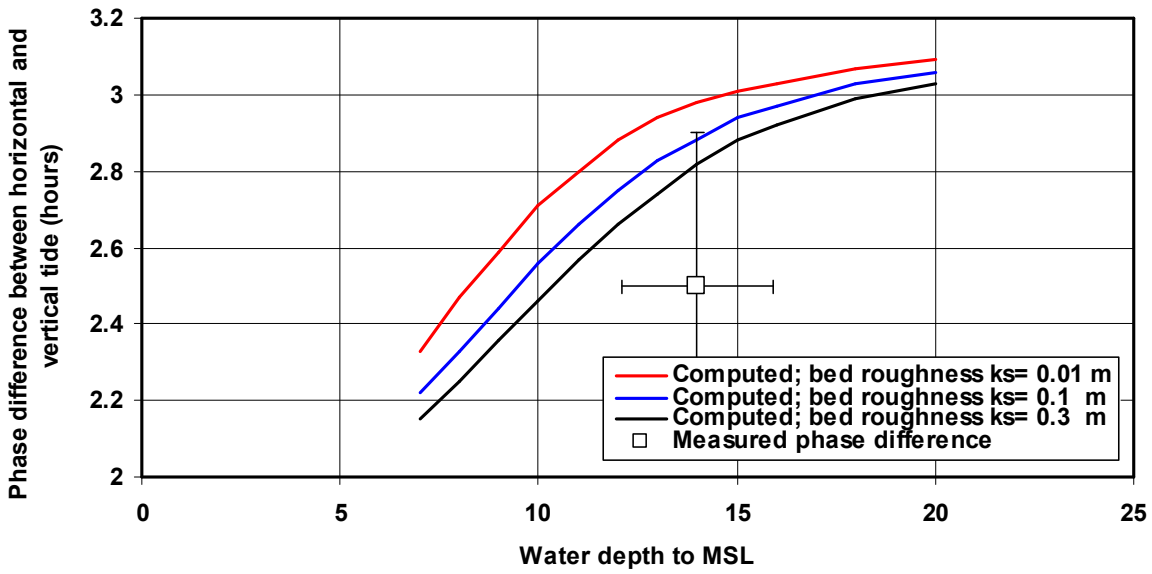

Figure 2.3.5 *Phase difference between horizontal and vertical tide as function of water depth and bed roughnes, Humber estuary*

Salinity intrusion along the estuary

The volume ratio number of the Humber estuary is R= V_{river}/V_{tide}= $\pi Q_r T/\hat{Q}T$= $\pi Q_r/\hat{Q} \cong 0.01$ (< 0.1) resulting in well-mixed conditions.

The linearized analytical model has been used to estimate the salinity intrusion length (**Kuijper and Van Rijn, 2011**).
The model computes the cross-section-averaged and tide-averaged salinity distribution along the estuary at high water slack (HWS).

Additional input data are:

- salinity at mouth (S_o);
- freshwater river discharge (Q_r).

Figure 2.3.6 shows the cross-section averaged salinity at HWS along the Humber estuary and River Ouse for water depth values in the range of 10 to 14 m, based on a schematization with two channel sections. The salinity at the mouth has been set to 30 promille. The river discharge has been set to Q_r= 250 m^3/s and the bed roughness is k_s= 0.1 m. The maximum salinity intrusion at HWS varies between $L_{s,max}$= 75 km for a water depth h_o at the mouth of 10 m and $L_{s,max}$= 100 km for a water depth h_o of 14 m. The observed maximum salinity intrusion is about 80 km. The model slightly overpredicts the observed intrusion length. Measured depth-mean salinities are taken from the plots given by **Falconer and Lin (1997)**. The error bars are related to reading errors. It is unknown whether these data refer to HSW (high watyer slack) or not.
Tidal data and fresh water data are unknown. The model data of salinity based on spring tide conditions and a fresh water discharge of 250 m^3/s are somewhat larger (10% to 40%).
The computed salinity intrusion lengths are shown in **Figure 2.3.7** for various input conditions (varying Q_r in the range of 100 to 1000 m^3/s and k_s in te range of 0.01 to 0.1 m). The 'measured' width-averaged water depth is estimated to be in the range of 12 to 16 m.

The salinity intrusion length reduces roughly by about 30 km for an increase of the fresh water discharge from 100 to 1000 m^3/s. This latter value is estimated to be the upper limit of the river discharge.

An increase of the water depth at the mouth from h_o= 10 to 16 m leads to an increase of the salinity intrusion by about 20 km.

A decrease of the bed roughness from k_s= 0.1 m to k_s= 0.01 m leads to an increase of the salinity intrusion length by about 15 km.

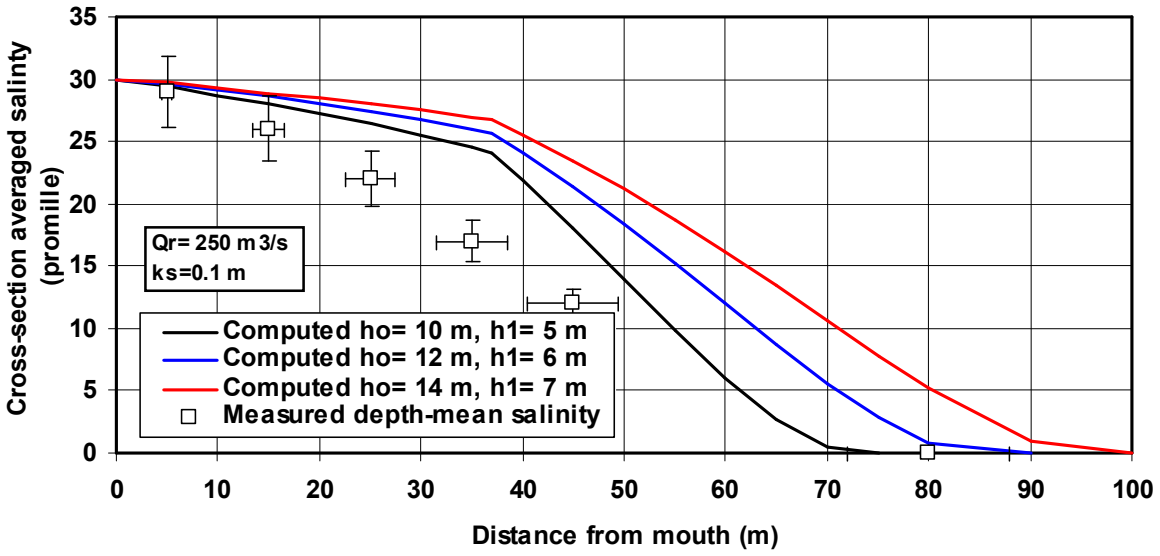

Figure 2.3.6 *Cross-section-averaged salinity at HWS along the Humber estuary and River Ouse, East coast of England*

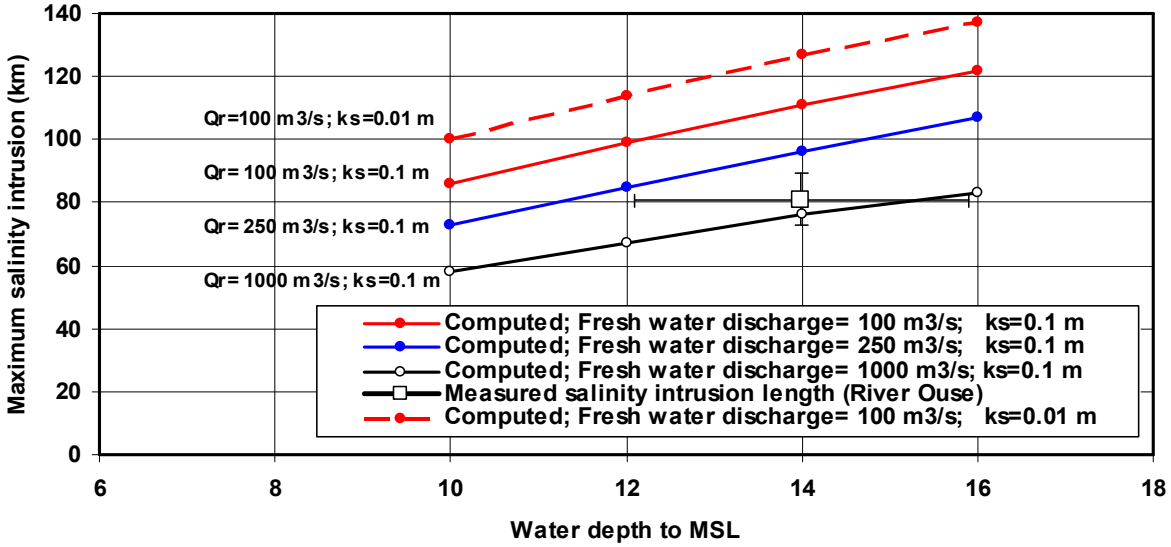

Figure 2.3.7 *Maximum salinity intrusion (at HWS) as function of water depth, river discharge and bed roughness, Humber estuary, east coast of England*

Tide-averaged net velocities

Sediment import and export are related to net tide-averaged velocities consisting of (Annex A3 and B2):

1. River velocity $u_r = Q_r/A$ with Q_r = river discharge and A = area of cross-section;
2. Stokes drift velocity $\overline{u}_s = -0.25\,(H/h_o)\cos\varphi$ with H = tidal range, h_o=water depth to MSL, φ = phase shift between horizontal and vertical tide (+ = seaward and – = landward);
3. Net maximum velocity near the bed related to salinity-gradient in well-mixed conditions is $u_{sa} = -0.035\,Mh^2$ with $M = g^{0.5}\,[C/\{\gamma\,(|\hat{\overline{u}}|+|\overline{u}_r|)\,h\}]\,(h/\rho_o)\,(\partial\rho_{sa}/\partial x)$, C= Chézy coefficient, $\rho_{sa} = \rho_o + 0.77\,S$, ρ_o= fresh water density, S= salinity (promille);
4. Net velocity related to tidal asymmetry $\Delta\hat{\overline{u}} = |\hat{\overline{u}}_{flood} - \hat{\overline{u}}_{ebb}|$ in landward or in seaward direction.

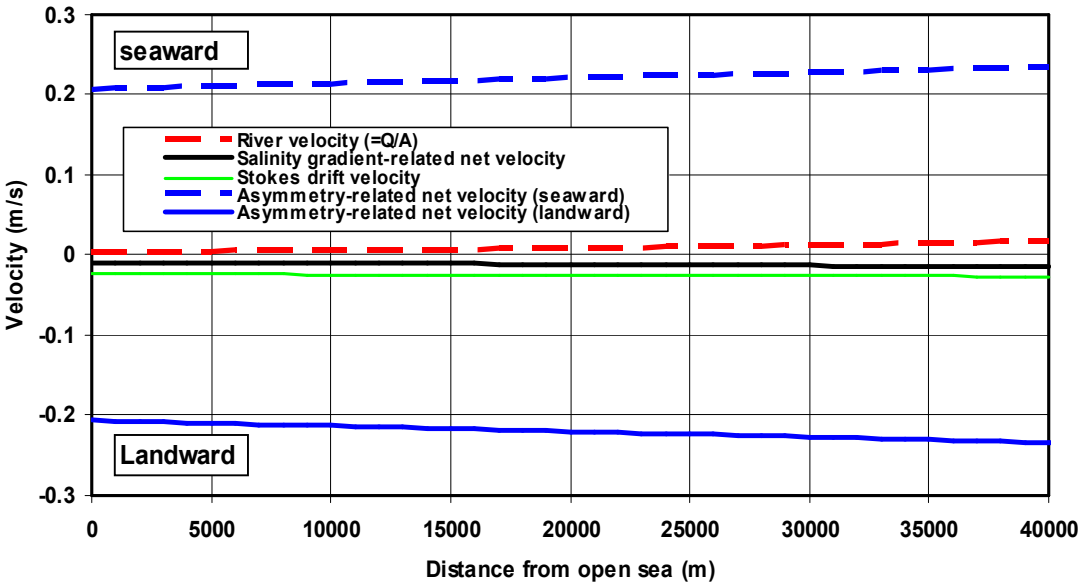

Figure 2.3.8 *Net velocities as function of distance along Humber estuary*

Figure 2.3.8 shows net velocities along the Humber for h_o= 12 m, k_s= 0.1 m and Q_r= 250 m^3/s. The river velocity decreases in seaward direction from approximately about 0.02 m/s to about zero due to the increasing width (water depth = 12 m is constant).
The landward-directed Stokes drift is almost constant (about 0.02 m/s) along the Humber.
The net velocity near the bed related to the salinity gradient is about 0.01 m/s in landward direction. It gradually increases up to 0.015 m/s at x= 40 km and decreases to zero beyond x= 40 km.

The net velocity related to the tidal asymmetry is approximately $\Delta\hat{\overline{u}} = 0.2\,\hat{\overline{u}}$ (based on measured values) resulting a value of about 0.2 m/s along the Humber. This compoment can be in landward and seaward direction depending on geometrical parameters (channel configuration). The net tide-averaged velocities are dominated by the net asymmetry-related velocities and hence the sediment import or export in the Humber estuary is largely determined by the net asymmetry-related velocities.

2.4 Elbe estuary

2.4.1 Physical parameters

The Elbe estuary consists of the tidal Elbe river which originates in the Karkonosze mountains of the Czech Republic and flows through Germany over 630 km passing the city of Hamburg (largest German seaport) at about 110 km from the mouth at Cuxhaven (North Sea), see **Figure 2.4.1.** The mean annual fresh water discharge is about 700 m^3/s with a variation range of 200 to 3600 m^3/s. The mouth of the estuary is characterized by a narrow deep channel and a very wide tidal flood plain up to 2 m above LAT (Hakensand, Medem sand, Norder Grunde), see also Admiralty Chart No. 3261. The total width of the mouth is about 15 km. The width of the deep channel is in the range of 1500 to 3000 m. The area below LAT of the deep channel at the mouth is in the range of about 20000 to 40000 m^2.

Information of various cross-sections along the estuary and river is given at site:
http://www.portaltideelbe.de/Projekte/FRA1999/Beweissicherung/Ergebnispraesentation/profile_elbe/index.html.

Some data of the width of the main channel are given **in Table 2.4.1**. Some cross-sections are shown in **Figure 2.4.2**.

The tide penetrates over about 140 km up to Geesthacht, where a **weir** is located. The weir is generally closed for discharges smaller than about 1200 m^3/s.
To allow the passage of large shipps, the Elbe river has been deepened gradually from about 4.5 m in 1843 to about 15 m below LAT (Lowest Astronomical Tide) in 2010. **Figure 2.4.3** shows a longitudinal profile through the fairway of the Elbe river up to Geesthacht. Landward of Hamburg the water depth is significantly smaller (about 5 m).

Large sand waves are present along the bed of the Elbe river with heights in the range of 1 to 3 m and lengths in the range of 50 to 150 m (**Nasner 1974, Stehr, 1975**). The bed material (d_{50}) is in the range of 0.3 to 0.5 mm.

Tidal data have been supplied by the Hamburg Port Authority, see **Table 2.4.1**.
The tide at the mouth is semi-diurnal with a flood period of 5 hrs 5 min and an ebb period of 7 hrs 20 min.

The tidal range in the mouth at Cuxhaven is now (2010) about 3 m during springtide. Due to the increase of the water depth by dredging activities, the tidal wave penetration along the Elbe river has gone up significantly over time, as shown by the tidal HW and LW values at Hamburg (Station St. Pauli) in **Figure 2.4.4**.
The tidal range was about 1.9 m in 1870 and is now about 3.6 to 3.8 m (2008).

The flood tide has a steeply ascending curve and the ebb tide has a more gently falling curve. This causes a considerable flood current dominance in the upper parts of the estuary.

The salinity penetration is about 65 km from Cuxhaven. The salinity at Cuxhaven is about 18 promille.

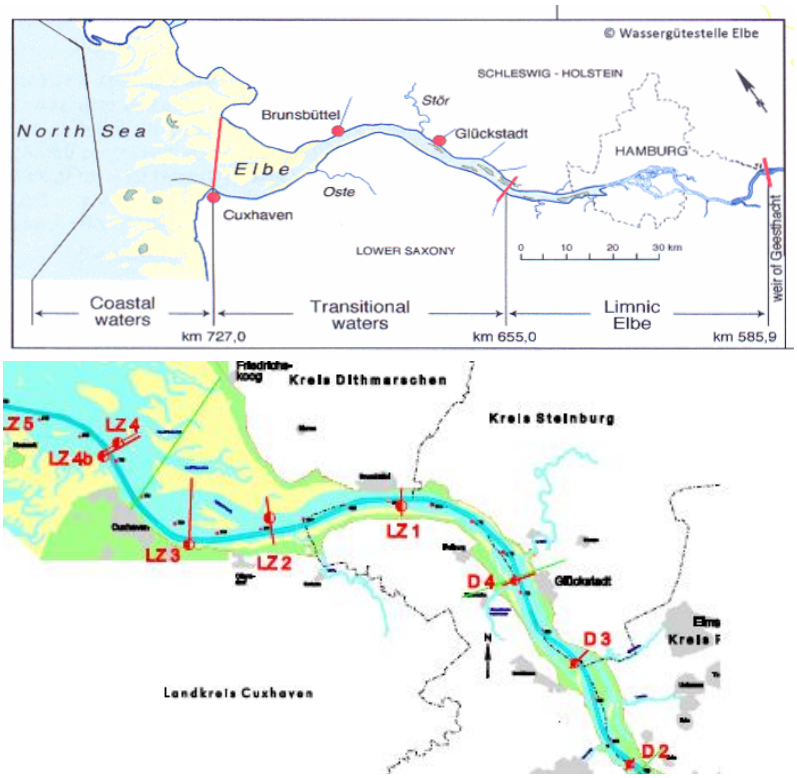

Figure 2.4.1 *Elbe estuary and river, Germany*

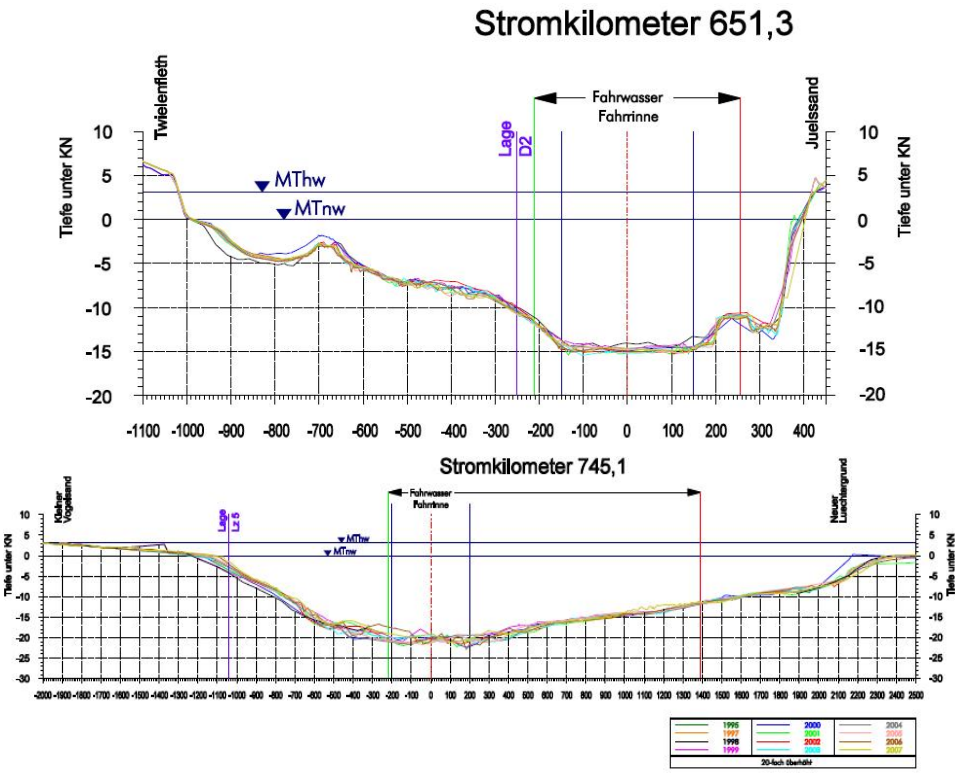

Figure 2.4.2 *Cross-sections of river (651 km) and estuary mouth (745 km); Cuxhaven= 724 km*

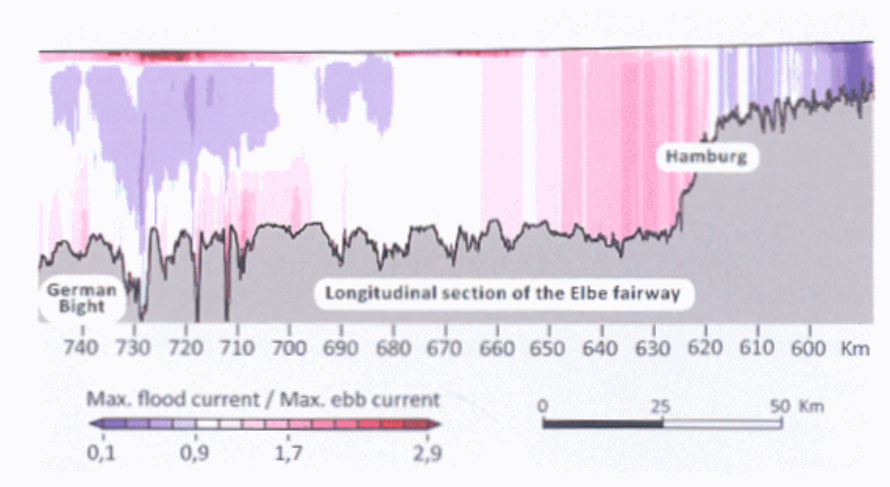

Figure 2.4.3 *Longitudinal profile Elbe estuary and river, Germany*

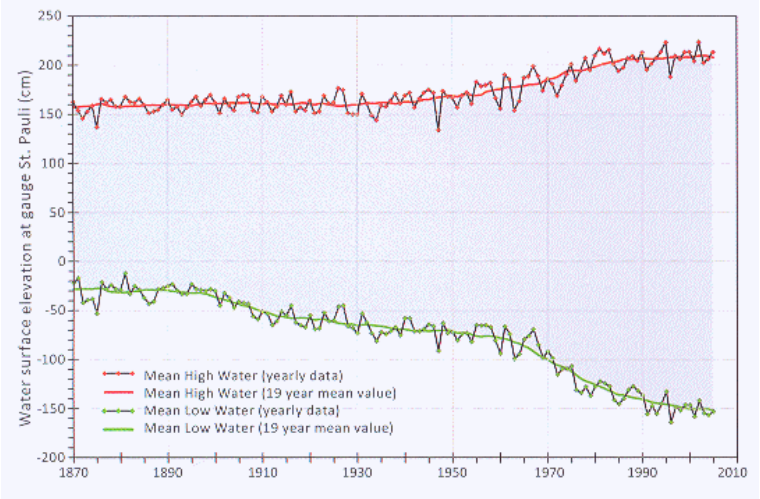

Figure 2.4.4 *Tidal range at Hamburg, Germany*

Table 2.4.1 *Tidal data (spring tide) of 2 to 5 November 2009*

Station	Km	Width (m)	HW (m)	LW (m)	Tidal range (m)
Profile 745	745	3500			
Profile 731	731	3000			
Cuxhaven	724	1500-3000	6.60	3.59	3.01
Profile 717	717	2000			
Profile 703	703	2000			
Brunsbüttel	696	1300	6.45	3.63	2.82
Profile 686	686	1500			
Glückstadt	674	1300	6.57	3.71	2.86
Profile 667	667	1000			
Stadersand	654	800	6.75	3.65	3.10
Profile 644	644	700			
Hamburg (St. Pauli)	623	400	7.06	3.33	3.73

2.4.2 Simulation results

The linearized analytical model (spreadsheet tidalmotion.xls; Van Rijn, 2011) has been used to compute the tidal range values along the Elbe estuary and river. The cross-section is schematized to a rectangular profile with an effective water depth (to MSL). The water depth is assumed to be constant along the channel section. Tidal reflection at the weir location has been neglected.

The basic input data are:

- tidal amplitude and tidal period at mouth ($\hat{\eta}_o = 0.5H_o$ and T);
- effective width (b_o);
- effective width-averaged water depth to MSL (h_o);
- converging length scale (L_b);
- effective bed roughness of Nikuradse (k_s)

The effective depth is about 15 m to LAT and is almost constant up to Hamburg. The effective depth to MSL is set to h_o=16.5 m.
The converging length scale (L_b) has been determined by plotting the cross-sectional area as function of distance to the mouth, see **Figure 2.4.5**. The area varies between 33000 m^2 at x= 0 km to 15000 m^2 at x= 60 km; the area at x= 100 km is about 6000 m^2. The converging length scale between the mouth and x= 60 km is about L_b= 75 km. The converging length scale from x= 60 km to x= 100 km is about 40 km

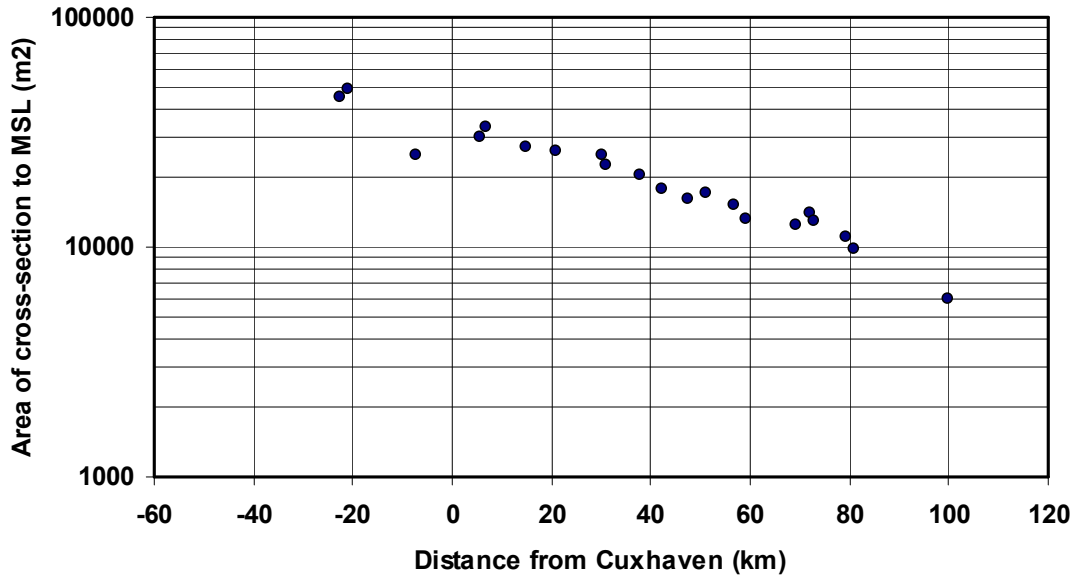

Figure 2.4.5 *Cross-sectional area (to MSL) as function of distance along Elbe estuary and river, Germany*

To evaluate the effect of the bulk geometrical parameters, three types of schematizations have been used:

A. Two converging channels up to Hamburg with
   Channel 1: b_o= 2 km at x= 0 km (Cuxhaven) and L_b= 75 km, h_o= 16.5 m (to MSL);
   Channel 2: b_{60}=0.9 km at x= 60 km and L_b= 40 km, h_o=16.5 m; b_{100}=330 m Hamburg
B. One converging channel with b_o= 3 km at x= 0 km (Cuxhaven), L_b = 50 km and h_o=16.5 m; b_{100}= 400 m (Hamburg)
C. One converging channel with b_o= 2.5 km at x= −21 km (Open Sea), L_b = 60 km and h_o=16.5 m;b_{100}= 340 m (Hamburg).

The tidal amplitude ($\hat{\eta}_o$) at the mouth is set to 1.5 m with T= 45000 s (springtide).

The bed roughness is assumed to be in the range of 0.1 to 1 m based on the presence of fairly large sand waves (Nasner, 1974; Stehr, 1975).

Tidal range along the estuary

Analysis of measured data shows that the tidal range decreases slightly between Cuxhaven and Glückstadt from 3 m to 2.86 m (see **Table 2.4.1**) and increases between Glückstadt and Hamburg from 2.86 m to 3.73 m (see **Table 2.4.1**). This latter increase may be caused by tidal reflection against the weir at Geesthacht. The tidal range at Geesthacht where the weir is located is about 2.3 m.

The measured ratio of the tidal range at 100 km and that at the mouth is about H_{100}/H_o= 1.23. The observed tidal range values between the mouth and Hamburg have been used to estimate the effective roughness involved using schematizations A, B and C.

Figures 2.4.6 to **2.4.8** show the tidal range as a function of distance from the mouth using a water depth of h_o= 16.5 m and various length scale values and roughness values for schematizations A,B and C.

The tidal range between Cuxhaven and Stadersand (distance of about 70 km) which is approximately constant, can be simulated quite well by the model using all schematisations. The converging lengthscale is of the order of 50 to 75 km. The computed tidal range values at the inland stations Brunsbuttel and Gluckstadt are too large.

The increase of the tidal range between Stadersand and Hamburg may be caused by the funelling effect (width decreases from about 900 to 350 m) and tidal reflection against the weir at Geesthacht.
Neglecting the reflection effect, the tidal range at Hamburg due to the funelling effect can be represented by the analytical model using bed roughness values in the range of 0.1 and 0.5 m. These relatively large values are quite realistic given the presence of relatively large sand waves and dunes along the Elbe estuary and river (Nasner, 1974; Stehr, 1975).

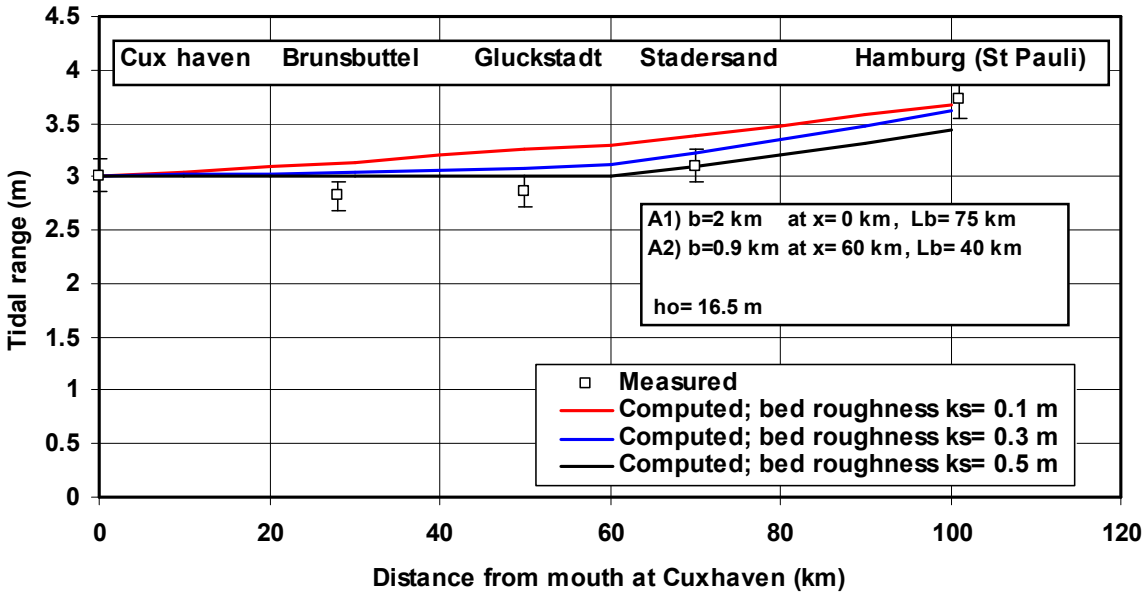

Figure 2.4.6 *Tidal range along Elbe estuary and river based on schematization A (two channels)*

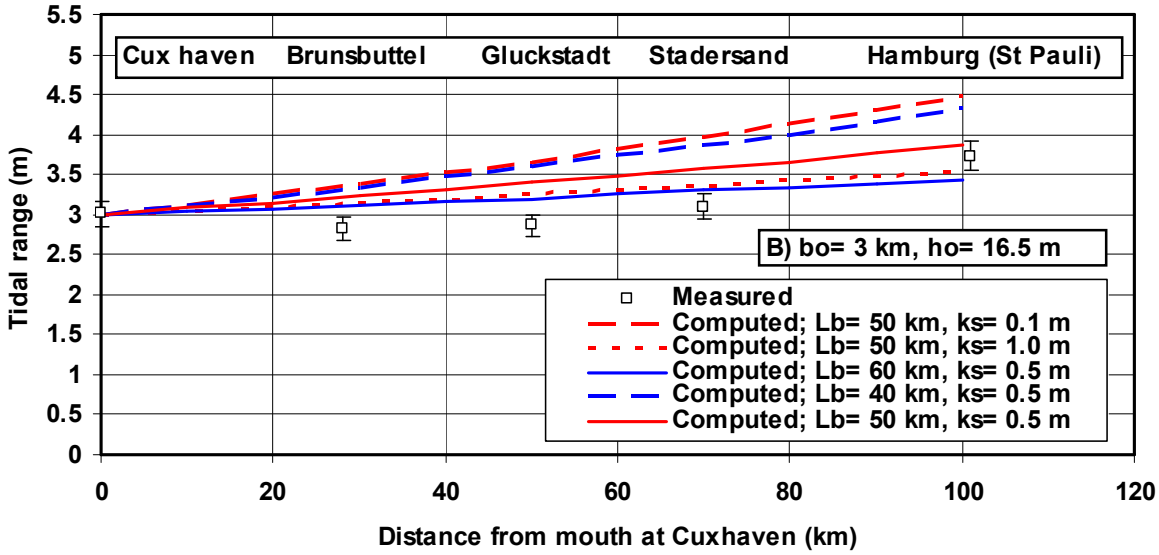

Figure 2.4.7 *Tidal range along Elbe estuary and river based on schematization B (one channel)*

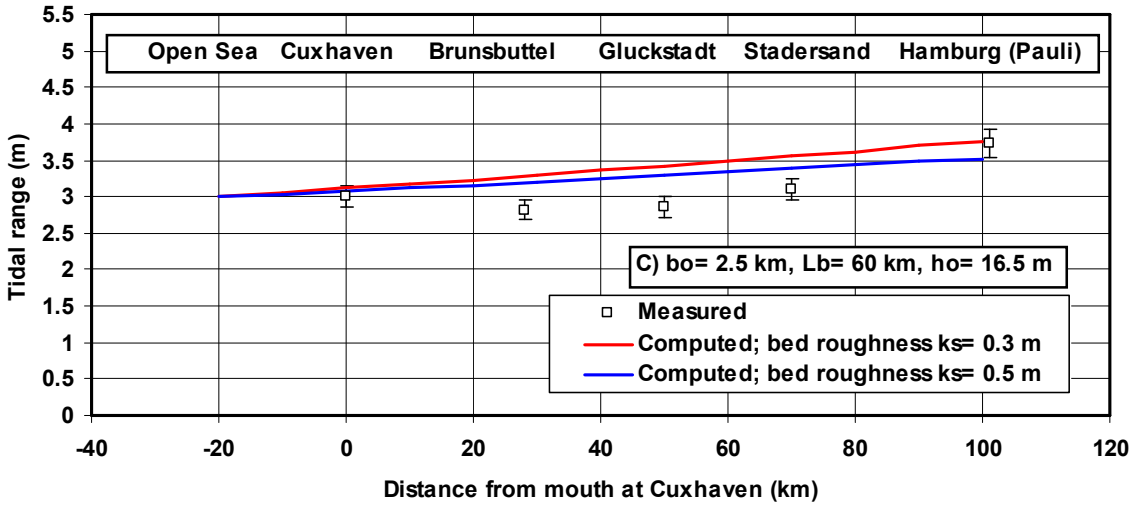

Figure 2.4.8 *Tidal range along Elbe estuary and river based on schematization C (one channel with mouth at open sea)*

Figure 2.4.9 shows the ratio (H_{100}/H_o) of the tidal range at Hamburg (100 km from mouth) and at the mouth Cuxhaven as function of the water depth and bed roughness for Schematization A, neglecting tidal reflection. The water depth was varied in the range of 7 to 30 m. The bed roughness was varied in the range of 0.1 to 0.5 m.

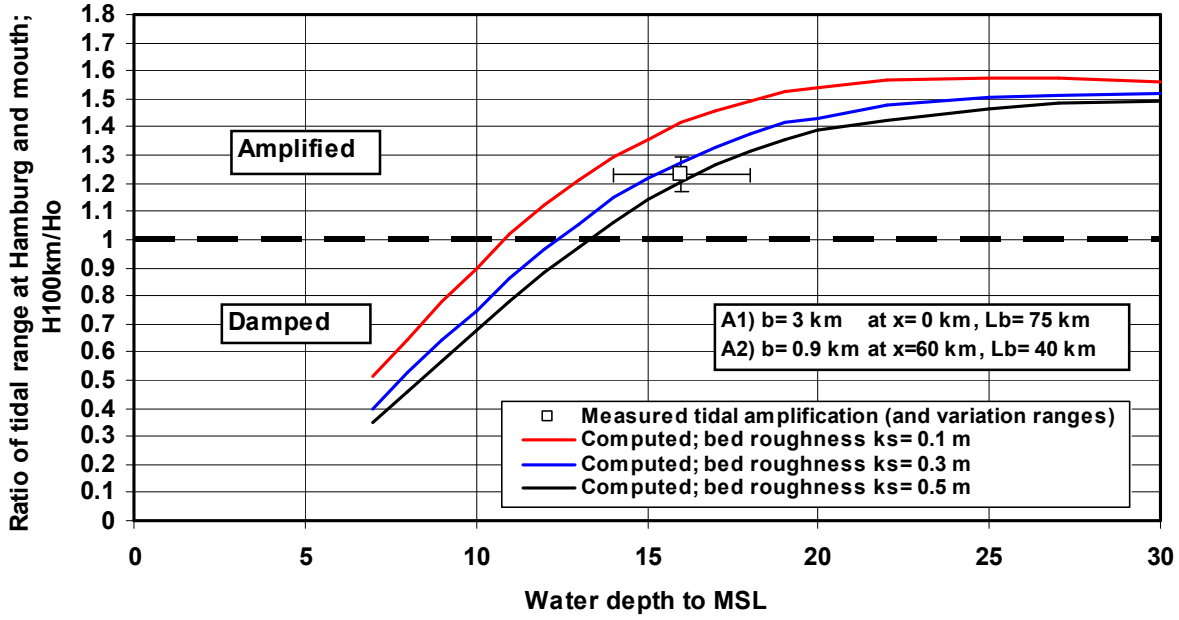

Figure 2.4.9 *Ratio of tidal range at Hamburg and mouth based on schematization A (two channels), Elbe*

Figure 2.4.10 shows the ratio (H_{100}/H_o) of the tidal range at Hamburg (100 km from mouth) and at the mouth Cuxhaven as function of the water depth and bed roughness for Schematization B, neglecting reflection effects. The water depth was varied in the range of 7 to 30 m. The bed roughness was varied in the range of 0.1 to 0.5 m.
Both schematizations A and B yield very similar results.

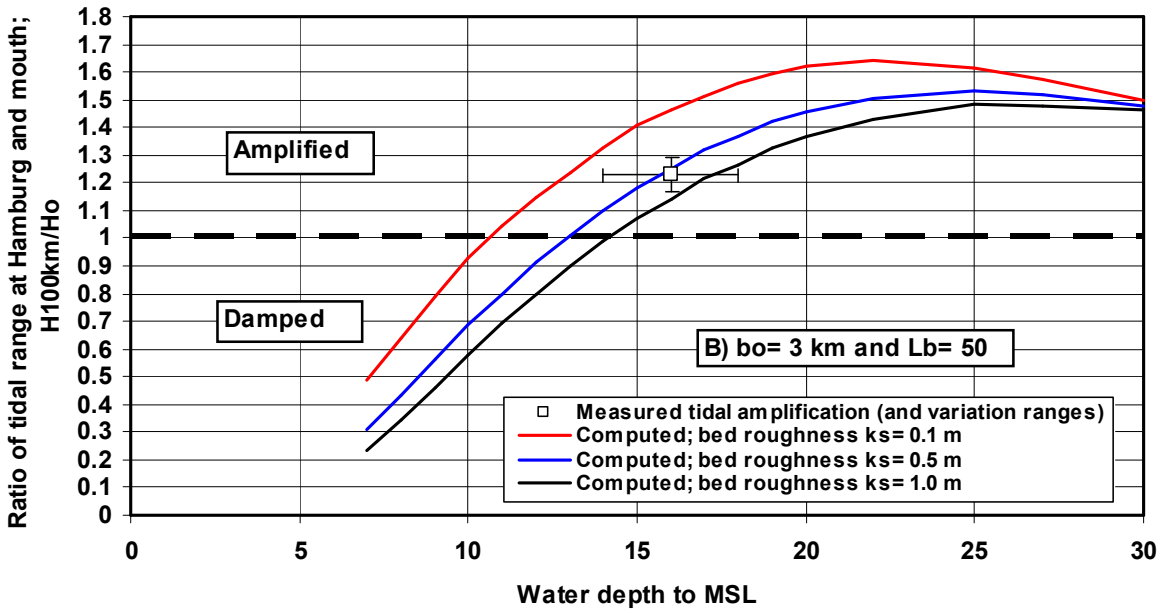

Figure 2.4.10 *Ratio of tidal range at Hamburg and mouth based on schematization B (one channel), Elbe*

Using a small bed roughness of k_s= 0.1 m, the tide is amplified for water depths larger than about 11 m.
The maximum amplification occurs for a water depth of about 25 m.
A further increase of the water depth yields a slight reduction of the amplification.
The tide is damped for water depths smaller than about 11 m.
Using a bed roughness of k_s= 0.5 m, the tide is amplified for water depths larger than about 13 m.
The predicted values of H_{100}/H_o are in good agreement with measured data for a water depth of about h_o= 16.5 m and a bed roughness of k_s= 0.5 m (Chézy coefficient of 47 $m^{0.5}/s$) for both schematizations A and B, provided that tidal reflection is neglected. The errors bars are estimates for the uncertainties involved.
The phase difference between the horizontal and vertical tide is in the range of 1.7 to 2.5 hours for water depths in the range of 7 to 30 m (not shown).

Overall, it can be concluded that the analytical model can reasonably well simulate the tidal range along the Elbe up to Stadersand, where tidal reflection most probably is not so important. All schematisations lead to an almost constant tidal range or a slightly increasing tidal range up to Stadersand. The bed roughness value is of the order of 0.3 to 0.5 m, which is relatively large but not unrealistic given the presence of relatively large bed forms over the major part of the channel reach. The simulation results between Stadersand and Hamburg are questionable as the tidal reflection (which may be of the order of 1 m) is not included in the simulation.

Salinity intrusion along the estuary

The volume ratio number of the Elbe estuary is R= V_{river}/V_{tide}= $\pi Q_r T/\hat{Q}T$= $\pi Q_r/\hat{Q} \cong 0.08$ (<0.1) resulting in well-mixed conditions.
The linearized analytical model has been used to estimate the salinity intrusion length (Kuijper and Van Rijn, 2011). This model computes the cross-section-averaged salinity distribution along the estuary at high water slack (HWS).

Additional input data are:

- salinity at mouth (S_o);
- freshwater river discharge (Q_r).

The salinity at the mouth (Cuxhaven) is set to 18 promille based on the results of the 3D-BAW model supplied by the Hamburg Port Authority. The river discharge is set to Q_r = 750 m^3/s (also used by 3D model) and the bed roughness has been varied in the range of 0.1 to 1 m.
The maximum salinity intrusion during the neap-spring tidal cycle according to the 3D-model (is about 65 km landward of Cuxhaven and about 90 km from open sea. The 3D-model results refer to tide-averaged conditions, whereas the analytical model refers to HWS (high water slack).
Figure 2.4.11 shows computed tide-averaged and cross-section averaged salinities of the 3D-model and the analytical model at HWS (Schematization A). The analytical model results are fairly close to the 3D-model results for a bed roughness of k_s= 0.5 m.

Figure 2.4.12 shows computed the tide-averaged and cross-section averaged salinities of the 3D-model and the analytical model at HWS (Schematization C). The analytical model results are somewhat too large compared to the 3D-model results for both bed roughness values.

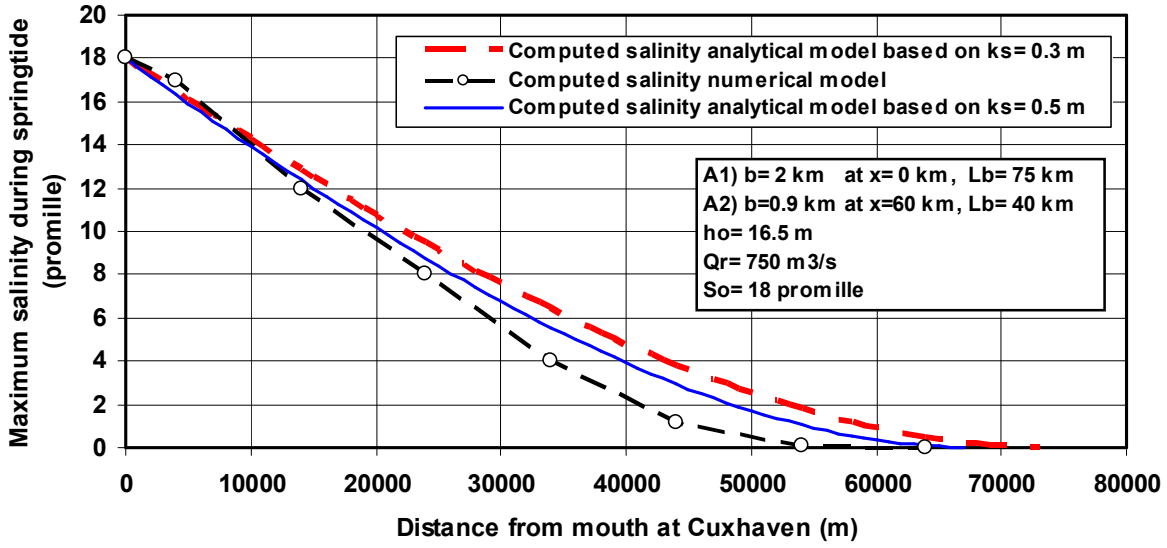

Figure 2.4.11 *Tide-averaged and cross-section-averaged salinity along Elbe estuary (Schematization A)*

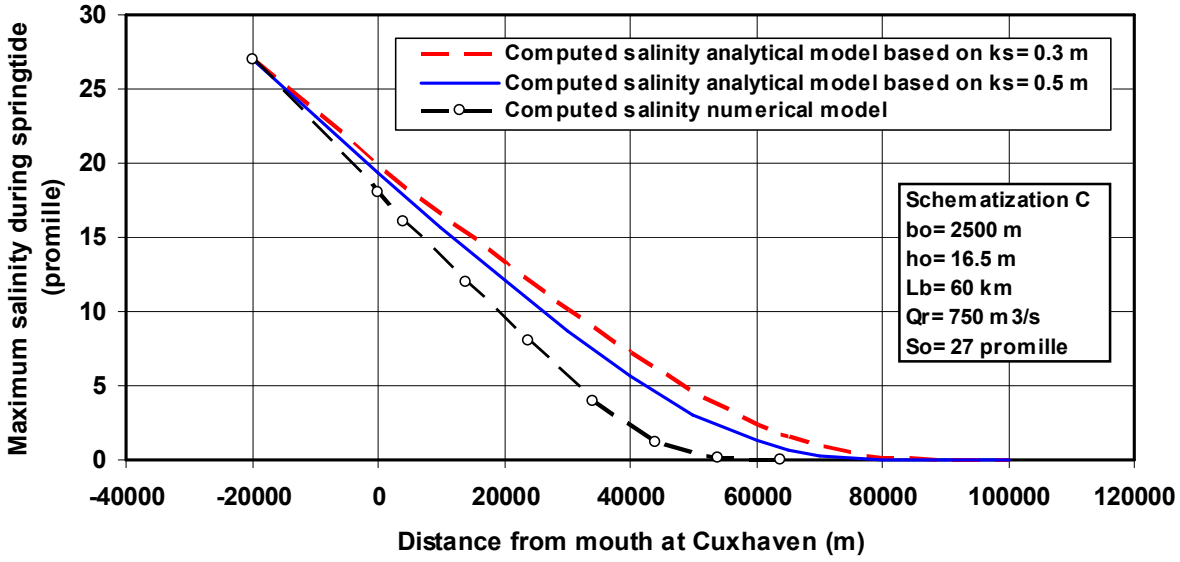

Figure 2.4.12 *Tide-averaged and cross-section-averaged salinity along Elbe estuary (Schematization C)*

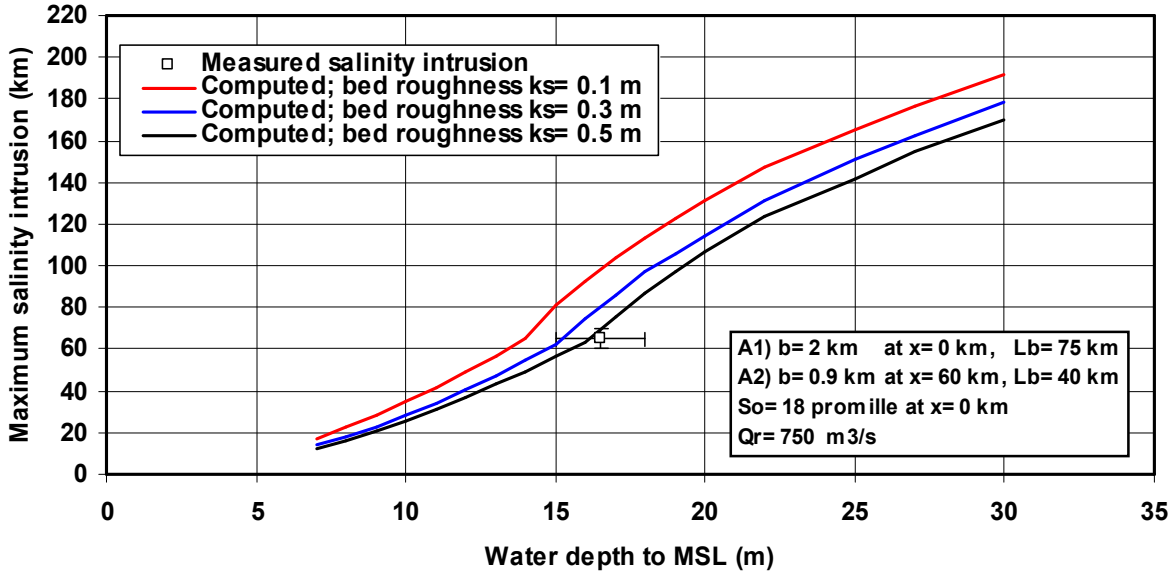

Figure 2.4.13 *Maximum salinity intrusion as function of water depth and bed roughness based on schematization A (two channels), Elbe*

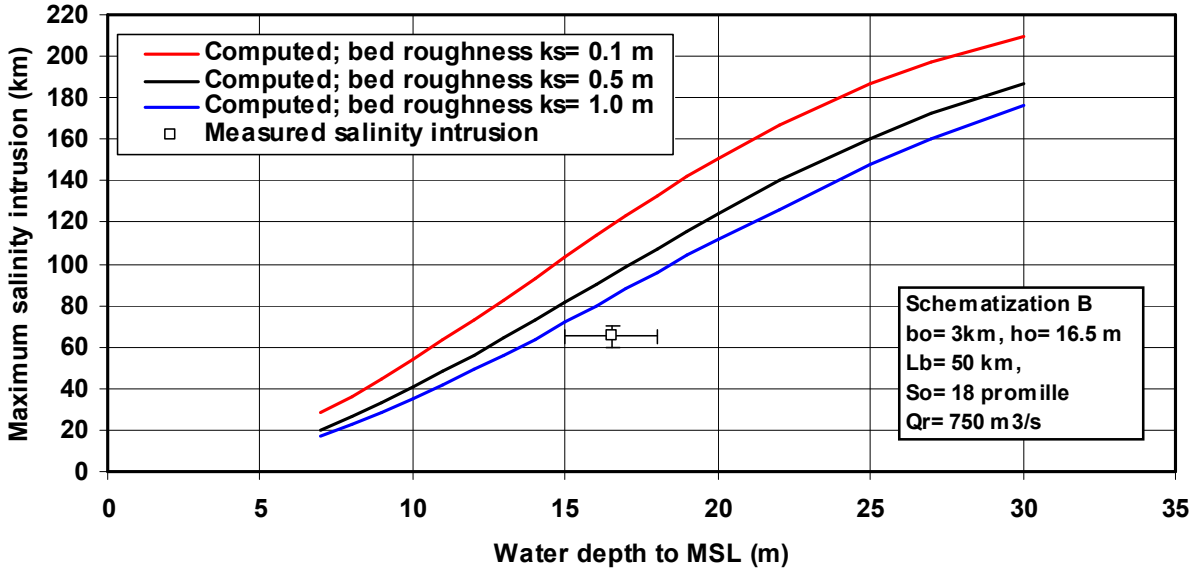

Figure 2.4.14 *Maximum salinity intrusion as function of water depth and bed roughness based on schematization B (one channel), Elbe*

Figures 2.4.13 and 2.4.14 show the maximum salinity intrusion along the Elbe estuary for water depth values in the range of 7 to 35 m, based on schematizations A and B of the analytical model.
The maximum salinity intrusion according to the analytical model varies between $L_{s,max}$= 10 km for small water depths to about 200 km for large water depths.
The analytical model overpredicts the observed intrusion length, particularly for smaller bed roughness values. The computed salinity intrusion is about 65 to 105 km for a water depth of 16.5 m and bed roughness values in the range of 0.1 to 0.5 m (based on schematization A).
Using schematization B, the computed salinity intrusion of the analytical model is considerably larger in the range of 85 to 125 km. The salinity intrusion of the analytical model is strongly related to the depth and width of the mouth. The salinity intrusion increases with increasing depth and width.
Schematization A uses a width at the mouth (Cuxhaven) of about 2000 m in line with the measured data; but Schematization B includes a width of 3000 m resulting in a larger salinity intrusion.

Tide-averaged net velocities

Sediment import and export are related to net tide-averaged velocities consisting of (Annex A3 and B2):

1. River velocity $u_r = Q_r/A$ with Q_r = river discharge and A = area of cross-section;
2. Stokes drift velocity $\overline{u}_s = -0.25\,(H/h_o)\cos\varphi$ with H = tidal range, h_o=water depth to MSL, φ = phase shift between horizontal and vertical tide (+ = seaward and – = landward);
3. Net maximum velocity near the bed related to salinity-gradient in well-mixed conditions is $u_{sa} = -0.035\,Mh^2$ with $M = g^{0.5}\,[C/\{\gamma\,(|\hat{\overline{u}}|+|\overline{u}_r|)\,h\}]\,(h/\rho_o)\,(\partial\rho_{sa}/\partial x)$, C= Chézy coefficient, $\rho_{sa} = \rho_o + 0.77\,S$, ρ_o = fresh water density, S= salinity (promille);
4. Net velocity related to tidal asymmetry $\Delta\hat{\overline{u}} = |\hat{\overline{u}}_{flood} - \hat{\overline{u}}_{ebb}|$ in landward or in seaward direction.

Figure 2.4.15 shows the peak flood and peak ebb velocities along the Elbe based on the 3D BAW model. Depth-averaged velocities in the fairway are shown. Ebb dominance can be observed in the entrance section up to 20 km Landward of Cuxhaven. Farther landward flood dominance is present which increases strongly beyond x= 60 km.

The net peak velocities $\Delta\hat{\bar{u}} = |\hat{\bar{u}}_{flood} - \hat{\bar{u}}_{ebb}|$ are in the range of 0.1 to 0.2 m/s in the entrance section (based on measured values).

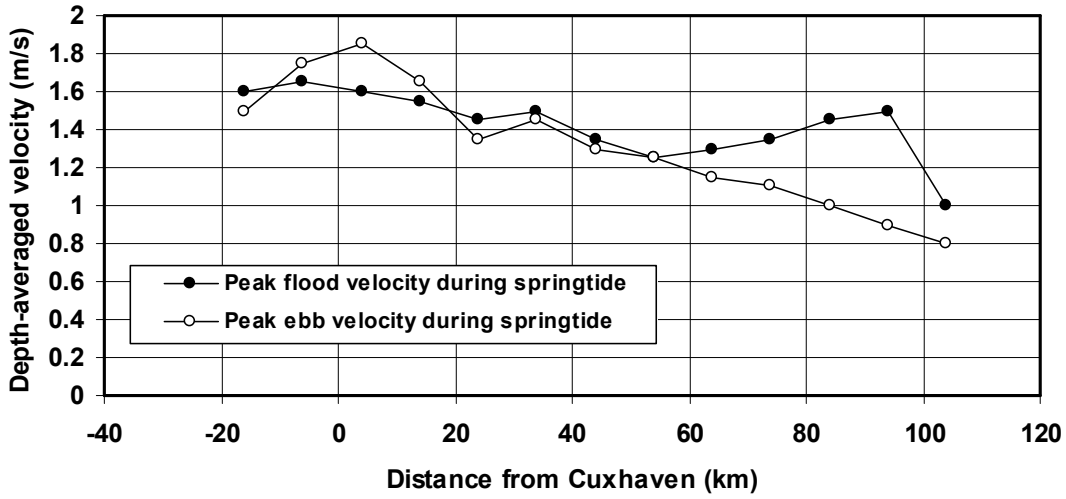

Figure 2.4.15 *Peak flood and peak ebb velocities of spring tide along Elbe*

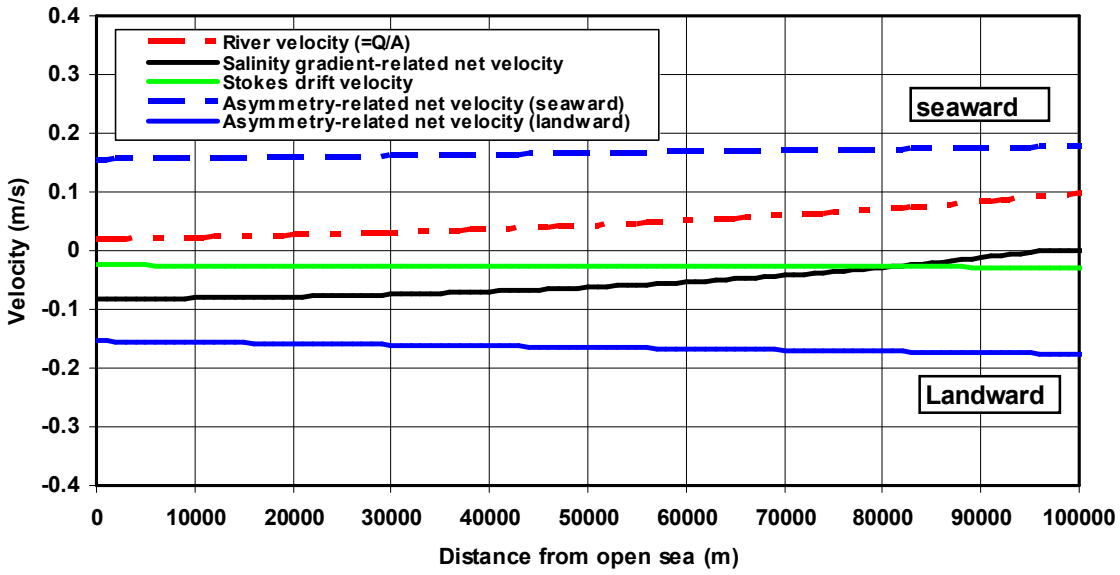

Figure 2.4.16 *Net velocities as function of distance along Elbe (Schematization C)*

Figure 2.4.16 shows net velocities along the Elbe for Schematization C with the mouth at open sea and k_s= 0.5 m (Q_r= 750 m^3/s, L_b= 60 km).
The river velocity decreases in seaward direction from 0.1 m/s to about 0.03 m/s due to the increasing width (water depth = 16.5 m is constant).
The landward-directed Stokes drift is almost constant (about 0.03 m/s) along the Elbe.
The net velocity related to the salinity gradient in the entrance section of the Elbe is about 0.07 m/s at the mouth (in landward direction) decreasing to zero at about 90 km from the mouth.
The net velocity related to the tidal asymmetry is approximately 0.15 m/s along the Elbe. The plotted values are assumed to be equal to $\Delta\hat{\bar{u}} = 0.2\,\hat{\bar{u}}$ with $\hat{\bar{u}}$ = peak tidal velocity of analytical model. This net velocity can be in landward and seaward direction depending on geometrical parameters (channel configuration).

The net velocities are dominated by the net asymmetry-related values, but the net density-related velocity also is important in the Elbe estuary. The net river velocity is important in landward section of the estuary.

Figure 2.4.17 shows similar results for schematization B with the mouth at Cuxhaven.

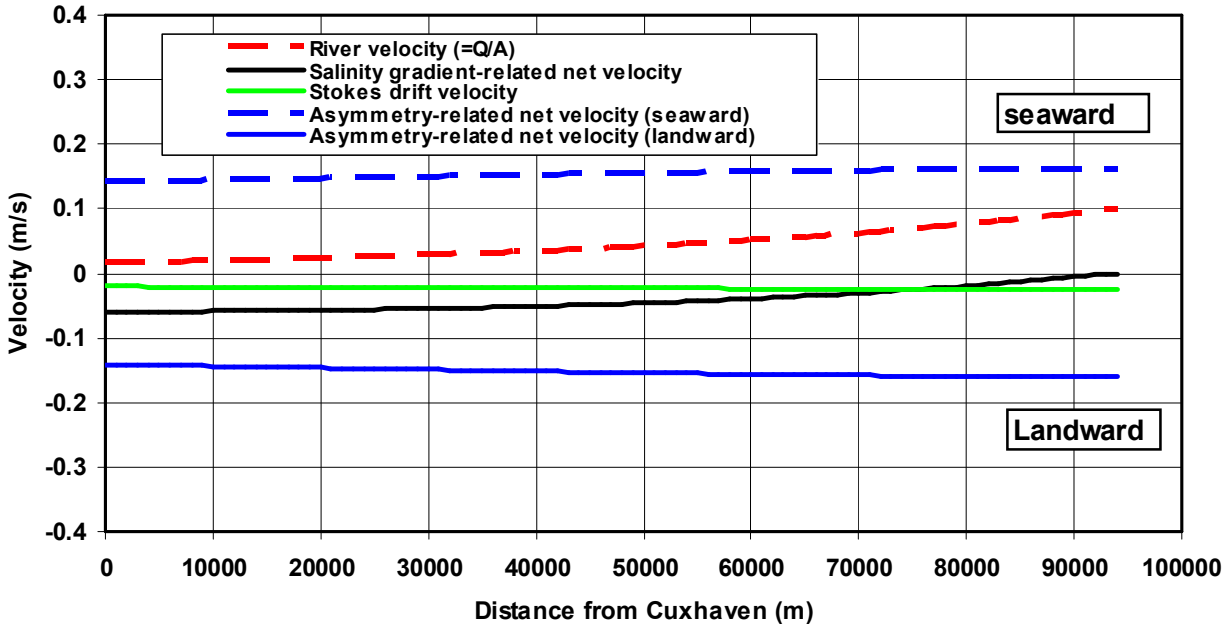

Figure 2.4.17 *Net velocities as function of distance along Elbe (Schematization B)*

2.5 Weser estuary

2.5.1 Physical parameters

The Weser estuary consists of the tidal Weser river which has a length of about 90 km. The mouth is widest (width of about 10.5 km) at Fedderwardersiel. The overall width at Bremerhaven (14 km from the mouth at Fedderwardersiel) is about 1.7 km. The two large cities of Bremerhaven and Bremen (about 66 km from Bremerhaven) are situated along the Weser river, see **Figure 2.5.1**. The tidal influence reaches up to the **Hemelinger Wehr** which is about 5 km upstream of Bremen. The Weir was built in 1906 to enable shipping upstream of Hemelingen.

The mean annual fresh water discharge is about 330 m^3/s. The mouth of the estuary is characterized by a narrow deep channel and very wide tidal flats up to 2 m above LAT (Grosse Platte and Wurster Watt), see also Admiralty Chart No. 3405. The total width of the mouth at Fedderwardersiel is about 10.5 km. The width of the deep channel is in the range of 600 m at Bremerhaven to about 1000 m at the mouth of Fedderwardersiel. The area below MSL of the deep channel at the mouth is about 13000 m^2.

Some data of the width of the main channel are given **in Table 2.5.1**. Some cross-sections are shown in **Figure 2.5.2**.

The tide penetrates over about 70 km up to Hemelingen, where a weir is located. To allow the passage of large ships, the Weser River has been deepened gradually up to 13 below MSL (Mean Sea level) in 2010.

Table 2.5.1 *Tidal data (spring tide) of 2006 to 2009 (Waterways and Shipping Office, Bremerhaven, 2011)*

Station	Km	Width (m)	HW (m)	LW (m)	Tidal range (m)
Bremen	0	150	7.6	3.25	4.35
Vegesack	17.9	220	7.4	3.3	4.1
Farge	27.5	350	7.1	3.0	4.1
Elsfleth	33.4	400	7.2	3.2	4.0
Brake	40.4	450	7.3	3.2	4.1
Rechtenfleth	46.5	500	7.0	3.0	4.0
Nordenham	55.8	600	6.9	2.9	4.0
Bremerhaven	66.7	600	6.8	2.8	4.0
Fedderwardersiel	80.7	1000			4.0

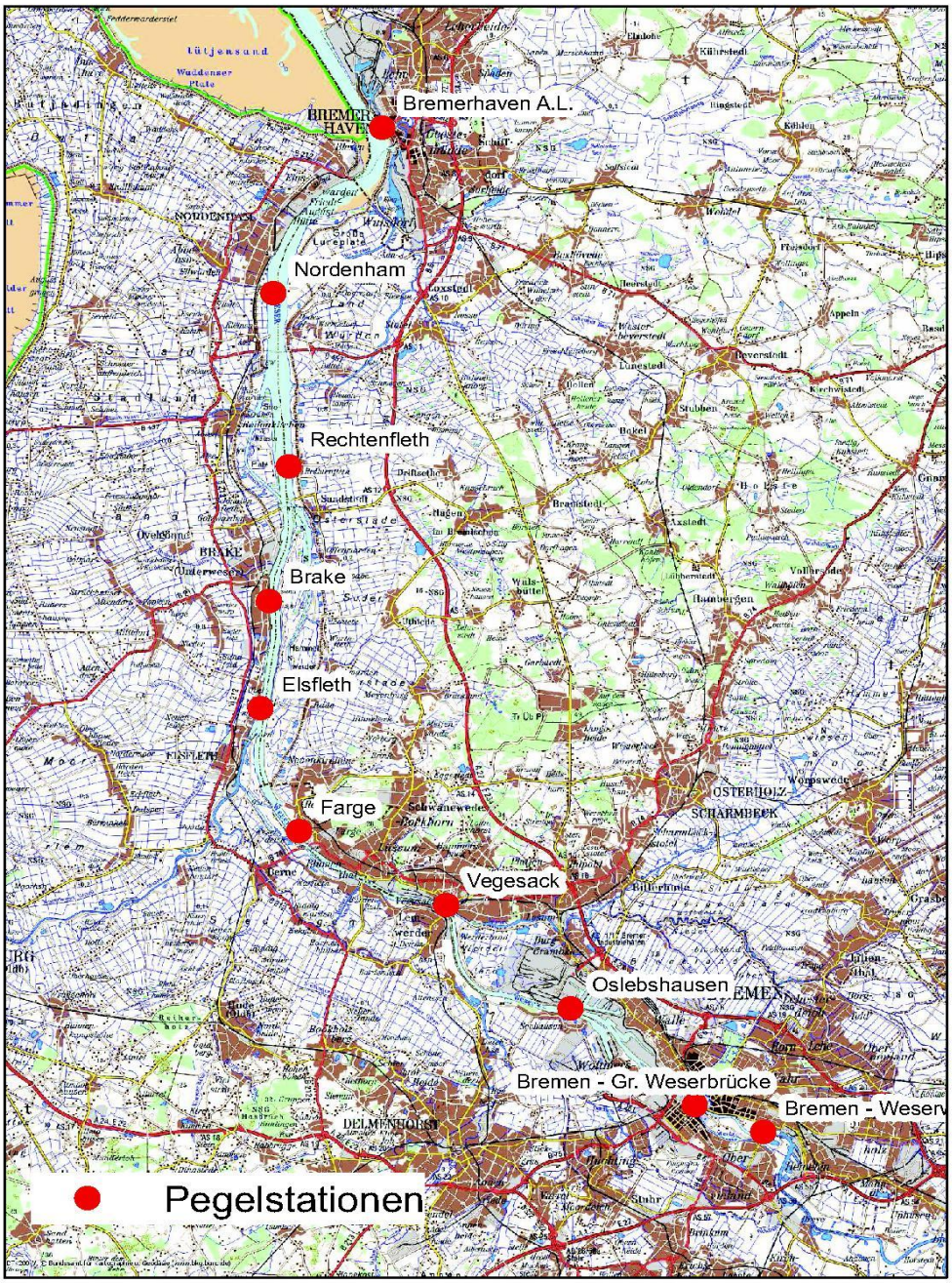

Figure 2.5.1 *Plan view of Weser estuary and river, Germany (Waterways and Shipping Office, Bremerhaven, 2011)*

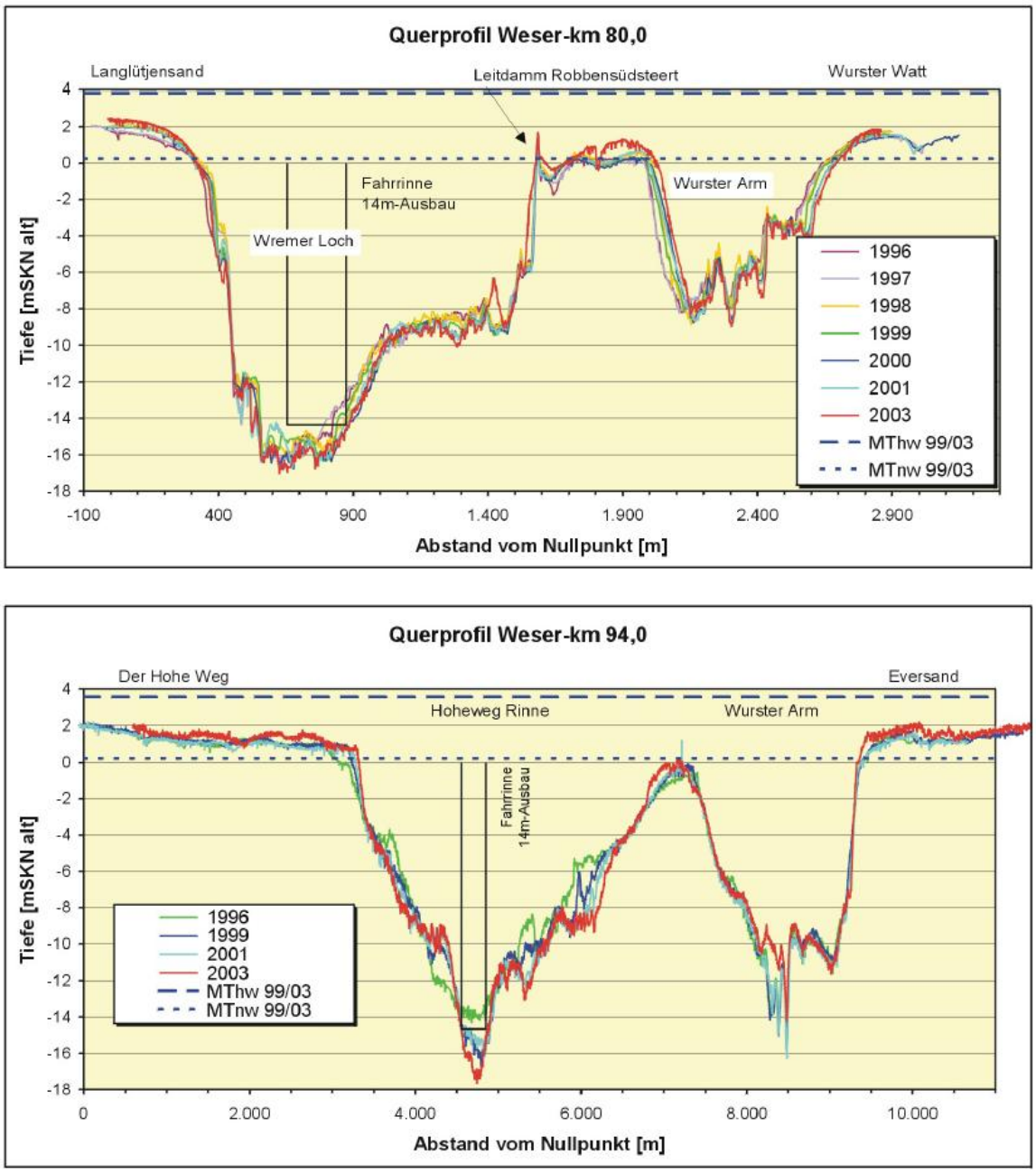

Figure 2.5.2 *Cross-sections of Estuary mouth (80 and 94 km from Bremen); Bremerhaven= 67 km (GfL, Bioconsult, KÜFOG, 2006)*

Figure 2.5.3 shows a longitudinal profile through the fairway of the Weser river between Bremen (x= 0 m) and the Mouth (> 80 km). Large sand waves are present along the bed of the Weser river with heights in the range of 1 to 3 m and lengths in the range of 50 to 150 m (Nasner 1974, Stehr, 1975). The bed material (d_{50}) was in the range of 0.3 to 0.5 mm.

Tidal data have been supplied by local authorities, see **Table 2.5.1**. The tide is semi-diurnal with a flood period of about 5 hrs and an ebb period of 7 hrs 20 min at the mouth.
Due to the increase of the water depth by dredging activities, the tidal wave penetration along the Weser river has gone up significantly over time. The spring tidal range in Bremen was about 0.3 m in 1880 and is now about 4.4 m (2010).
The tidal range in the mouth at Bremerhaven is now (2010) about 4 m during springtide. The tidal range is about constant with values of 4 to 4.1 m between the mouth Fedderwardersiel and Vegesack (about 18 km downstream of Bremen). The tidal range increases slightly up to 4.35 m between Vegesack and Bremen, most likely due to reflection of the tidal wave against the weir at Hemelingen (5 km upstream of Bremen).
The salinity intrusion is about 45 km from Fedderwardersiel, where the maximum salinity is about 23 promille. The maximum salinity at Bremerhaven is about 19 promille.

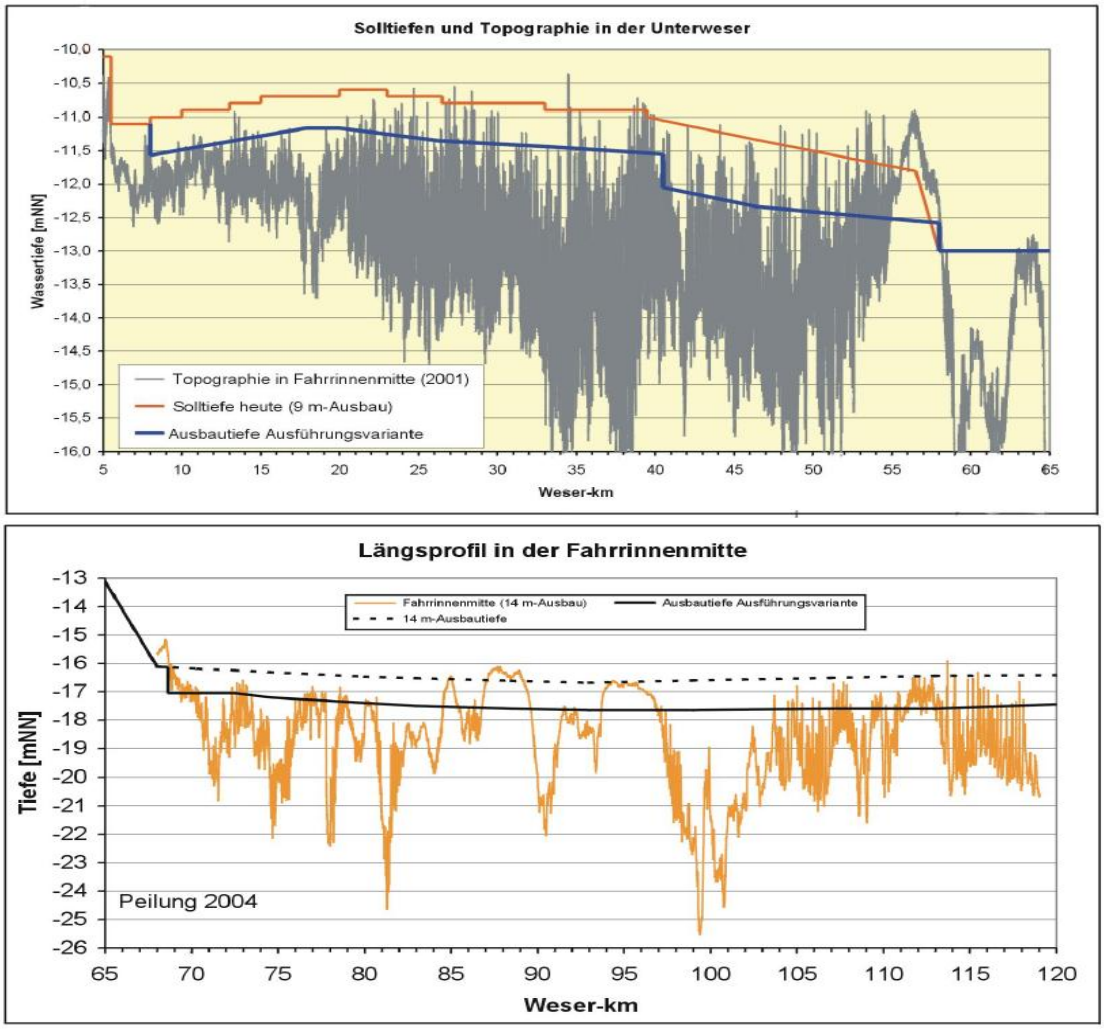

Abbildung 9: Längsprofile der Unter- und Außenweser von km 0-65 bzw. 65-120 (PG WAP schriftl.)

Figure 2.5.3 *Longitudinal profile Weser estuary and river, Germany (GfL, Bioconsult, KÜFOG, 2006)*

2.5.2 Simulation results

The linearized analytical model (spreadsheet tidalmotion.xls; Van Rijn, 2011) has been used to compute the tidal range values along the Weser estuary and river neglecting reflection effects at the Hemelingen wehr. The cross-section is schematized to a rectangular profile with an effective water depth (to MSL). The water depth is assumed to be constant along the channel section.
The basic input data are:

- tidal amplitude and tidal period at mouth ($\hat{\eta}_o = 0.5H_o$ and T);
- effective width (b_o);
- effective width-averaged water depth to MSL (h_o);
- converging length scale (L_b);
- effective bed roughness of Nikuradse (k_s)

The effective depth is about 13 m to MSL and is almost constant up to Bremen (navigation depth). The effective depth to MSL is set to h_o= 13 m.
The converging length scale between the mouth at x= 80.7 km (Fedderwardersiel) and x= 0 km (Bremen) is crudely estimated to be about L_b= 45 km. Only one schematization has been used with b_o= 1000 m at Fedderwardersiel and b= 170 m at Bremen in reasonable agreement with measured data (Admiralty Chart).
The tidal amplitude ($\hat{\eta}_o$) at the mouth of Fedderwardersiel is set to 2 m with T= 45000 s (springtide).
The bed roughness is assumed to be in the range of 0.1 to 0.5 m based on the presence of fairly large sand waves (Nasner, 1974; Stehr, 1975).

Tidal range along the estuary

Analysis of measured data shows that the tidal range is about constant between the mouth Fedderwardersiel and Vegesack and increases up to 4.35 m between Vegesack and Bremen, as shown in **Figure 2.5.4.** The uncertainty error of the tidal range is assumed to be about 5%. Between Vegesack and Bremen there is a slight increase of the tidal range of about 0.3 to 0.4 m, most probably due to tidal reflection effects (Hemelingen wehr).

The measured ratio of the tidal range at 80 km and that at the mouth is about H_{80}/H_o= 1.09.
Computed tidal range values are shown for k_s = 0.03 m to 0.5 m. Slight amplification occurs for k_s= 0.1 to 0.3 m. The amplification increases considerably for a small bed roughness of k_s= 0.03 m. Slight damping occurs for a bed roughness of k_s = 0.5 m. The transition from amplification to damping occurs for k_s = 0.35 m.
Neglecting reflection effects, the tidal range at Bremen can be represented quite well using bed roughness values in the range of 0.1 and 0.3 m. These relatively large values are quite realistic given the presence of relatively large sand waves and dunes along the Weser estuary and river (Nasner, 1974; Stehr, 1975). Removal of these sand waves by dredging will lead to small k_s-values and a significant increase of tidal amplification along the Weser.

Figures 2.5.5 shows the ratio (H_{80}/H_o) of the tidal range at Bremen and at the mouth Fedderwardersiel (80 km from Bremen) as function of the water depth and bed roughness (neglecting reflection effects). The water depth was varied in the range of 5 to 25 m. The bed roughness was varied in the range of 0.1 to 0.5 m.

Using a small bed roughness of k_s= 0.1 m, the tide is amplified for water depths larger than about 11 m.

The maximum amplification occurs for a water depth of about 20 m. Increasing the water depth yields a slight reduction of the amplification. The tide is damped for water depths smaller than about 11 m.
Using a bed roughness of k_s= 0.5 m, the tide is amplified for water depths larger than about 14 m.
The predicted values of H_{80}/H_o are in good agreement with measured data for a water depth of about h_o= 13 m and a bed roughness of k_s= 0.2 m (neglecting reflection effects). The uncertainty error of the water depth is assumed to be about 1 m.

The phase difference between the horizontal and vertical tide is in the range of 1.7 to 2.8 hours for water depths in the range of 5 to 25 m (not shown).

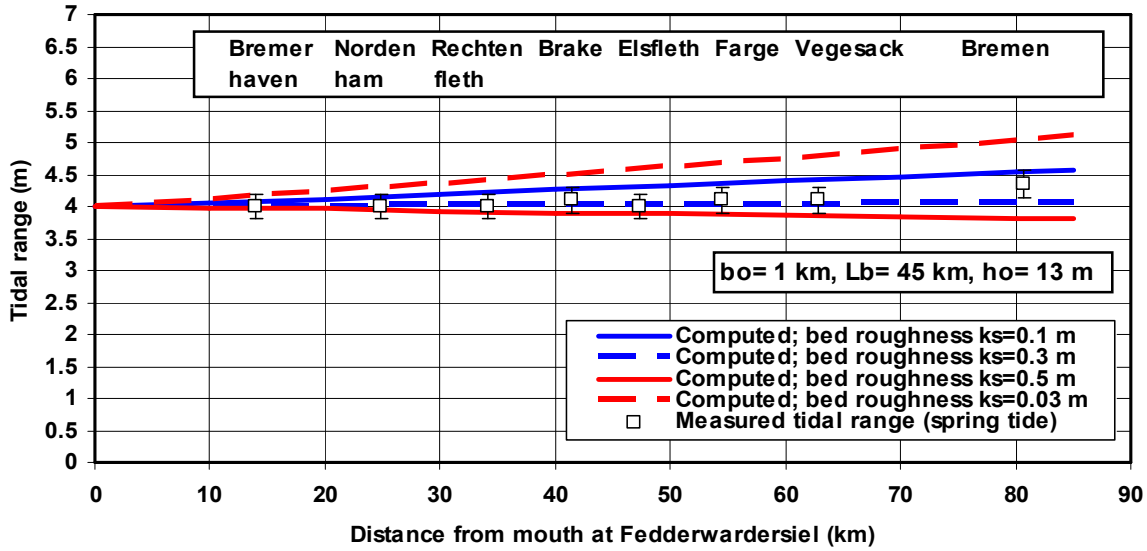

Figure 2.5.4 *Tidal range along the Weser estuary and river, Germany*

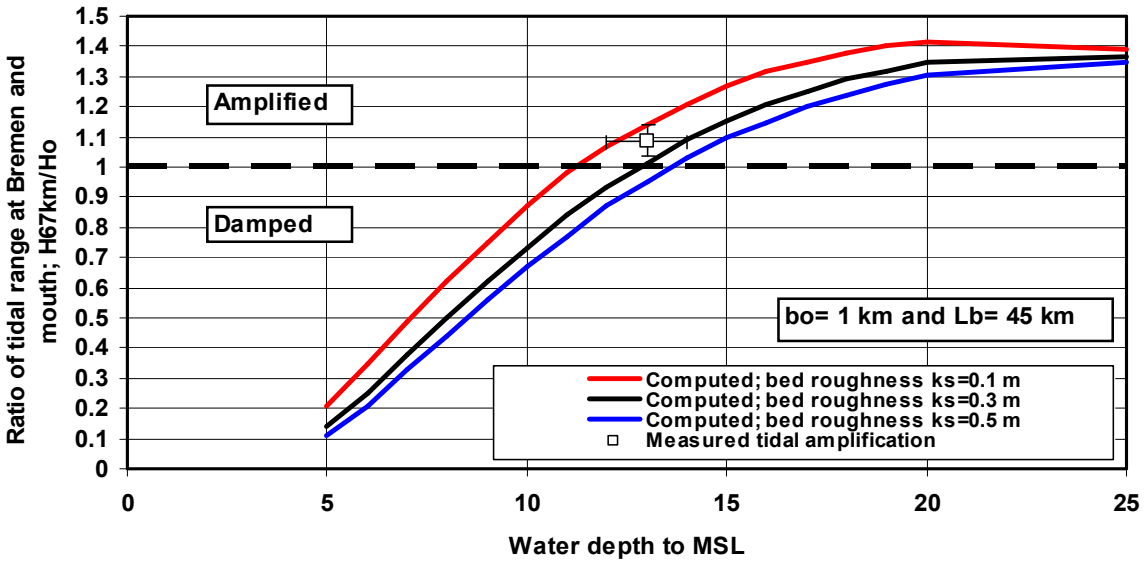

Figure 2.5.5 *Ratio of tidal range at Bremen and mouth Fedderwardersiel, Weser*

Overall, it can be concluded that the analytical model can reasonably well simulate the tidal range along the Weser up to Vegesack, where tidal reflection most probably is not so important. The schematisation used leads to an almost constant tidal range for roughness values in the range of 0.1 to 0.3 m. These relatively large values are not unrealistic given the presence of relatively large bed forms over the major part of the channel reach. The simulation results between Vegesack and Bremen are questionable as the tidal reflection (which may be of the order of 0.5 m) is not included in the simulation.

Salinity intrusion along the estuary

The volume ratio number of the Weser estuary is $R= V_{river}/V_{tide}= \pi Q_r T/ \hat{Q} T= \pi Q_r/ \hat{Q} \cong 0.09$ (<0.1) resulting in well-mixed conditions.
The linearized analytical model has been used to estimate the salinity intrusion length (Kuijper and Van Rijn, 2011).
The model computes the cross-section-averaged salinity distribution along the estuary at high water slack (HWS).

Additional input data are:

- salinity at mouth (S_o);
- freshwater river discharge (Q_r).

Figure 2.5.6 shows monthly-averaged river discharge and monthly-averaged salinity values at various stations along the Weser in the period June 1997 to June 2003. The salinity values are relatively small if the river discharge is relatively large.

Figure 2.5.7 shows measured salinity values along the Weser estuary. The salinity intrusion from Fedderwardersiel is about 50 km up to Elsfleth. The maximum salinity at Fedderwardersiel (Station 80.7 km) is about 23 promille. The maximum salinity at Bremerhaven is about 19 promille (Station 66.7 km).

Figure 2.5.8 shows computed cross-section averaged maximum salinities (at HWS) of the calibrated analytical salinity intrusion model and measured values from **Figure 2.5.7**. The river discharge is set to Q_r = 180 m^3/s based on measured data (see legend of **Figure 2.5.7**). The salinity at the mouth (Fedderwardersiel) is set to 23 promille.
The measured salinity distribution based on **Figure 2.5.7** (Q_r= 180 m^3/s) is somewhat different from the computed distribution. The computed salinities decrease for increasing bottom roughness.

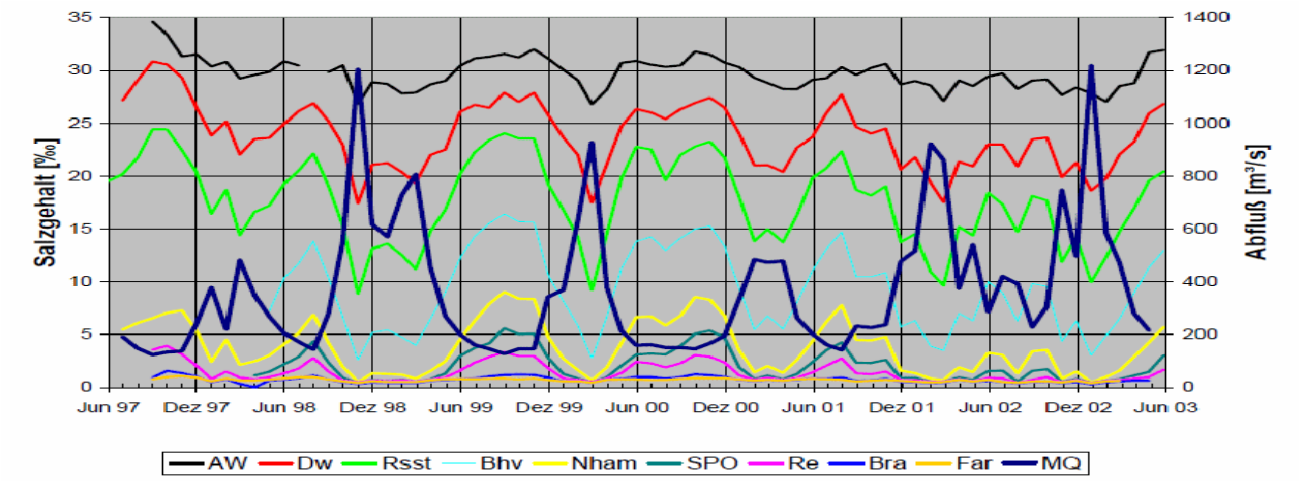

Figure 2.5.6 *Montly-averaged river discharge (MQ-curve) and montly-averaged salinity at various stations along the Weser estuary in period June 1997 to June 2003 (AW= Alte Weser, Dw= Dwarsgat, Rsst= Robbensudsteert, Bhv= Bremerhaven, Nham= Nordenham, SPO= Strohauser Plate Ost, Re= Rechtenfleth, Bra= Brake, Far= Farge)*
(GfL, Bioconsult, KÜFOG, 2006)

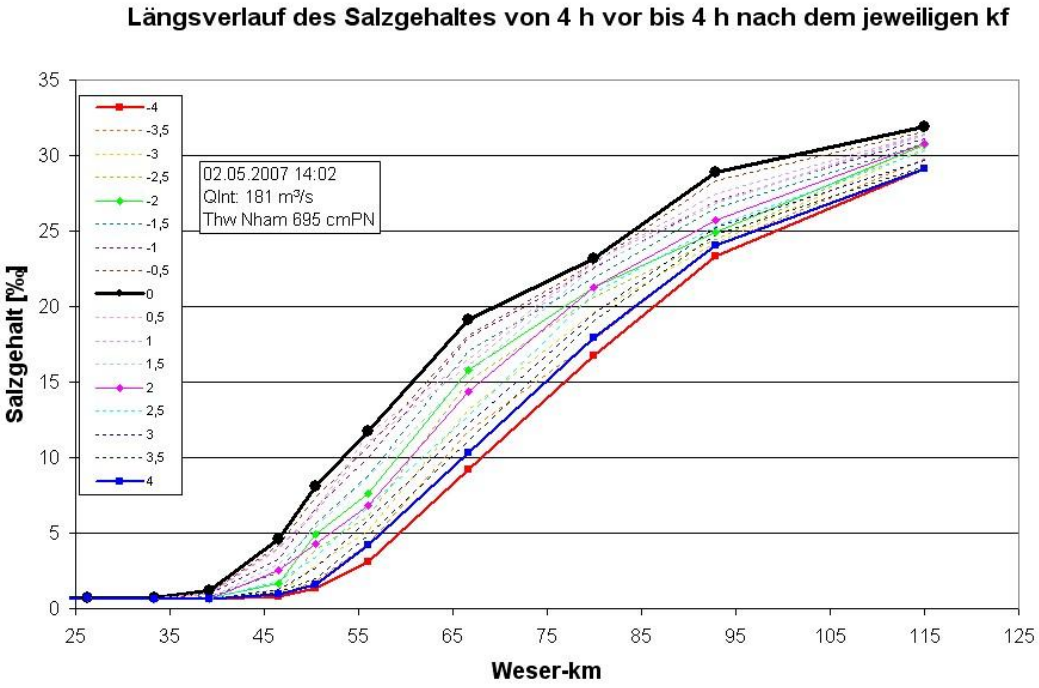

Figure 2.5.7 *Salinity along Weser estuary at various times within the tidal cycle (kf= high water slack) (Station 0= Bremen; Station 66.7 = Bremerhaven; Station 80.7= Fedderwardersiel)*
(Waterways and Shipping Office,Bremerhaven, 2011)

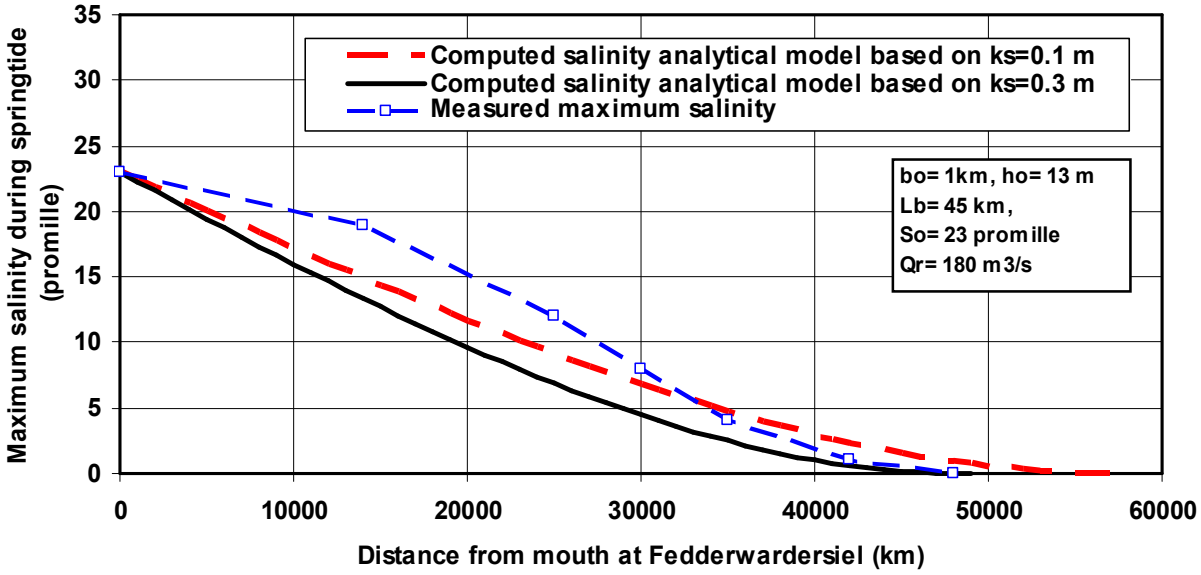

Figure 2.5.8 *Cross-section-averaged salinity (at HWS) during springtide along Weser estuary*

Figure 2.5.9 shows the computed cross-section averaged salinity intrusion at HWS along the Weser estuary for water depth values in the range of 5 to 25 m. The river discharge is set to the annual average value Q_r = 330 m^3/s. The salinity at the mouth (Fedderwardersiel) is set to 23 promille.

The maximum salinity intrusion computed according to the analytical salinity model varies between $L_{s,max}$= 7 km for small water depths to about 110 km for large water depths.

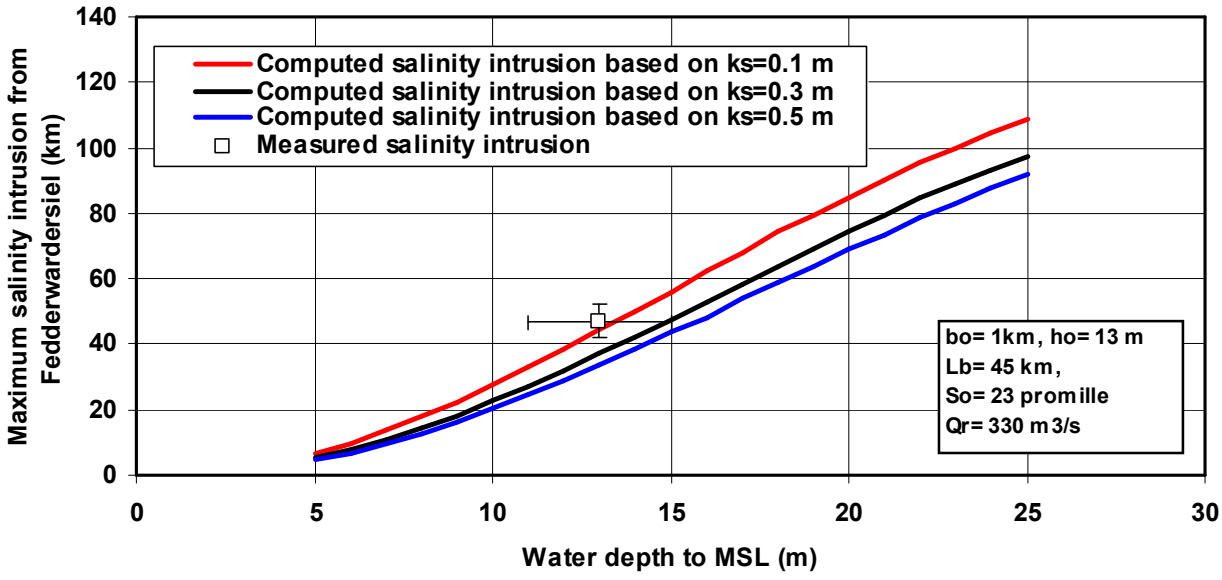

Figure 2.5.9 *Maximum salinity intrusion (at HWS) as function of water depth and bed roughness, Weser estuary*

Tide-averaged net velocities

Sediment import and export are related to net tide-averaged velocities consisting of (Annex A3 and B2):

1. River velocity $u_r = Q_r/A$ with Q_r = river discharge and A = area of cross-section;
2. Stokes drift velocity $\overline{u}_s = -0.25\,(H/h_o)\cos\varphi$ with H = tidal range, h_o=water depth to MSL, φ = phase shift between horizontal and vertical tide (+ = seaward and – = landward);
3. Net maximum velocity near the bed related to salinity-gradient in well-mixed conditions is: $u_{sa} = -0.035\,Mh^2$ with $M = g^{0.5}\,[C/\{\gamma\,(|\hat{\overline{u}}|+|\overline{u}_r|)\,h\}]\,(h/\rho_o)\,(\partial\rho_{sa}/\partial x)$, C= Chézy coefficient, $\rho_{sa} = \rho_o + 0.77\,S$, ρ_o= fresh water density, S= salinity (promille);
4. Net velocity related to tidal asymmetry $\Delta\hat{\overline{u}} = |\hat{\overline{u}}_{flood} - \hat{\overline{u}}_{ebb}|$ in landward or in seaward direction.

Analysis of numerical depth-averaged velocities of the 3D BAW model along the fairway in the mouth region (near Fedderwardersiel) shows peak flood and ebb values in the range of 1.2 to 1.6 m/s. The maximum net peak velocities $\Delta\hat{\overline{u}} = |\,|\hat{\overline{u}}_{flood} - \hat{\overline{u}}_{ebb}|$ is in the range of 0.1 to 0.3 m/s (based on computed values). Both ebb and flood dominance is present depending on the local geometry of the channels.

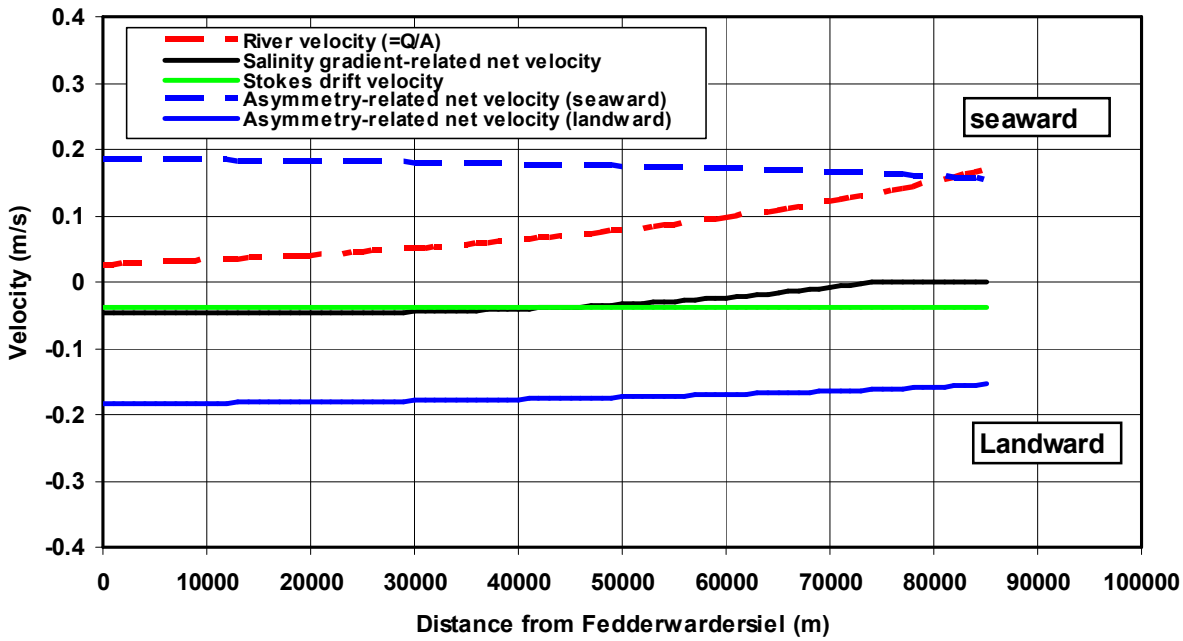

Figure 2.5.10 *Net velocities as function of distance along Weser estuary*

Figure 2.5.10 shows net velocities along the Weser with the mouth at Fedderwardersiel, Q_r= 330 m^3/s and k_s= 0.3 m.
The river velocity decreases in seaward direction from 0.15 m/s to about 0.03 m/s due to the increasing width (water depth = 13 m is constant).
The landward-directed Stokes drift is almost constant (about 0.03 m/s) along the Weser. Near the mouth the Stokes-drift is about 0.03 m/s in landward direction.
The net velocity related to the salinity gradient in the entrance section of the Weser is about 0.03 m/s at the mouth (in landward direction) decreasing to zero at about 75 km from the mouth.
The net peak velocity related to the tidal asymmetry is approximately 0.2 m/s along the Weser. This component can be in landward and seaward direction depending on geometrical parameters (channel configuration) and is much larger than the other components. The net river velocity is important in landward section of the estuary.
Sediment import or export in the Weser Estuary is largely determined by the net asymmetry-related velocities.

3 Summary and conclusions

The present report deals with the simulation of tidal wave propagation and salinity intrusion in four major (TIDE) estuaries in north-west Europe:

- Scheldt (Netherlands-Belgium),
- Humber (United Kingdom),
- Elbe (Germany) and
- Weser (Germany).

Simulation results have been compared with measured data of the four estuaries. The simulation results are based on relatively simple analytical models for tidal wave propagation and salinity intrusion in exponentially converging channels of constant depth. The exponentially converging width is represented as $b= b_o e^{-x/Lb}$ with L_b= converging width scale derived from known cross-sections along the estuary and b_o= effective width at mouth.
The basic input parameters are presented in **Table 3.1**. The model output parameters are presented in **Table 3.2**. The mouths of the four estuaries are shown in **Figure 3.3**.
The model includes the bottom friction effect and the funelling effect due to the decrease of the width. Tidal reflection effects at closed ends have been neglected. The model was tuned by using a geometrical parameter (converging length scale) and the bed roughness. The model results show that some basic features of tidal propagation can be simulated reasonably well quite well despite the crude schematizations used. Given the limitations of the analytical model, a crude schematization of the planform of the estuary is sufficiently adequate to get a first order estimate of the tidal parameters involved.

In all cases the measured tidal range values in the entrance of the estuaries and tidal rivers considered can be simulated reasonably well by the analytical model. The predicted tidal range values in the landward section of the tidal rivers were less good due to strongly decreasing water depth (Humber) and the presence of weirs in both German tidal rivers (reflection effects).
The prediction of the salinity intrusion by the analytical model was less good for the Scheldt and Weser Estuaries (overprediction).

All four estuaries are well-mixed estuaries as the peak tidal discharges are much larger than the fresh water river discharges.

Geometrical characteristics
The mouths of the Humber, Elbe and Weser are characterized by the presence of relatively large tidal flat areas above LAT bordering the banks (green areas of **Figure 3.3**). The widths of the main channels conveying the tidal discharges are relatively small. The mouth of the Scheldt estuary does not have substantial tidal tidal flats above LAT.

The Scheldt estuary has a relatively strong convergence of the width. The width (below LAT) of the Scheldt reduces from 25 km at the mouth (between Westkapelle and Zeebrugge) to about 2 km at 60 km from the mouth. The area of the cross-section at the mouth below LAT is about 120.000 m^2. The mean depth over the width at the mouth is about 5 m below LAT. The width at the line Vlissingen to Breskens at 15 km from the mouth is about 3500 m and the area of the cross-section below MSL is about 60000 m^2, yielding a mean depth of about 17 m below LAT. The deepest channel has a depth of about 22 m below LAT. The mean depth

over the estuary up to Antwerp is about 7 m below LAT and about 10 m below MSL. This latter value has been used in the simulations as the base depth.

The Humber estuary also has a relatively strong convergence of the width. The width of the Humber reduces from 6 km at the mouth to about 1 km at 37 km (Humber bridge) from the mouth. The mouth of the Humber is partly closed by a long spit (Spurn head spit). The effective opening of the mouth between Spurn Head and Tetney High Sands on the other bank is about 6000 m. The area of the cross-section below LAT at the mouth is about 80.000 m^2. The largest depth of the channel in the mouth is about 20 m below LAT. The mean depth below LAT at the mouth is about 13 m. Landward of Humber Bridge, the depth rapidly decreases to smaller values. The base depth between the mouth and Humber bridge used in the simulations is 12 m below MSL.

The Elbe and Weser estuaries have a relatively weak convergence of the width. The width (below LAT) of the Elbe reduces from 3 km at the mouth to about 0.4 km at 100 km (Hamburg) from the mouth. The width of the Weser reduces from 1 km at the mouth to about 0.15 km at 80 km (Bremen) from the mouth.
The channel depths of the Elbe and Weser estuaries are quite large and almost constant over long distance (80 to 100 km) to accomodate the passage of large vessels to the cities of Hamburg and Bremen.
Large-scale tidal sand waves and dunes (heights of 1 to 3 m and lengths of 50 to 150 m) are present along the bed of the Elbe and Weser.

Hydrodynamic characteristics (tides and river discharges)
The mean annual fresh water input of the four estuaries is largest for the Elbe river (700 m^3/s) and smallest for Scheldt river (about 100 m^3/s).
The tidal ranges at the mouths of the estuaries vary in the range of 3 m (Elbe) to 6 m (Humber). The Elbe, Weser and Scheldt have meso-tidal conditions. The Humber has macro-tidal conditions. The tides in all four estuaries have a semi-diurnal period.

Analysis of the tidal data shows that the tidal amplitude at the mouth is amplified in landward direction in all four estuaries. The amplification between the mouth and inland stations is largest (factor 1.3 to 1.5) for the Scheldt and smallest for the Weser (factor 1.05 to 1.1). The results are shown in **Figure 3.1**. A larger tidal range at the mouth leads to larger flow velocities in the estuary and thus to a larger contribution of bottom friction resulting in a smaller amplification effect (blue curves). The turning point from amplification ($H/H_o>1$) to damping ($H/H_o<1$) occurs for $L_b/h_o \cong 4500$ (**Van Rijn, 2011**). The Weser estuary is relatively close to this turning point.

The tidal amplitude along the Scheldt estuary is gradually amplified up to Rupelmonde (at about 105 km from the mouth) landward of Antwerp due to funneling and reflection against the landward boundary at Bath. The tidal data show relatively large tidal amplification between Hansweert and Antwerp due to reflection. Landward of Antwerp the tidal amplitude gradually dampens due to bottom friction in shallow river depths.
The tidal amplitude along the Humber estuary is gradually amplified up to Humber Bridge (at 37 km from the mouth). The maximum amplification is about 1.15. The amplification due to funnelling is substantially counteracted by damping due to the rapidly decreasing depth in landward direction and the presence of large tidal flats within the estuary. Landward of Humber bridge the tidal gradually dampens due to bottom friction in very shallow river depths.
The amplitude of the tidal wave is almost constant over large distances in both the Elbe and Weser Estuaries. Damping is not so significant as the depths remain rather large, although

the bed forms in both estuaries are quite large (presence of large sand waves with heights in the range of 1 to 3 m). Removal of these sand waves by regular dredging will lead to smaller bed roughness values and hence an increase of tidal amplification. The funneling effect is not very significant along the Elbe and Weser as the width reduces very gradually. In both rivers, weirs are present (upstream of Hamburg (Elbe) and Bremen (Weser)) causing reflection of the tidal wave and increase of the tidal amplitude over the most landward end of both estuaries.

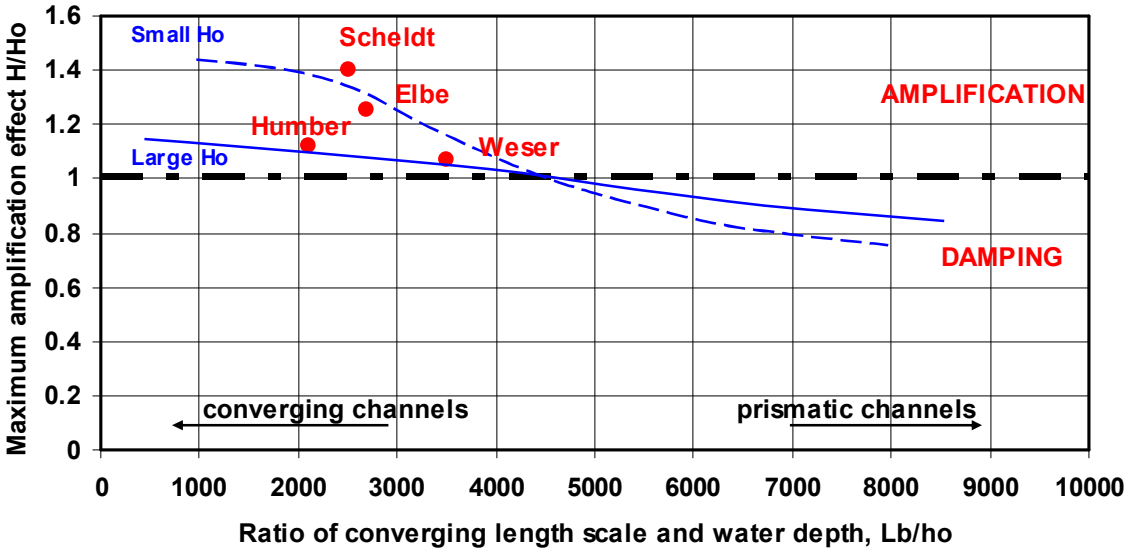

Figure 3.1 *Amplification effect as function of converging length scale (L_b), water depth (h_o) and tidal range (H_o)*

Tidal asymmetry is caused by the variable depth under the wave crest and trough resulting in a variable wave speed. As a result the wave crest will be more peaked with larger peak flood velocities than peak ebb velocities. Tidal circulations in both horizontal and vertical directions are present in all four estuaries. Horizontal circulations mainly occur due to geometrical configuration of the flood and ebb channels in the mouth region. Tidal asymmetry and horizontal circulation will lead to differences in the peak flood and ebb velocities of the order of 0.1 to 0.3 m/s in the mouth region.
Vertical circulations may occur due to the Stokes drift and horizontal density differences. The net velocities associated with these vertical density-rleated circulations vary in the range of 0.01 to 0.1 m/s. Net density-induced velocities are largest in the mouth of the Elbe with values of about 0.05 to 0.1 m/s in landward direction. These values are smaller in the range of 0.01 to 0.05 m/s in the mouths of the other estuaries. The Stokes drift velocity in landward direction is of the order of 0.03 m/s in all estuaries.
The net seaward velocities due to the fresh river discharges are almost zero in the Scheldt and Humber Estuaries and relatively large with values of 0.1 to 0.15 m/s at the landward end of the Weser and Elbe Estuaries.

Salinity characteristics

The volume ratio number (R= V_{river}/V_{tide}= $\pi Q_r T/\hat{Q}T$= $\pi Q_r/\hat{Q}$) of all four estuaries is smaller than 0.1 which means the presence of well-mixed conditions.
The salinity intrusion is approximately 120 km in the Scheldt, about 80 km in the Humber, about 65 km in the Elbe and about 50 km in the Weser. The salinity intrusion is largest in the Scheldt Estuary with the widest mouth (25 km) and the smallest river discharge (about 100 m^3/s). The salinity intrusion is smallest in the Weser with the smallest effective width (1 km) at the mouth. The Weser (and also the Elbe) are characterized by the presence of very regular river channels without typical flood and ebb channels as present in the Scheldt and Humber Estuaries resulting in less horizontal mixing and circulation. The results are shown in **Figure 3.2**.

The salinity intrusion depends on the tidal characteristics (water depth h_o, peak tidal velocity $\hat{u}_o$), the converging length scale (L_b), the bed roughness (k_s), the salinity at the mouth (S_o) and the fresh water river velocity ($Q_r/(b_o h_o)$).

The latter parameter varies over the year depending on rain fall and snow melt in the upstream catchment area. The converging length scale is a geometrical parameter and is alsmost constant for each estuary. The salinity intrusion decreases for increasing river discharge (blue curves). The salinity intrusion increases weakly with decreasing bed roughness (decreasing friction). The water depth and the bed roughness can be influenced by dredging activities.

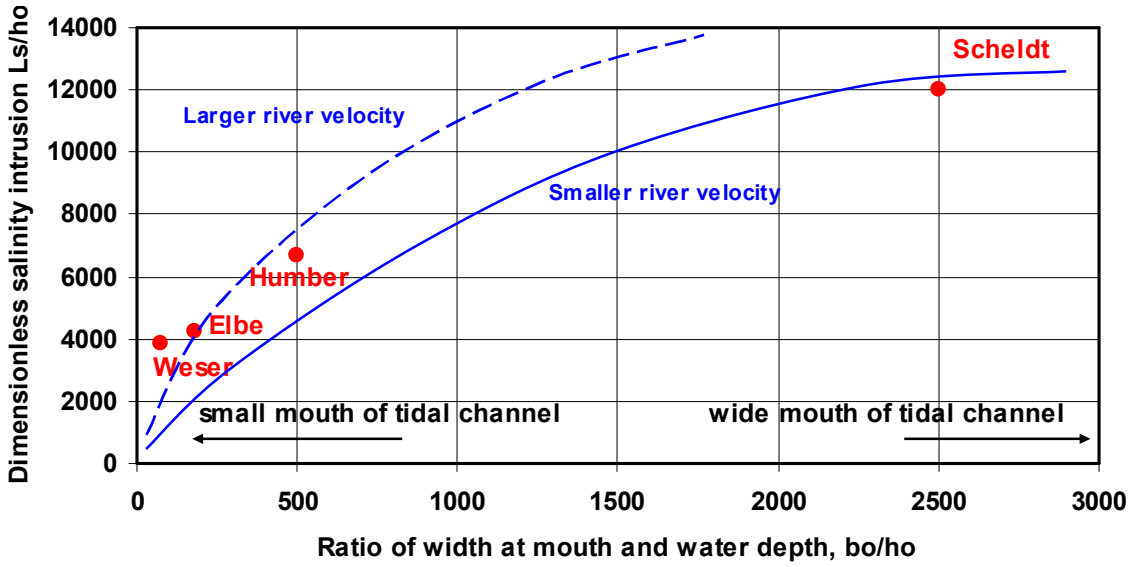

Figure 3.2 *Dimensionless salinity intrusion (L_s/h_o) as function of dimensionless width at mouth of tidal channel (b_o/h_o)*

Table 3.1 *Input parameters*

Input Parameters	Scheldt	Humber	Elbe	Weser
Tidal amplitude springtide at mouth ($\hat{\eta}_o$ in m)	2.1 (meso)	3 (macro)	1.5 (meso)	2 (meso)
Effective water depth to MSL (h_o in m)	10 (over 60 km)	12 (over 37 km) 6 (inland)	16.5 (over about 100 km)	13 (over about 80 km)
Effective width at mouth (b_o in m)	25000	6000	3000	1000
Tidal period (T in s)	45000	45000	45000	45000
Length scale converging width and cross-sectional area (L_b, L_a in m)	25000	25000	50000	45000
Effective bed roughness (k_s in m)	0.03 - 0.1	0.01 - 0.1	0.1 - 0.5	0.1 - 0.3
Mean annual river discharge (Q_r in m^3/s)	120	250	700	330
Salinity at mouth (S_o in promille)	30	30	18	18

Table 3.2 *Output parameters*

Output Parameters	Scheldt	Humber	Elbe	Weser
Estuary number Volume ratio Well-mixed <0.1 Part. mixed 0.1-1 Stratified >1	0.001 (well-mixed)	0.01 (well-mixed)	0.07 (wel-mixed)	0.09 (well-mixed)
Peak tidal velocity at mouth ($\hat{\overline{u}}_o$ in m/s)	0.8 - 0.85	0.95 – 1.0	0.65 - 0.7	0.90 – 0.95
Maximum amplification of tidal amplitude at mouth	1.3 to 1.5 (due to funelling and end reflection)	1.1 to 1.15 (due to funelling	1.2 to 1.3 (due to funelling and end reflection at weir)	1.05 to 1.1 (due to end reflection at weir; smaller than Elbe due to smaller depth)
Phase difference between horizontal and vertical tide (in hours)	2.5 to 3	2.5 to 3	2 to 2.5	2 to 2.5
Effective wave speed (m/s)	17	22	17	13
Frictionless wave speed $(gh_o)^{0.5}$	10	11	13	11
Salinity intrusion (km)	120	80	70	50

(North Sea on left)
Scheldt mouth, The Netherlands

(North Sea on right)
Humber mouth, England

(North Sea on left)
Elbe mouth, Germany

(North Sea on left)
Weser mouth, Germany

Figure 3.3 *Mouth of Scheldt, Humber, Elbe and Weser*
Yellow = land;
green = flats above LAT;
blue = 0 to -5 m LAT;
white = deeper than -5 m LAT

A Analytical model for tides in prismatic and convergent estuaries

A.1 Definitions

Basically, an estuary is the (widened) outlet of a river to the sea and is governed by the oscillating tidal flow coming from the (saline) sea and by the quasi-steady (fresh) water flow coming from the river in a complicated hydraulic system consisting of channels and shoals. Sometimes, a narrowing bay without river inflow is also known as an estuary. Drowned valleys (rias) and fjords also are examples of estuaries. A bay connected to the sea by a narrow channel (tidal inlet) is known as a lagoon or semi-enclosed basin. An alluvial channel with a movable sediment bed (banks are usually fixed) is a highly dynamic morphological system with meandering channels and shoals; sediments may be imported from riverine and marine sources. Sediments may also be exported over the seaward boundary of the estuary depending on the tidal asymmetry characteristics and the magnitude of the fresh water discharge of the river (density differences). Stratified or well-mixed flow conditions depend on the ratio of the fresh water river discharge and the saline tidal discharge.

The shape of alluvial estuaries is similar all over the world, see **Dyer (1997), McDowell and O'Connor (1977), Savenije (2005)** and **Prandle (2009)**. The width and the area of the cross-section reduce in upstream (landward) direction with a river outlet at the end of the estuary resulting in a converging (funnel-shaped) channel system, see **Figure A1**. The bottom of the tide-dominated section is almost horizontal. Often, there is a mouth bar at the entrance of the estuary. Tidal flats or islands may be present along the estuary (deltas).

Davies (1964) has classified tidal estuaries based on the tidal range H into:

- micro-tide (H < 2 m),
- meso-tide (2 < H < 4 m),
- macro-tide (H > 4 m).

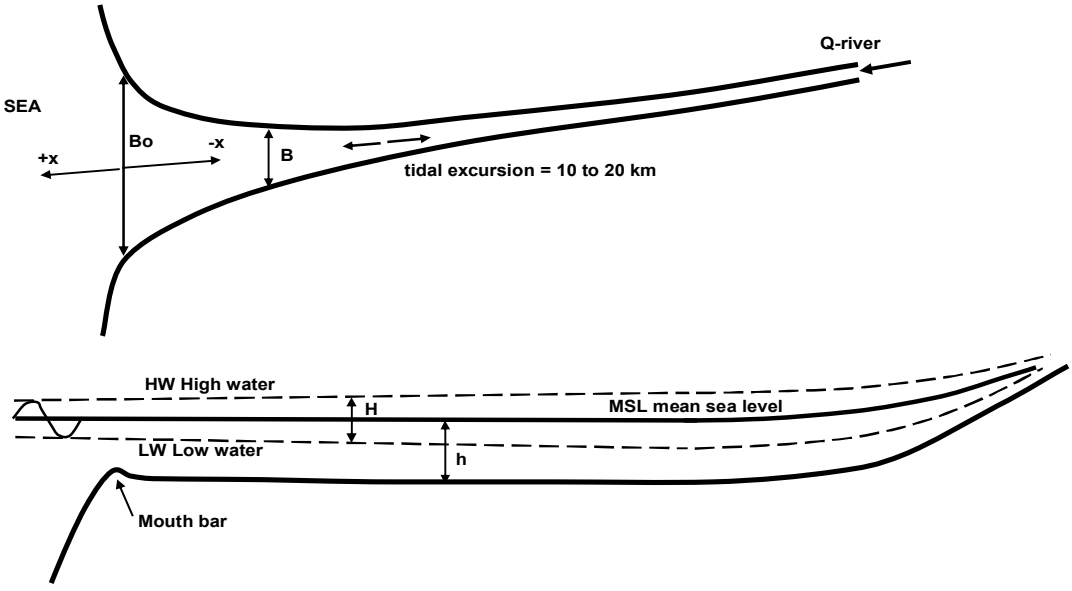

Figure A1 *Tidal estuary (plan shape and longitudinal section)*

A typical feature of estuaries is shallowness towards the landward end, although the water depth in the mouth of the estuary can be quite large (order of 10 to 20 m). Both shoaling and bottom friction are important, the latter becoming dominant in the river section with smaller water depths causing the tide to damp out.

The tidal flow is bi-directional in the horizontal section on the seaward side of the estuary and uni-directional in the sloping river section on the landward side of the estuary.

The tidal range (H) in estuaries is affected by the following dominant processes:

- shoaling or amplification due to the decrease of the width and depth in landward direction,
- damping due to bottom friction,
- deformation due to non-linear effects,
- (partial reflection) at landward end of the estuary.

As a result of these processes there is a phase difference between the vertical (water levels) and horizontal (currents) tide. The horizontal tide has a phase lead of about 1 to 3 hours with respect to the vertical tide.

The variation of the tidal range H along the estuary can be classified, as follows:

- tidal range is constant $H = H_o$ (defined as an ***ideal*** or ***synchronous*** estuary);
- tidal range increases $H > H_o$ (***amplified*** estuary);
- tidal range decreases $H < H_o$ (***damped*** estuary).

with: H = tidal range and H_o = tidal range at entrance (mouth).

The offshore astronomical tide is composed of various constituents. The most important constituent is the semi-diurnal M_2-component. The first harmonic of this constituent is M_4. Generally, the M_4-component is small offshore, but rapidly increases within estuaries due to bottom friction and channel geometry (see **Speer and Aubrey, 1985; Parker, 1991**). The M_2-component and its first harmonic M_4 dominate the non-linear processes within estuaries. Non-linear interaction between other constituents is also possible in shallow estuaries.
Analysis of field observations has shown that the interaction of M_2 and its first harmonic M_4 explains the most important features of tidal asymmetries. The type of tidal distortion (flood or ebb dominance) depends on the relative phasing of M_4 to M_2.

The basic causes of tidal deformation or tidal asymmetry are (see **Speer and Aubrey, 1985**; **Friedrichs, 1993; Friedrichs and Aubrey, 1988; Parker, 1991**):

- frictional damping, which is largest at low tide with smaller water depths resulting in flood dominance (ebb velocities are smaller than flood velocities);
- large volumes of water above wide tidal flats by which the flood velocities in the main channel are slowed down (drag in side planes) resulting in ebb dominance (flood velocity smaller than ebb velocity).

A.2 Mass and momentum equations and solutions

The mass balance and momentum balance equations for a simple prismatic channel with constant cross-sections read, as ($h = h_o+\eta$ and thus $\partial h/\partial x = \partial h_o/\partial x + \partial\eta/\partial x = + I_b + \partial\eta/\partial x$):

$$\frac{\partial \eta}{\partial t} + \frac{h\,\partial \bar{u}}{\partial x} + \frac{\bar{u}\,\partial \eta}{\partial x} = 0 \qquad \text{(A1)}$$

$$\frac{\partial \bar{u}}{\partial t} + \frac{\bar{u}\,\partial \bar{u}}{\partial x} + \frac{g\,\partial \eta}{\partial x} + \frac{g\,|\bar{u}|\,\bar{u}}{C^2 h} = 0 \qquad \text{(A2)}$$

with: η = water level elevation with respect to horizontal mean sea level (MSL), $\hat{\eta}$ = tidal amplitude, $\bar{u}$ = depth-averaged velocity, h = water depth, h_o = water depth to horizontal mean sea level, I_b = bottom slope, C = Chézy-coefficient.

These two equations contain several non-linear terms ($h\,\partial\bar{u}/\partial x$, $\bar{u}\,\partial\eta/\partial x$; $\bar{u}\,\partial\bar{u}/\partial x$ and $|\bar{u}|\,\bar{u}$), which can only be taken into account properly by using a numerical solution method. To find analytical solutions, these terms have either to be neglected or to be linearized. Since, analytical solutions are instructive to reveal the effects of bottom friction and width convergence, various methods will be explored below both for prismatic and converging channels.

The classical solution of the linearized mass and momentum balance equations for a ***prismatic*** channel of constant depth and width is well-known (**Hunt, 1964; Dronkers, 1964; Ippen, 1966; Verspuy, 1985; Parker, 1984; Friedrichs, 1993 and Dronkers, 2005**). This solution for a prismatic channel represents an exponentially damped sinusoidal wave which dies out gradually in a channel with an open end or is reflected in a channel with a closed landward end. In a frictionless system with depth h_o both the incoming and reflected wave have a phase speed of $c_o = (gh_o)^{0.5}$ and have equal amplitudes resulting in a standing wave with a virtual wave speed equal to infinity due to superposition of the incoming and reflected wave. Including (linear) friction, the wave speed of each wave is smaller than the classical value c_o (damped co-oscillation). Using this classical approach, the tidal wave propagation in funnel-type estuary can only be computed by schematizing the channel into a series of sections, each with its own constant width and depth, following **Dronkers (1964)** and many others. Unfortunately, this approach eliminates to large extent the effects of convergence in width and depth on the complex wave number and thus on the wave speed (**Jay, 1991**). A better approach is to represent the planform of the estuary by a geometric function. When an exponential function with a single length scale parameter (L_b) is used, the linearized equations can still be solved analytically and are of an elegant simplicity.

The solution for a funnel-type channel with exponential width ($b = b_o\, e^{-x/Lb}$ and L_b= converging length scale of about 10 to 100 km) and constant depth is less well-known.
Hunt (1964) was one of the first to explore analytical solutions for converging channels using exponential and power functies to represent the width variations. Both **LeFloch (1961)** and **Hunt (1964)** have given solutions for exponentially converging channels with constant depth. However, their equations are not very transparent.

Furthermore, they have not given the full solution including the precise damping coefficient and wave speed expressions for both amplified and damped converging channels. **Hunt (1964)** briefly presents his solution for a converging channel and focusses on an application for the Thames Estuary in England. The analytical model is found to give very reasonable results fitting the friction coefficient. **Hunt** shows that strongly convergent channels can produce a single forward propagating tidal wave with a phase lead of the horizontal and vertical tide close to 90^o, mimicking a standing wave system (apparent standing wave). A basic feature of this system is that the wave speed is much larger than the classical value $c_o = (gh_o)^{0.5}$, in line with observations. For example, the observed speed of the tidal wave in the amplified Scheldt Estuay in The Netherlands is between 13 and 16 m/s, whereas the classical value is about 10 m/s.

Parker (1984) has given a particular solution for a converging tidal channel with a closed end focussing on the tidal characteristics (only M_2-tide) of the Delaware Estuary (USA). He shows that the solution based on linear friction and exponential decreasing width yields very reasonable results for the Delaware Estuary fitting the friction coefficient.

Harleman (1966) also included the effect of the width convergence by combining **Greens' law** and the expressions for a prismatic channel. Predictive expressions for the friction coefficient and wave speed were not given. Instead, he used measured tidal data to determine the friction coefficient and wave length.

Godin (1988) and **Prandle and Rahman (1980)** have addressed a channel with both converging width and depth. They show that the analytical solution can be formulated in terms of Bessel functions for tidal elevations and tidal velocities in open and closed channels. However, the complex Bessel functions involved do obscure any immediate physical interpretation. Therefore, their results were illustrated in diagrammatic form (contours of amplitude and phase) for a high and low friction coefficient.

Like **Hunt, Jay (1991)** based on an analytical perturbation model of the momentum equation for convergent channels (including river flow and tidal flats) has shown that a single, incident tidal wave may mimic a standing wave by having an approximately 90^o degree phase difference between the tidal velocities and tidal surface elvations and a very large wave speed without the presence of a reflected wave. The tidal wave behaviour to lowest order is dominated by friction and the rate of channel convergence.

Friedrichs and Aubrey (1994) have presented a first-order solution of tidal wave propagation which retains and clarifies the most important properties of tides in strongly convergent channels with both weak and strong friction. Their scaling analysis of the continuity and momentum equation clearly shows that the dominant effects are: friction, surface slope and along-channel gradients of the cross-sectional area (rate of convergence). Local advective acceleration is much smaller than the other parameters. The solution of the first order equation is of constant amplitude and has a phase speed near the frictionless wave speed, like a classical progressive wave, yet velocity leads elevation by 90^o, like a classical standing wave. The second order solution at the dominant frequency is also a uni-directional wave with an amplitude which is exponentially modulated. If inertia is finite and convergence is strong, the amplitude increases along the channel, whereas if inertia is weak and convergence is limited, amplitude decays.

Lanzoni and Seminara (1998) have presented linear and non-linear solutions for tidal propagation in weakly and strongly convergent channels by considering four limiting cases defined by the relative intensity of dissipation versus local inertia and convergence. In weakly dissipative channels the tidal propagation is essentially a weakly non-linear problem. As channel convergence increases, the distortion of the tidal wave is enhanced and both the tidal wave speed and height increase leading to ebb dominance. In strongly dissipative channels the tidal wave propagation is a strongly non-linear process with strong distortion of the wave profile leading to flood dominance. They use a non-linear parabolic approximation of the full momentum equation.

Prandle (2003) has presented localized analytical solutions for the propagation of a single tidal wave in channels with strongly convergent triangular cross-sections, neglecting the advective terms and linearizing the friction term. The solutions apply at any location where the cross-sectional shape remains reasonably congruent and the spatial gradient of tidal elevation amplitude is relatively small (ideal or synchronous estuary). Analyzing the tidal characteristics of some 50 estuaries, he proposed an expression for the bed friction coefficient as function of the mud content yielding a decreasing friction coefficient for increasing mud content.

Finally, **Savenije et al. (2008)** have presented analytical solutions of the one-dimensional hydrodynamic equations in a set of four equations for the tidal amplitude, the peak tidal velocity, the wave speed and the phase difference between horizontal and vertical tide. Only bulk parameters are considered; hence the time effect is not resolved. Since reflection is not considered, their equations cannot deal with closed end channels. Various approaches have been used to arrive at their four equations. According to the authors, the combination of different approaches may introduce inconsistencies, which may limit the applicability of the equations. This may not be a real problem as long as measured data sets are available for calibration of the tidal parameters.

Herein, it will be shown that the linearized solution for a converging channel of constant depth with and without reflection can be expressed by transparent equations which are very similar to the classical expressions for a prismatic channel. These expressions are easily implemented in a spreadsheet model allowing quickscan computations of the dominant tidal parameters in the initial stage of a project (feasibility studies).

It is noted that the linearized solution cannot deal with the various sources of non-linearity such as quadratic friction, finite amplitude, variation of the water depth under the crest and trough, effects of river flow and effects of tidal flats causing differences in wave speed and hence wave deformation (see **Jay, 1991**). Multiple tidal constituents and overtides cannot be taken into account by analytical models including bottom friction. The offshore astronomical tide is composed of various constituents. The most important constituent is the semi-diurnal M_2-component. The first harmonic of this constituent is M_4 (amplitude of about 0.1 m to 0.15 m in the Scheldt Estuary and fairly constant within the estuary). Generally, the M_4-component is small offshore, but may increase within estuaries due to bottom friction and channel geometry (see **Speer and Aubrey, 1985; Parker, 1991**). The M_2-component and its first harmonic M_4 dominates the non-linear processes within estuaries. Non-linear interaction between other constituents is also possible in shallow estuaries. Analysis of field observations has shown that interaction of M_2 and its first harmonic M_4 explains the most important features of tidal asymmetries. The type of tidal distortion (flood or ebb dominance) depends on the relative phasing of M_4 to M_2.

In shallow friction-dominated estuaries generally, a saw-tooth type of tidal wave (sometimes a tidal bore) is generated, which cannot be represented by higher harmonics.

Nowadays, we have sophisticated numerical models to deal with the non-linearities involved and the multiple constituents, if present. One-dimensional numerical models can be setup easily and quickly and produce fairly accurate results if the geometry and topography is resolved in sufficient detail. Analytical models can only deal with schematized cases, but offer the advantage of simplicity and transparency. Simple spreadsheet solutions can be made for a quickscan of the parameters involved. The influence of basic human interventions such as channel deepening and widening can be assessed quickly. These simple models can be easily combined with salt intrusion models, sediment transport models, ecological models, etc for a quick first analysis of the problems involved. Based on this, the parameter range can be narrowed down substantially so that the minimum number of numerical model runs need to be made.

Analytical solutions are given in **Appendix B, C** and **D**.

A.3 Basics of tidal wave propagation and salinity intrusions

Tidal amplification

The principle of tidal wave amplification defined as the increase of the wave height due to the gradual change of the geometry of the system (depth and width), can be easily understood by considering the wave energy flux equation, which is known as **Green's law (1837)**.
This phenomenon is also known as wave shoaling or wave funneling.
The total energy of a sinusoidal tidal wave per unit length is equal to:

$$E = 0.125\rho g\, b\, H^2 \qquad \text{(A3)}$$

with b= width of channel, H = wave height.

The propagation velocity of a sinusoidal wave is given by: $c_o = (gh_o)^{0.5}$ with h_o= water depth.

Assuming that there is no reflection and no loss of energy (due to bottom friction), the energy flux F= E c is constant resulting in:

$$E_o c_o = E_x c_x$$
$$H_x/H_o = (b_x/b_o)^{-0.5} (h_x/h_o)^{-0.25} \qquad \text{(A4)}$$

Thus, the tidal wave height H_x increases for decreasing width and depth in landward direction. The wave length $L = c_o T$ will decrease as c_o will decrease for decreasing depth resulting in a shorter and higher wave.

Tidal wave speed

The wave speed $c = (g\ h_o)^{0.5}$ of a frictionless tidal wave in a deep, prismatic channel can be derived from the mass balance and momentum balance equations.

The wave speed in a converging estuary can be expressed as (Van Rijn, 2011)

$$c = \alpha_1\ c_o \qquad \text{(A5)}$$

with: $$\alpha_1 = [L/(4L_b)]^{0.5}\ \frac{[1 + \exp(0.5L/L_b)]^{0.5}}{[-1 + \exp(0.5L/L_b)]^{0.5}} \qquad \text{(A6)}$$

$c_o = (gh_o)^{0.5}$

L = tidal wave length,

L_b= converging length scale ($b = b_o\ e^{-x/Lb}$).

The α_1-coefficient is approximately equal to $\alpha_1 = [L/(4L_b)]^{0.5}$ for L_b << L. (or L/L_b>>1).

The α_1-coefficient is approximately equal to $\alpha_1 = 1$ for L_b >> L (or L/L_b<<1, prismatic channel).

The ratio c/c_o as function of L/L_b is shown in **Figure A2**. For most practical cases: $L_b \cong$ 10 to 25 km and L ≅ 300 to 500 km, the α_1-coefficient is about 1.7 to 3.5 for L/L_b= 12 to 50.

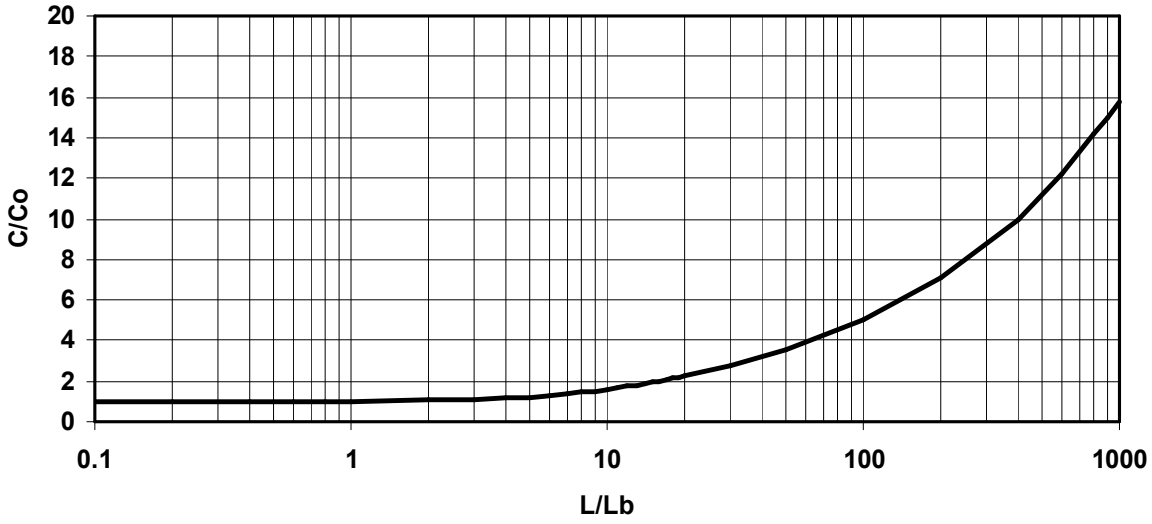

Figure A2 *Ratio c/c_o as function of L/L_b*

Thus, the frictionless wave speed in a strongly converging estuary is **strongly amplified**.

Wave speed data of the Scheldt Estuary yield $c/c_o \cong$ 1.2 to 1.6. Equation (3.6) yields $\alpha_1 \cong 2$ for the Scheldt Estuary using L ≅ 400 km and $L_b \cong$ 25 km, which is somewhat larger than measured values (as friction has been neglected to derive Equation A6).

The tidal wave speed is reduced by **bottom friction**, which can be expressed as (Van Rijn, 2011):

$$c = \alpha_2 (g h_o)^{0.5} \qquad \text{(A7)}$$

with: $\alpha_2 = [1/(1 + m\ T)]^{0.5}$, m = friction coefficient (> 0) and T = tidal period.

Since the α_2-coefficient is always smaller than 1, the wave speed is reduced by bottom friction.

Phase shifts between vertical and horizontal tide

Bottom friction and channel geometry (shoaling) cause a phase shift between the horizontal tide (current velocities) and the vertical tide (water levels). A phase shift of 3 hours ($\cong 90^o$) represents a standing wave pattern. In the Scheldt Estuary (The Netherlands) the horizontal tide reverses earlier (about 1 to 2.5 hours) than the vertical tide, as shown in **Figure A3;** see also **De Kramer (2002)**.
The time period with nearly zero current velocities is known as **Slack Water**.

The vertical and horizontal tides can be represented as:

$$\eta = \hat{\eta} \cos(\omega t) \qquad \text{(A8)}$$

$$\bar{u} = \hat{\bar{u}} \cos(\omega t + \varphi_1) = \hat{\bar{u}} \cos(\omega t + 90^o - \varphi_2) \qquad \text{(A9)}$$

with: $\hat{\bar{u}}$ = peak tidal velocity (positive velocity is flood velocity), φ_1 = phase lead (if $\varphi_1 < 0$, then phase lag; horizontal tide reverses later); $\varphi_1 + \varphi_2 = 90^o$; $\varphi_1 = 0^o$ for a frictionless progressive wave, $\varphi_1 = 90^o$ for a standing wave.

Thus: $\varphi_1 = 0^o$: progressive tidal wave in prismatic channel (no friction),
$\varphi_1 = 90^o$: standing tidal wave (phase lead of 3 hours in semi-diurnal conditions),
$\varphi_1 = 0^o$ to 90^o: mixed tidal wave.

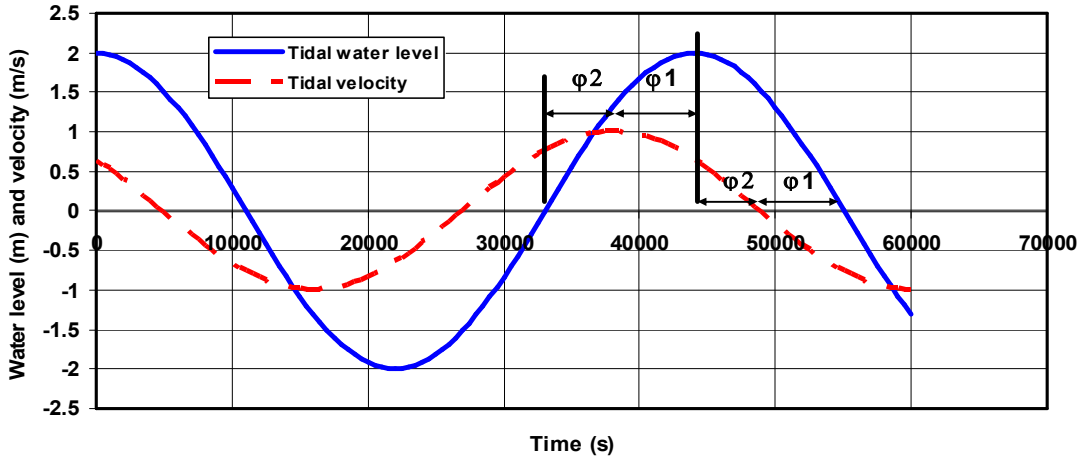

Figure A3 *Phase shift between vertical and horizontal tide; flood velocity is positive ($\varphi_1 = 0^o$ and $\varphi_2 = 90^o$ for progressive wave) ($\varphi_1 = 90^o = 0.5\pi$ and $\varphi_2 = 0^o$ for standing wave)*

The phase angle is defined with respect to the time moment of zero-crossing of the vertical tide.

The phase difference between the vertical and horizontal tide can also be defined as the phase difference φ_2 between HW (High Water of vertical tide) and HWS (High Water Slack of horizontal tide), which is a phase lag as the reversal of the horizontal tide (HWS) is later than reversal of the vertical tide (HW).

The phase lead of the velocity with respect to the water level variation can be expressed as (Van Rijn, 2011):

$$\cos\varphi_1 = h_o \hat{\bar{u}}_o T \frac{(\mu_D+\beta)}{(\pi H_o)} \qquad \text{(A10)}$$

with:
φ_1= phase lead of velocity with respect to water level elevation,
h_o = water depth to MSL, H_o= tidal range at mouth,
T= tidal wave period,
$\hat{\bar{u}}_o$= peak tidal velocity at mouth,
μ_D= $1/L_w$= damping coefficient (positive value),
β = $1/L_b$ = convergence coefficient (positive value).

Thus, the phase lead increases with increasing damping coefficient (greater bottom friction) and increasing convergence (larger β or smaller L_b).
Equation (A10) is only valid for a damped estuary with a gradually reducing width (weakly converging estuary) and decreasing tidal range, which implies that $L_b \cong$ 100 km or larger ($\beta <$ 0.00001).
The damping length L_W also is of the order of 100 km or larger (μ_D <0.00001).

Stokes drift
Due to the tidal variation of the water level, the net discharge over the tidal cycle is not zero. The velocity defined as $\bar{u}_{Stokes} = q_{Stokes}/T$ is known as the **Stokes** drift:

$$q_{stokes} = (1/T) \int_0^T q\, dt = (1/T) \int_0^T (\bar{u} h)\, dt \qquad \text{(A11)}$$

$$\bar{u}_{stokes} \cong 0.5 (\hat{\eta}/h_o) \cos\varphi_1 \quad \hat{\bar{u}} \qquad \text{(A12)}$$

The Stokes drift velocity is maximum for φ_1 = 0 (no phase shift between horizontal and vertical tide) and zero for φ_1= 90° (standing wave system). Generally, φ_1 = 60° to 85°.
Using: $\hat{\eta}/h_o \cong$ 0.2, cosφ= 0.5 and $\hat{\bar{u}} \cong$ 1 m/s, resulting in: $\bar{u}_{stokes} \cong$ 0.05 m/s in landward direction.
Since the Stokes drift leads to the accumulation of fluid within the estuary, the mean water level will gradually go up towards the landward end of the estuary resulting in a water level gradient by which a return flow is driven (vertical circulation).

B Analytical solution of tidal wave equations for prismatic channels

B.1 Schematization and basic equations

In a prismatic channel with constant cross-section (depth and width are constant), the phase shift between the horizontal and the vertical tide is caused by bottom friction. This can be illustrated by the analytical solution of the mass and momentum balance equations for a prismatic channel (cross-section is constant, bottom slope is constant, see **Figure A1**), see also **Dronkers (1964)**, **Hunt (1964), Ippen (1966), Verspuy (1985)** and **Dronkers (2005)**.

The basic assumptions are:

- channel depth (h_o) to MSL is assumed to be constant in space and time: ($h = h_o + \eta$); h_o = constant (bottom of **Figure B1** is assumed to be horizontal);
- convective acceleration ($\overline{u}\,\partial\overline{u}/\partial x = 0$) is neglected;
- linearized friction is used;
- fluid density is constant;
- river discharge (Q_r) is constant;
- x-coordinate is negative in landward direction and positive in seaward direction.

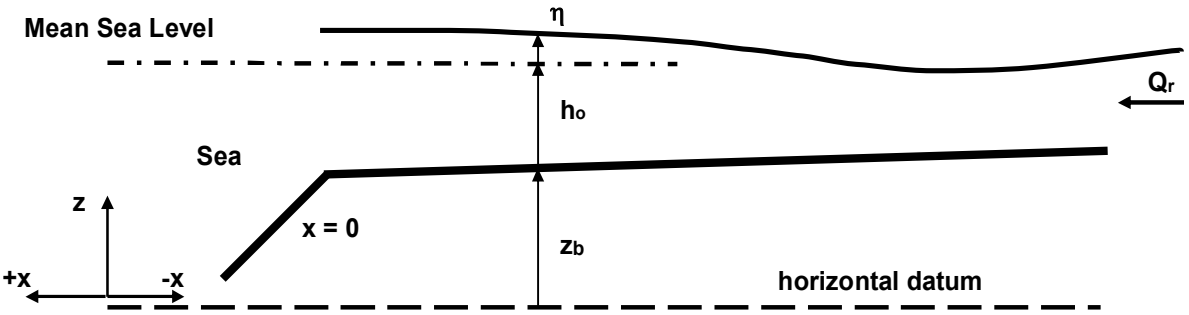

Figure B1 *Tidal wave in a prismatic tidal channel (constant width)*

Due to linearization of the friction term the solution can be represented by a sinusoidal function in time and space. Non-linear effects (higher harmonics) deforming the tidal wave profile are not included.
It is remarked that only one (primary) tidal wave is included (M_2-component).

The equations of continuity and motion for depth-averaged flow are:

$$\frac{b\,\partial\eta}{\partial t} + \frac{\partial Q}{\partial x} = 0 \qquad \text{(B1)}$$

$$\frac{1}{A}\frac{\partial Q}{\partial t} + \frac{g\,\partial\eta}{\partial x} + \frac{Q\,|Q|}{C^2 A^2 R} = 0 \qquad \text{(B2)}$$

in which:
A = b h_o = area of cross-section, b_s= b = surface width, h_o = depth to MSL (mean sea level), R = hydraulic radius ($\cong h_o$ if b>>h_o) and C = Chézy-coefficient (constant).

An analytical solution can be derived when the friction term is linearized. The equation of motion becomes:

$$\frac{1}{A}\frac{\partial Q}{\partial t} + \frac{g}{}\frac{\partial \eta}{\partial x} + n Q = 0 \qquad \text{(B3)}$$

in which:
n is a constant friction factor, n = $(8g|\hat{Q}|)/(3\pi C^2A^2R)$= **Lorentz**-friction parameter ($m^{-2}s^{-1}$) in the case Q_r = 0, m = n A = $(8g|\hat{Q}|)/(3\pi C^2AR)$= **Lorentz**-friction parameter (1/s), (**1922, 1926**), $\hat{Q}$= characteristic peak tidal discharge (average value over traject), C = Chézy-coefficient, R = hydraulic radius.
Assuming a rectangular cross-section and the width and depth to be constant in space and time (b = constant, h $\cong$ h_o = constant), Equations (A13) and (A15) can also be expressed as:

$$\frac{\partial \eta}{\partial t} + \frac{h_o}{}\frac{\partial \overline{\overline{u}}}{\partial x} = 0 \qquad \text{(B4)}$$

$$\frac{\partial \overline{\overline{u}}}{\partial t} + \frac{g}{}\frac{\partial \eta}{\partial x} + m\,\overline{\overline{u}} = 0 \qquad \text{(B5)}$$

in which: $\overline{\overline{u}}$= cross-section averaged velocity, $\hat{u}$= amplitude of tidal velocity, m = $(8g|\hat{u}|)/(3\pi C^2R)$ = friction coefficient. In the case of a very wide channel (b>>h_o): $\overline{\overline{u}} \cong \overline{u}$ = depth-averaged velocity and R $\cong$ h_o.
In the case of a **compound** cross-section consisting of a main channel and tidal flats it may be assumed that the flow over the tidal flats is of minor importance and only contributes to the tidal storage. The discharge is conveyed through the main channel. This can to some extent be represented by using: $c_o = (g\,h_{eff})^{0.5}$ with $h_{eff} = A_c/b_s = \alpha_h h_c$ and $\alpha_h = A_c/(b_s h_c) = (b_c/b_s) h_c = (b_c/b_s) h_o$, A_c= area of main channel (= $b_c h_c = b_c h_o$), $h_c = h_o$= depth of main channel, b_c= width of main channel and b_s= surface width.
The transfer of momentum from the main flow to the flow over the tidal flats can be seen as additional drag exerted on the main flow (by shear stresses in the side planes between the main channel and the tidal flats). This effect can be included crudely by increasing the friction in the main channel.
If the hydraulic radius (R) is used to compute the friction parameters (m and C) and the wave propagation depth (h_{eff}= R), the tidal wave propagation in a compound channel will be similar to that in a rectangular channel with the same cross-section A.

B.2 Types of boundary conditions

The various types of boundary conditions (in complex notation; index c) are presented in **Table B1**.

Table B1 *Types of boundary conditions*

Boundary Case	**Entrance of channel x = 0**	**Exit of channel x = L**
I Channel of infinite length	Open: $\hat{\eta}_{c,o}$ = given (known	Open: $\hat{\eta}_{c,L} = 0$, $\hat{Q}_{c,L} = 0$ or $\hat{Q}_{c,L} = Q_{river}$
II Channel of finite length	Open: $\hat{\eta}_{c,o}$= given (known) $\hat{Q}_{c,o}$ = given (known)	Open: $\hat{\eta}_{c,L}$ = unknown, $\hat{Q}_{c,L}$ = unknown
III Channel closed at end	Open: $\hat{\eta}_{c,o}$ = given (known)	Closed: $\hat{Q}_{c,L} = 0$
IV Channel between two large tidal basins	Open: $\hat{\eta}_{c,o}$ = given (known)	Open: $\hat{\eta}_{c,L}$ = given
V Channel between large basin and lake with constant level	Open: $\hat{\eta}_{c,o}$ = given (lnown)	Open: $\hat{\eta}_{c,L} = 0$

B.3 Analytical solutions

The analytical solution with and without reflection is summarized in **Table B2 (**see **Van Rijn, 2011)**.

Table B.2 *Analytical solutions for prismatic and converging channels (with and without reflection)*

TYPE OF WAVE	PRISMATIC CHANNELS	CONVERGING CHANNELS
Excluding reflection at landward end (channel open at end)	$\eta_{x,t} = \hat{\eta}_o\,[e^{-\mu x}]\,[\cos(\omega t - kx)]$ $\overline{\overline{u}}_{x,t} = \hat{\overline{u}}_o\,[e^{-\mu x}]\cos(\omega t - kx+\varphi)$ with: $\hat{\overline{u}}_o = -(\hat{\eta}_o/h_o)(\omega/k)[\cos\varphi]$ μ = friction parameter k = wave number φ = phase lead x = horizontal coordinate; positive in landward direction	$\eta_{x,t} = \hat{\eta}_o\,[e^{-\varepsilon x}]\,[\cos(\omega t - kx)]$ $\overline{\overline{u}}_{x,t} = \hat{\overline{u}}_o\,[e^{-\varepsilon x}]\cos(\omega t - kx+\varphi)$ with: $\varepsilon = -0.5\beta + \mu$ $\hat{\overline{u}}_o = -(\hat{\eta}_o/h_o)(\omega/k)[\cos\varphi]$ $c = \omega/k$, $\tan\varphi = \sin\varphi/\cos\varphi = (0.5\beta+\mu)/k$, $\sin\varphi = (0.5\beta+\mu)/[(0.5\beta+\mu)^2 + k^2]^{0.5}$ $\cos\varphi = (k)/[(0.5\beta+\mu)^2 + k^2]^{0.5}$, μ = friction parameter k = wave number φ = phase lead (between hor. and vert. tide) $\beta = 1/L_b$ = convergence parameter x = horizontal coordinate; positive in landward direction
Including reflection at landward end (channel closed at end)	$\eta_{x,t} = 0.5\,\hat{\eta}_o\,(f_A)^{-1}\,[e^{-\mu(x-L)}\cos(\omega t - k(x-L)) + e^{\mu(x-L)}\cos(\omega t + k(x-L))]$ $\overline{\overline{u}}_{x,t} = 0.5\,\omega\,(\hat{\eta}_o/h_o)(f_A)^{-1}\,(k^2+\mu^2)^{-0.5}$ $[e^{-\mu(x-L)}\cos(\omega t - k(x-L) + \varphi) - e^{\mu(x-L)}\cos(\omega t + k(x-L) + \varphi)]$ with: f_A = amplification/damping factor = $[\cos^2(kL) + \sinh^2(\mu L)]^{0.5}$ L = channel length x = horizontal coordinate; **positive** in landward direction	$\eta_{x,t} = 0.5\,\hat{\eta}_o\,(f_A)^{-1}\,[e^{(\varepsilon 1)x+\mu L}\cos(\omega t - k(x-L)) + e^{(\varepsilon 2)x-\mu L}\cos(\omega t + k(x-L))]$ $\overline{\overline{u}}_{x,t} = 0.5\omega(\hat{\eta}_o/h_o)(f_A)^{-1}(k^2+\mu^2)^{-0.5}$ $[e^{(\varepsilon 1)x+\mu L}\cos(\omega t - k(x-L) + \varphi) - e^{(\varepsilon 2)x-\mu L}\cos(\omega t + k(x-L) + \varphi)]$ with: $\varepsilon_1 = 0.5\beta - \mu$ $\varepsilon_2 = 0.5\beta + \mu$ f_A = amplification/damping factor = $= [\cos^2(kL) + \sinh^2(\mu L)]^{0.5}$ L = channel length; x = horizontal coordinate; **positive** in landward direction

C Analytical solutions of tidal wave equations for converging channel

C.1 Schematization and basic equations

An analytical solution of the mass and momentum balance equations can also be obtained for a converging channel (funnel type; see **Figure C1**), if the channel width is represented by an exponential function ($b = b_o e^{\beta x}$), see also **Hunt (1964), Mazumder and Bose (1995)** and **Prandle (2009)**.

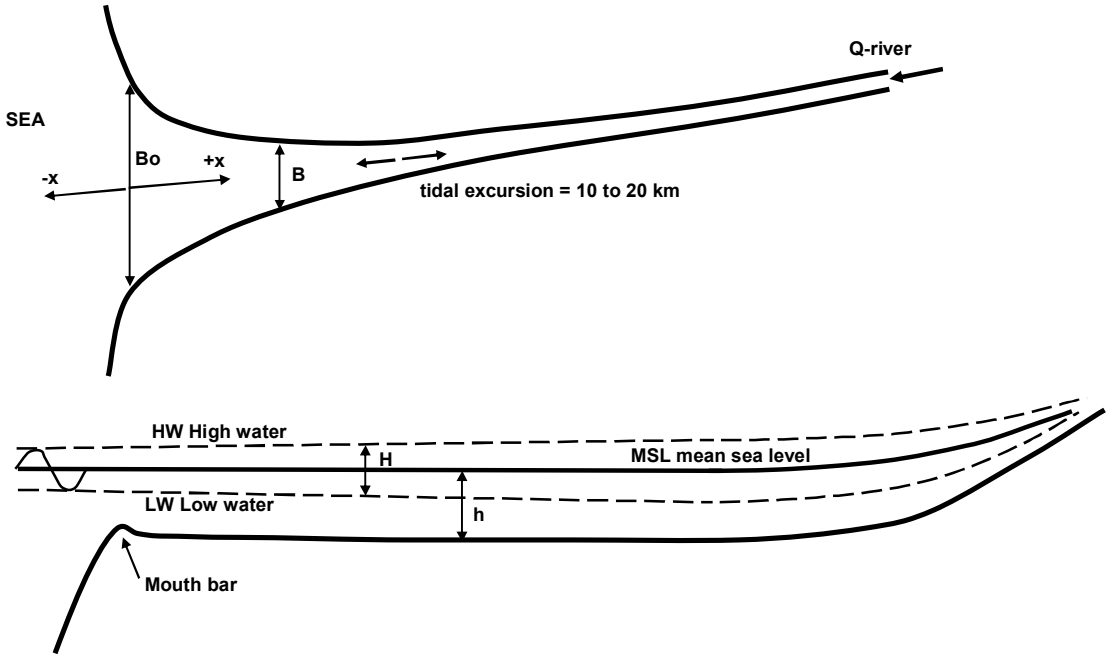

Figure C1 *Tidal estuary (planform and longitudinal section)*

The basic assumptions are:

- bottom is assumed to be horizontal ($I_b = 0$); channel depth to MSL is assumed to be constant in space and time ($h = h_o+\eta$); depth h_o = constant;
- width is $b = b_o e^{\beta x}$ with $\beta=1/L_b$= convergence coefficient, L_b = converging length scale, constant in time;
- convective acceleration ($\overline{u}\,\partial\overline{u}/\partial x = 0$) is neglected;
- linearized friction is used;
- fluid density is constant.

The equations of continuity and motion for depth-averaged flow are:

$$\frac{b\,\partial\eta}{\partial t} + \frac{\partial Q}{\partial x} = 0 \qquad \text{(C1)}$$

$$\frac{1}{A}\frac{\partial Q}{\partial t} + \frac{g}{\partial x}\frac{\partial \eta}{} + \frac{Q\,|Q|}{C^2 A^2 R} = 0 \qquad \text{(C2)}$$

in which:
A = b h_o = cross-section area, b = width, h_o= depth to mean sea level, R = hydraulic radius and C = Chézy-coefficient are constants.

An analytical solution can be found when the friction term is linearized, as follows:

$$\frac{1}{A}\frac{\partial Q}{\partial t} + \frac{g}{\partial x}\frac{\partial \eta}{} + n\,Q = 0 \qquad \text{(C3)}$$

in which: n is a constant friction factor, $n = (8g\,|\hat{Q}|)/(3\pi C^2 A^2 R)$.

The mass balance equation can be expressed as (A = b h and $h = h_o+\eta$):

$$\frac{b}{\partial t}\frac{\partial \eta}{} + \frac{b\,h_o}{\partial x}\frac{\partial \overline{\overline{u}}}{} + \frac{\overline{\overline{u}}\,b}{\partial x}\frac{\partial \eta}{} + \frac{\overline{\overline{u}}\,h_o}{\partial x}\frac{\partial b}{} = 0 \qquad \text{(C4)}$$

The gradient of the width is: $\partial b/\partial x = \beta\, b_o\, e^{\beta x} = \beta\, b$.
Neglecting the term $\overline{\overline{u}}\, b\, \partial\eta/\partial x$, the mass balance equation becomes:

$$\frac{b}{\partial t}\frac{\partial \eta}{} + \frac{b\,h_o}{\partial x}\frac{\partial \overline{\overline{u}}}{} + \overline{\overline{u}}\,\beta\, b\, h_o = 0 \qquad \text{(C5)}$$

or

$$\frac{\partial \eta}{\partial t} + \frac{h_o}{\partial x}\frac{\partial\ \overline{\overline{u}}}{} + \overline{\overline{u}}\ \beta\, h_o = 0 \qquad \text{(C6)}$$

The momentum equation can be simplified to:

$$\frac{\partial(b h_o \overline{\overline{u}})}{b\,h_o\ \partial t} + \frac{g}{\partial x}\frac{\partial \eta}{} + n\, b\, h_o\, \overline{\overline{u}} = 0 \qquad \text{(C7)}$$

or

$$\frac{\partial \overline{\overline{u}}}{\partial t} + \frac{g}{\partial x}\frac{\partial \eta}{} + m\ \overline{\overline{u}} = 0 \qquad \text{(C8)}$$

with: $\overline{\overline{u}}$= cross-section-averaged velocity, $m = nA = n\ b\ h_o = (8g\ |\hat{\overline{u}}|)/(3\pi C^2 R) \cong (8g\ |\hat{\overline{u}}|)/(3\pi C^2 h_o)$ = **Lorentz**-friction parameter (dimension 1/s), $\hat{\overline{u}}$= characteristic peak velocity (average value over traject), C= Chézy = coefficient, R = hydraulic radius.

In the case of a **compound** cross-section consisting of a main channel and tidal flats it may be assumed that the flow over the tidal flats is of minor importance and only contributes to the tidal storage. The discharge is conveyed through the main channel. This can to some extent be represented by using $c_o = (g\, h_{eff})^{0.5}$ with $h_{eff} = A_c/b_s = \alpha_h\, h_c$ and $\alpha_h = A_c/(b_s\, h_c) = (b_c/b_s)\, h_c = (b_c/b_s)\, h_o$, A_c= area of main channel $(= b_c\, h_c = b_c h_o)$, $h_c = h_o$= depth of main channel, b_c= width of main channel and b_s= surface width.
The transfer of momentum from the main flow to the flow over the tidal flats can be seen as additional drag exerted on the main flow (by shear stresses in the side planes between the main channel and the tidal flats). This effect can be included crudely by increasing the friction in the main channel.
If the hydraulic radius (R) is used to compute the friction parameters (m and C) and the wave propagation depth (h_{eff}= R), the tidal wave propagation in a compound channel will be similar to that in a rectangular channel with the same cross-section A.

C.2 Analytical solutions

Tidal range and peak tidal velocities
The solution is given by **Van Rijn (2011)** and is summarized in **Table B2**.
Three subcases (**Case A, B and C**) can be distinguished to determine the μ-parameter and the k-parameter, as follows:

Case A**: **Amplitude of water level and velocity are constant (ideal estuary)

$$\beta = 2\,\omega/c_o = 2\,k_o \quad \text{or} \quad 1/L_b = 2k_o \quad \text{or} \quad L_b = L_{wave,o}/(4\pi) \text{ or} \qquad \text{(C9)}$$
$$L_b = c_o/(2\,\omega) = (g\,h_o)^{0.5}T/(4\pi) = L_{wave,o.}/(4\pi)$$

Using: h_o = 3 m and T = 43200 s, $L_b \cong$ 20.000 m (20 km)
h_o = 5 m and T = 43200 s, $L_b \cong$ 25.000 m (25 km)
h_o = 10 m and T = 43200 s, $L_b \cong$ 35.000 m (35 km)

If $L_b = L_{wave,o}/(4\pi)$, then $\mu = k = k_o$ and the amplitudes of water level and velocity are constant ($\beta = 2\,k = 2\mu$).

Case B**: **Amplification is dominant

$$\beta \geq 2\,\omega/c_o \text{ or } L_b \leq (g\,h_o)^{0.5}T/(4\pi) \qquad \text{(C10)}$$

$$k = 0.5^{0.5}\,(\omega/c_o)\,\alpha^{0.5}\,[-1 + \{1 + m^2/(\omega^2\alpha^2)\}^{0.5}]^{0.5} \quad \text{with} \quad \alpha = 0.25\,\beta^2\,(c_o/\omega)^2 - 1$$
$$k = 0.5^{0.5}\,(k_o)\,\alpha^{0.5}\,[-1 + \{1 + m^2/(\omega^2\alpha^2)\}^{0.5}]^{0.5} \quad \text{with} \quad \alpha = 0.25\,\beta^2\,(1/k_o)^2 - 1 \quad \text{and } k_o = \omega/c_o$$

$$\mu = (m\,\omega)/(2\,c_o^2)\;(1/k) \quad \text{(positive damping parameter; } e^{\mu x} < 0 \text{ with } x < 0) \qquad \text{(A28)}$$
$$\mu \text{ can also be expressed as: } \mu = 0.5^{0.5}\,(\omega/c_o)\,\alpha^{0.5}\,[1 + \{1 + m^2/(\omega^2\alpha^2)\}^{0.5}]^{0.5}$$

The actual propagation velocity or phase velocity c can be expressed as:

$$c = \frac{L}{T} = \frac{\omega}{k} = \frac{c_o}{(0.5\alpha)^{0.5}\,(-1 + a_2)^{0.5}} \qquad \text{(C11)}$$

with: $a_2 = [1 + m^2/(\omega^2\alpha^2)]^{0.5}$

This latter expression yields a wave propagation velocity larger than that of a frictionless wave ($c > c_o$) in practical cases, since $(0.5\alpha)^{0.5}\,(-1 + a_2)^{0.5} < 1$. Practical values: $a_2 \cong 2$ to 3.

Tidal amplification is dominant in deep estuaries with strong width reduction (strong convergence).
In short estuaries a near-standing wave pattern can be generated with a phase lead close to 3 hours (relatively large 'apparent' wave speed).

<u>Case C</u>: Damping is dominant

$$\beta \leq 2\,\omega/c_o \text{ or } L_b \geq (g\,h_o)^{0.5}T/(4\pi) \qquad \text{(C12)}$$

$$k = 0.5^{0.5}\,(\omega/c_o)\,\alpha^{0.5}\,[1 + \{1+ m^2/(\omega^2\alpha^2)\}^{0.5}]^{0.5} \quad \text{with } \alpha = 1 - 0.25\,\beta^2\,(c_o/\omega)^2$$
$$k = 0.5^{0.5}\,(k_o)\,\alpha^{0.5}\,[1 + \{1+ m^2/(\omega^2\alpha^2)\}^{0.5}]^{0.5} \quad \text{with } \alpha = 1 - 0.25\,\beta^2\,(1/k_o)^2 \text{ and } k_o = \omega/c_o$$

$$\mu = (m\,\omega)/(2\,c_o^{\,2})\;(1/k) \qquad \text{(positive damping parameter; } e^{\mu x} < 0 \text{ with } x < 0) \qquad \text{(C14)}$$
μ can also be expressed as: $\mu = 0.5^{0.5}\,(\omega/c_o)\,\alpha^{0.5}\,[-1 + \{1+ m^2/(\omega^2\alpha^2)\}^{0.5}]^{0.5}$

The actual propagation velocity c is:

$$c = \frac{L}{T} = \frac{\omega}{k} = \frac{c_o}{(0.5\alpha)^{0.5}\,(1 + a_2)^{0.5}} \qquad \text{(C13)}$$

with: $a_2 = (1+ m^2/(\omega^2\alpha^2))^{0.5}$

This latter expression yields a wave propagation velocity which is smaller than that of a frictionless wave ($c < c_o$) in practical cases, since $(0.5\alpha)^{0.5}\,(1 + a_2)^{0.5} > 1$. Practical values: $a_2 \cong$ 1 to 5.

Summarizing, the variation of the tidal range H along an estuary can be, as follows:

- tidal range is constant $H = H_o$ and $c = c_o$ (*ideal* estuary; Case A);
- tidal range increases $H > H_o$ and $c > c_o$ (*amplified* estuary; Case B);
- tidal range decreases $H < H_o$ and $c < c_o$ (*damped* estuary; Case C).

with: H = tidal range, H_o = tidal range at entrance (mouth), c = wave propagation velcvocity (wave speed) and $c_o = (gh_o)^{0.5}$.

D Analytical solution of net tide-averaged velocities

Tide-averaged net velocity due fresh water discharge

The fresh water velocity can be computed as:

$$u_r = Q_r/A \qquad \text{(D1)}$$

with: Q_r = river discharge and A = area of cross-section;

Tide-averaged Stokes drift.

Due to the tidal variation of the water level, the net discharge over the tidal cycle is not zero.

The velocity defined as $\bar{u}_{net} = q_{net}/T$ is known as the **Stokes** drift.

$$q_{stokes} = (1/T)\ {}_0\int^T q\ dt = (1/T)\ {}_0\int^T (\bar{u}\, h)\ dt \qquad \text{(D2)}$$

Using: $\bar{u} = \hat{\bar{u}}\cos(\omega t+\varphi)$ (symmetrical tide; φ= phase lead of horizontal tide with respect to vertical tide) and $h = h_o + \hat{\eta}\cos\omega t$, it follows that:

$$\begin{aligned}
q_{stokes} &= (1/T)\ {}_0\int^T \{\hat{\bar{u}}\cos(\omega t+\varphi)\}\{h_o + \hat{\eta}\cos\omega t\}\ dt \\
&= (\hat{\bar{u}}\, h_o/T)\ {}_0\int^T \cos(\omega t+\varphi)\ dt + (\hat{\bar{u}}\,\hat{\eta}/T)\ {}_0\int^T \cos\omega t\cos(\omega t+\varphi)\ dt \\
&= (\hat{\bar{u}}\, h_o/T)\ {}_0\int^T(\cos\omega t\cos\varphi - \sin\omega t\sin\varphi)dt + \\
&\qquad (\hat{\bar{u}}\,\hat{\eta}/T)\ {}_0\int^T\{(\cos\omega t)^2\cos\varphi - \sin\omega t\cos\omega t\sin\varphi\}dt \\
&= (\hat{\bar{u}}\, h_o/T)[\cos\varphi\int\cos\omega t\ dt - \sin\varphi\int\sin\omega t\ dt] + \\
&\qquad (\hat{\bar{u}}\,\hat{\eta}/T)[\cos\varphi\int(\cos\omega t)^2 dt - 0.5\sin\varphi\int\sin 2\omega t\ dt] \\
&= (\hat{\bar{u}}\,\hat{\eta}/T)\cos\varphi\ {}_0\int^T(\cos\omega t)^2\ dt
\end{aligned}$$

The integrals ${}_0\int^T \cos\omega t\ dt$, ${}_0\int^T \sin\omega t\ dt$ and ${}_0\int^T \sin 2\omega t\ dt$ are zero as the functions are periodic over time T.

Thus:

$$\begin{aligned}
q_{stokes} &= (\hat{\bar{u}}\,\hat{\eta}/T)\cos\varphi\ {}_0\int^T(\cos\omega t)^2\ dt = (\hat{\bar{u}}\,\hat{\eta}/T)\cos\varphi\,(0.5T) = 0.5\,\hat{\bar{u}}\,\hat{\eta}\cos\varphi \\
\bar{u}_{stokes} &= 0.5\,(\hat{\eta}/h_o)\,\hat{\bar{u}}\cos\varphi \\
\bar{u}_{stokes} &= 0.25\,(H/h_o)\,\hat{\bar{u}}\cos\varphi \qquad \text{(D3)}
\end{aligned}$$

The Stokes drift velocity is maximum for $\varphi = 0$ (no phase shift between horizontal and vertical tide) and zero for $\varphi = 90^o$ (standing wave system). Generally, $\varphi = 60^o$ to 85^o.

Since the Stokes drift leads to the accumulation of fluid within the estuary, the mean water level will gradually go up towards the landward end of the estuary resulting in a water level gradient by which a return flow is driven (vertical circulation) with seaward-directed velocities near the bottom and landward-directed velocities near the surface.

E Asymmetry of peak tidal velocities due to higher harmonics (M2 and M4 components)

The tide is distorted in an asymmetric nature due to the variable depth under the wave crest and the wave trough introducing a variable wave speed, which can be represented by second harmonics.

Quadratic friction ($\overline{\overline{u}}^2$) causes maximum amplitude attenuation and minimum wave propagation at both maximum flood and maximum ebb; attenuation is minimum at slack water. The result of this asymmetry effect is a third harmonic (e.g. M_6) and other smaller odd harmonics.

When two tidal constituents are present there is a modulation of the distortion and attenuation effects, resulting in new compound tidal constituents For example, when M_2 and N_2 are in phase, so that their respective high waters occur at the same time; the total depth under the crest of the combined wave will be greater than when they are out of phase 14 days later. Similarly, the total depth under the trough when M_2 and N_2 are in phase will be smaller than when they are out of phase. Thus, M_4-generation due to greater depth at the crest than at the trough will be modulated by the 28 day variation of the combined M_2+N_2 effects, leading to a 28 day modulation of M_4 and a new constituent NM_4.

When the tidal velocity consists of two major constituents ($\overline{\overline{u}} = \hat{\overline{u}}_1 \cos \omega_1 t + \hat{\overline{u}}_2 \cos \omega_2 t$), the terms involving a product of constituents generate constituents at the difference frequency and at the sum frequency, which is illustrated below:

$$\overline{\overline{u}}^2 = (\hat{\overline{u}}_1 \cos \omega_1 t + \hat{\overline{u}}_2 \cos \omega_2 t)^2 =$$

$$\overline{\overline{u}}^2 = (\hat{\overline{u}}_1 \cos \omega_1 t)^2 + (\hat{\overline{u}}_2 \cos \omega_1 t)^2 + 2\,\hat{\overline{u}}_1\,\hat{\overline{u}}_2 \cos \omega_1 t \cos \omega_2 t$$

$$\overline{\overline{u}}^2 = (\hat{\overline{u}}_1 \cos \omega_1 t)^2 + (\hat{\overline{u}}_2 \cos \omega_1 t)^2 + \hat{\overline{u}}_1\,\hat{\overline{u}}_2 [\cos((\omega_1-\omega_2)t) + \cos((\omega_1+\omega_2)t)] \qquad \text{(E1)}$$

Maximum flood and ebb currents will be greatest when M_2 and N_2 currents are in phase. Because of quadratic friction, the loss when M_2 and N_2 are in phase will be greater than the sum of the individual losses of M_2 and N_2; the combined wave will travel slower and be damped more. The opposite will be true 14 days later. In real estuaries the phase difference between the vertical and horizontal tide will also have a pronounced effect on this.

In shallow friction-dominated estuaries generally, a saw-tooth type of tidal wave (sometimes a tidal bore) is generated, which cannot be represented by higher harmonics. Furthermore, the effect of a mean river flow may be important. A mean river flow makes the ebb current velocities larger and the flood current velocities smaller. Due to quadratic friction, the increased loss during the ebb phase is greater than the decreased loss during the flood phase. The result is a greater loss than if the mean flow is absent and thus greater damping of the tidal wave and a reduced tidal range. Friction effects being greater during ebb than during flood (asymmetry effects) also lead to the generation of M_4-harmonics; low waters are delayed and high waters are made earlier. When the river flow is greater than the tidal flow, the flow becomes uni-directional. When the river discharge increases, the mean sea level also increases due to frictional momentum loss from the mean flow. This increase in water depth increases the wave speed, via the non-linear continuity term.

The effect of storm surges (larger water depths) on the tide can also be explained in terms of changes in wave speed and frictional damping. The lower the frequency of the surge, the smaller the current velocities associated with the surge and the less important are the terms $\overline{\overline{u}}\,\partial\overline{\overline{u}}/\partial x$ and $\overline{\overline{u}}^2$. At the surge crest the total depth will be significantly larger and the tidal wave speed will increase. This will increase the tidal wave length and reduce the tidal velocities and therefore reduce frictional attenuation.

Linear tides are solutions of the first-order tidal equations (single progressive wave). Tidal waves are distorted in shallow water due to various non-linear terms ($\overline{\overline{u}}\,\partial\overline{\overline{u}}/\partial x$; $\overline{\overline{u}}\,\partial\eta/\partial x$) in the mass and momentum balance equations. Taking these effects into account, the tidal asymmetry can be determined (flood and ebb flows are different in strength and duration). This can be done by perturbation analysis using power series solutions. For example, the water level can be expressed as: $\eta = \hat{\eta}\cos(\omega t+kx) + \alpha\hat{\eta}^2\cos\{2(\omega t+kx)\}$, which is substituted in the solution to determine the coefficients. Phase differences between the first order and second order harmonics generally are neglected. The friction term generally is linearized.

If the flood duration (T_f) is shorter than the ebb duration (T_e), the peak flood velocity will be larger than the peak ebb velocity assuming that the total tidal inflow volume is, on average, equal to the total tidal outflow volume.

The area under half a sine-wave is equal to: $2\,(0.5T)\,\hat{u}/\pi$

The area under the flood part of the wave is: $2\,T_f\,\hat{u}_f/\pi$

The area under the ebb part of the wave is: $2\,T_e\,\hat{u}_e/\pi$

Thus: $2T_f\,\hat{u}_f/\pi = 2T_e\,\hat{u}_e/\pi$ and $T_f + T_e = T$ resulting in $\hat{u}_f/\hat{u}_e = T_e/T_f = (T-T_f)/T_f$

The peak discharges are: $\hat{Q}_f = b\,\hat{u}_f(h_o+\hat{\eta})$ and $\hat{Q}_e = b\,\hat{u}_e(h_o-\hat{\eta})$

$$\hat{Q}_f/\hat{Q}_e = [(T-T_f)/T_f][(h_o+\hat{\eta})/(h_o-\hat{\eta})] = [(T-T_f)/T_f][(1+\hat{\eta}/h_o)/(1-\hat{\eta}/h_o)]$$

$\hat{Q}_f/\hat{Q}_e$ = 1.3 to 1.7 for $\hat{\eta}/h_o$ in the range of 0.1 to 0.2

The offshore astronomical tide is composed of various constituents. The most important constituent is the semi-diurnal **M_2-component**. The first harmonic (overtide) of this constituent is the **M_4-component** causing tidal asymmetry.
Generally, the M_4-component is small offshore, but rapidly increases within estuaries due to bottom friction and channel geometry (see **Speer and Aubrey, 1985**). The M_2-component and its first harmonic M_4 dominate the non-linear processes within estuaries. Non-linear interaction between other constituents is also possible in shallow estuaries.
Analysis of field observations has shown that interaction of M_2 and its first harmonic M_4 explains the most important features of tidal asymmetries. The type of tidal distortion (flood or ebb dominance) depends on the relative phasing of M_4 to M_2.

The tidal velocity due to these M_2 and M_4 components can be described as:

$$\overline{u} = \overline{u}_2 + \overline{u}_4 \quad \text{with} \quad \overline{u}_2 = \hat{u}_2\cos(\omega t-\varphi_2) \quad \text{and} \quad \overline{u}_4 = \hat{u}_4\cos(2\omega t-\varphi_4)$$

Defining: $\omega t' = \omega t-\varphi_2$, it follows that $\omega t = \omega t'+\varphi_2$ and $2\omega t = 2\omega t'+2\varphi_2$ and thus:

$$\overline{u} = \hat{u}_2\cos(\omega t'-\varphi_2) + \hat{u}_4\cos(2\omega t'-\varphi_4) = \hat{u}_2\cos(\omega t') + \hat{u}_4\cos(2\omega t'-\phi) \qquad \text{(E2)}$$

A_u = tidal velocity asymmetry = $\hat{u}_4/\hat{u}_2$ and ϕ = relative M_2 - M_4 phase = $2\varphi_2-\varphi_4$

An undistorted tide has $A_u = 0$.
A distorted but symmetric tide has $\phi = \pm\ 90^o$ and $A_\eta > 0$
If M_4 has a velocity phase of -90^o to $+90^o$ relative to M_2 with $A_\eta>0$, then the distorted composite tide has $\hat{u}_{flood} > \hat{u}_{ebb}$ and is defined as flood dominant ($T_{flood}<T_{ebb}$).

If M_4 has a velocity phase of 90° to 270° relative to M_2 with A_η>0, then the distorted composite tide has $\hat{u}_{ebb} > \hat{u}_{flood}$ and is defined as ebb dominant ($T_{ebb} < T_{flood}$).
Figures E1 and **E2** show the tidal velocity for $\hat{u}_2$= 1 m/s, $\hat{u}_4$= 0.3 m/s and ϕ= 0°, 30°, 60° and 90° and for 270°, 300°, 330° and 360° (see also **Table E1**).

Flood dominance occurs for ϕ= 0° to 90° (and for 270° to 360°) with $\hat{u}_{flood} > \hat{u}_{ebb}$ and $T_{flood} > T_{ebb}$.
Thus: $\hat{u}_{flood}/\hat{u}_{ebb} > 1$ and $T_{flood}/T < 0.5$ for these conditions.

Flood dominance is characterized by a relatively short flood duration with a higher peak flood velocity.

Table E1 *Peak tidal velocities for M_2 tide superimposed by M_4 tide*

Phase difference	$\hat{u}_{\mathbf{flood}}$ (m/s)	$\hat{u}_{\mathbf{ebb}}$ (m/s)	$\hat{u}_{\mathbf{flood}}$ (m/s)	$\hat{u}_{\mathbf{ebb}}$ (m/s)
	$\hat{u}_4/\hat{u}_2$=0.2		$\hat{u}_4/\hat{u}_2$= 0.3	
0°	1.2	0.8	1.3	0.7
90°	1.07	1.07	1.14	1.14
180°	0.8	1.2	0.7	1.3
270°	1.07	1.07	1.14	1.14
360°	1.2	0.8	1.3	0.7

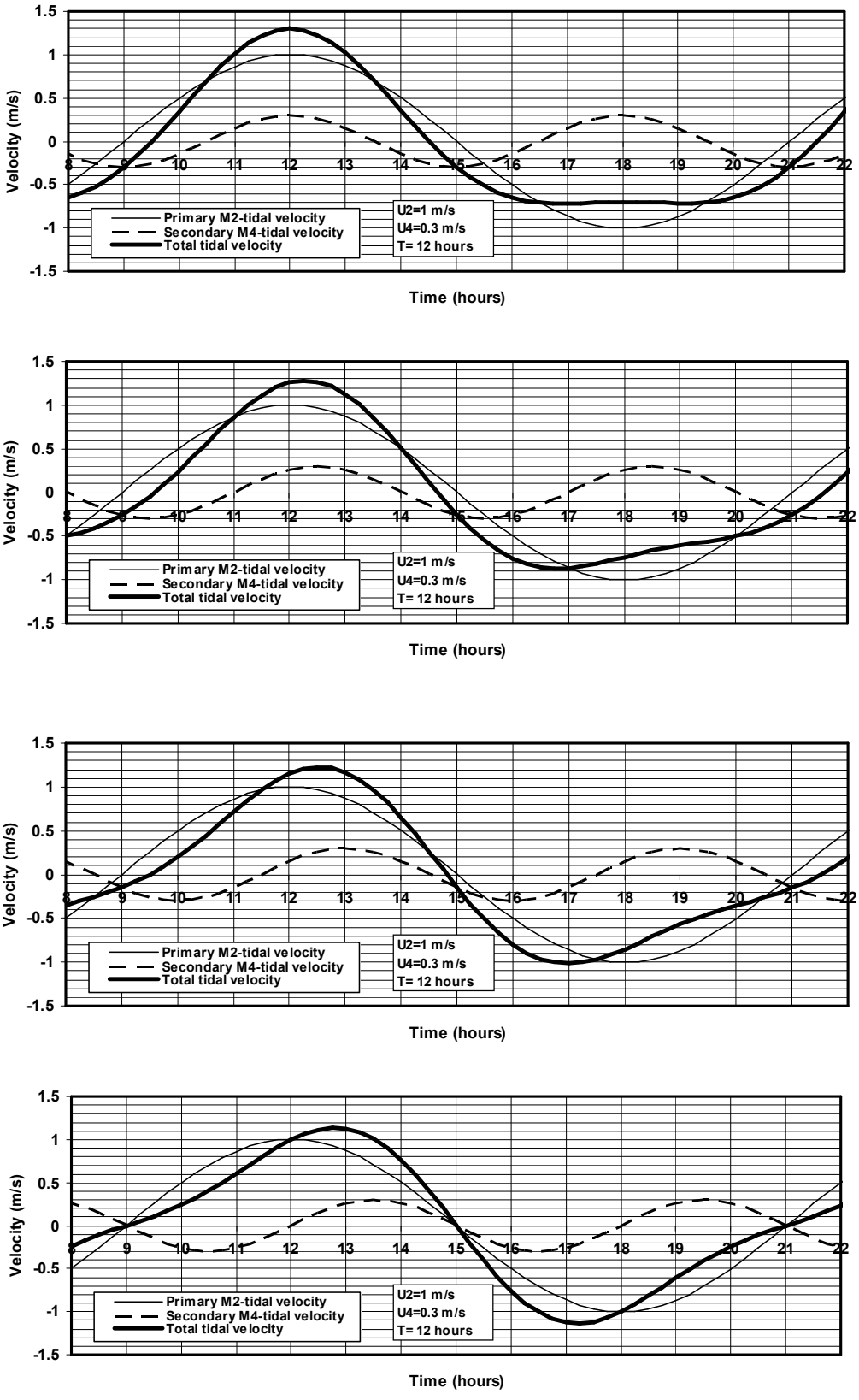

Figure E1 *Tidal velocity of M_2 and M_4-components as function of time for semi-diurnal tide; ϕ= 0° (top), 30°, 60° and 90° (bottom); flood dominance*

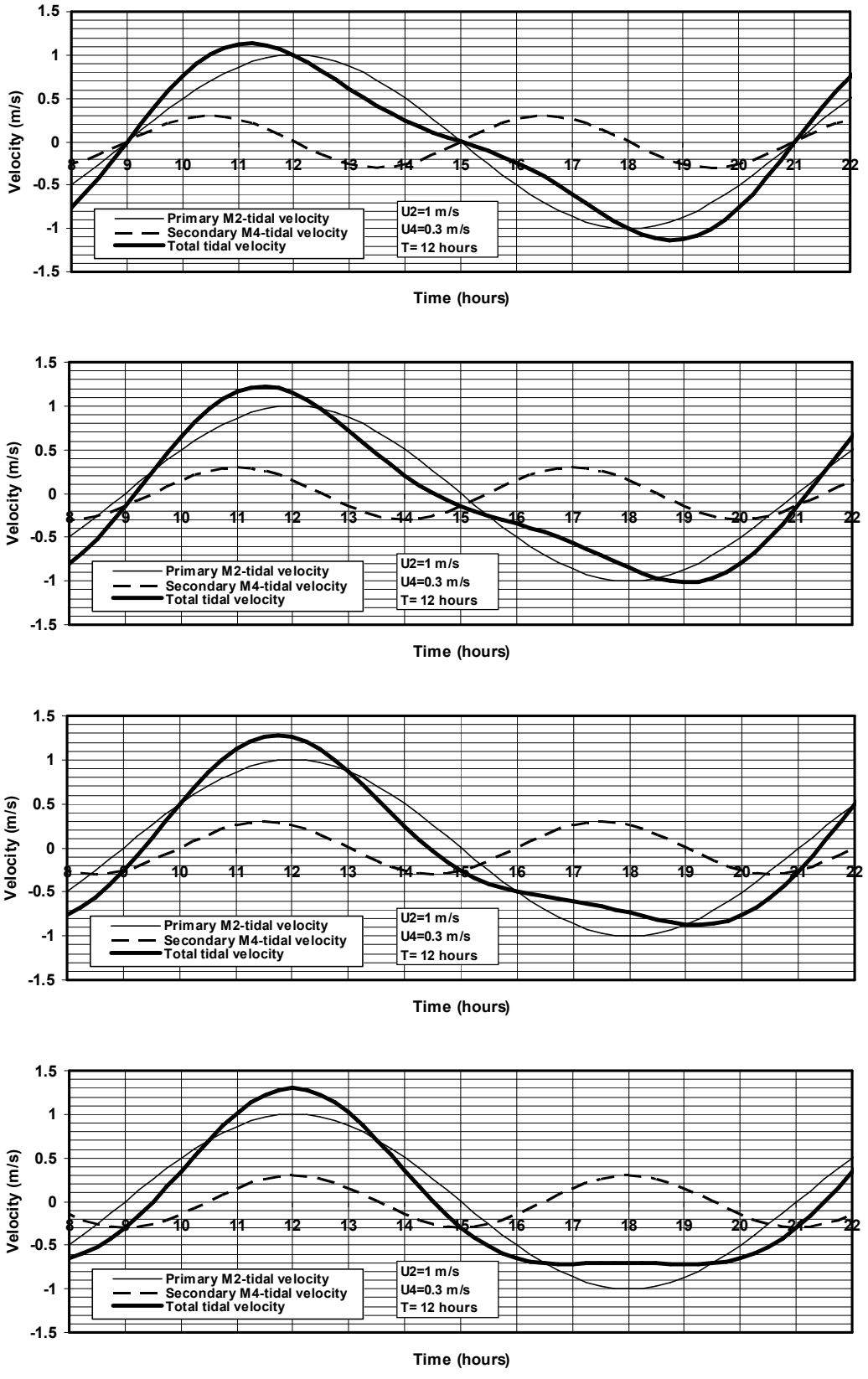

Figure E2 *Tidal velocity of M_2 and M_4-components as function of time for semi-diurnal tide; ϕ= 270^o (top), 300^o, 330^o and 360^o (bottom); flood dominance*

Figures E3 and **E4** show the ratio ratio $\hat{u}_{flood}/\hat{u}_{ebb}$ and the ratio T_{flood}/T as function of the phase difference ϕ based on Equation (A25) with velocity amplitudes $\hat{u}_2$= 1 m/s and $\hat{u}_4$= 0.2 and 0.3 m/s. The tidal period is T= 12 hours.
The peak flood velocity is larger than the peak ebb velocity for $\phi<90^o$ and $\phi>270^o$ (flood dominance).
The peak flood velocity is smaller than the peak ebb velocity for $90 \leq \phi \leq 270^o$ (ebb dominance).
The largest ratio $\hat{u}_{flood}/\hat{u}_{ebb}$ is about 1.8 for ϕ= 0^o and 360^o and $\hat{u}_4/\hat{u}_2$= 0.3 (flood dominance).
The smallest ratio $\hat{u}_{flood}/\hat{u}_{ebb}$ is about 0.55 for ϕ=180^o and $\hat{u}_4/\hat{u}_2$= 0.3 9 (ebb dominance).
The smallest ratio T_{flood}/T is about 0.42 for ϕ= 0^o and 360^o and $\hat{u}_4/\hat{u}_2$= 0.3 (flood dominance).
The largest ratio T_{flood}/T is about 0.58 for ϕ= 180^o and $\hat{u}_4/\hat{u}_2$= 0.3 (ebb dominance).

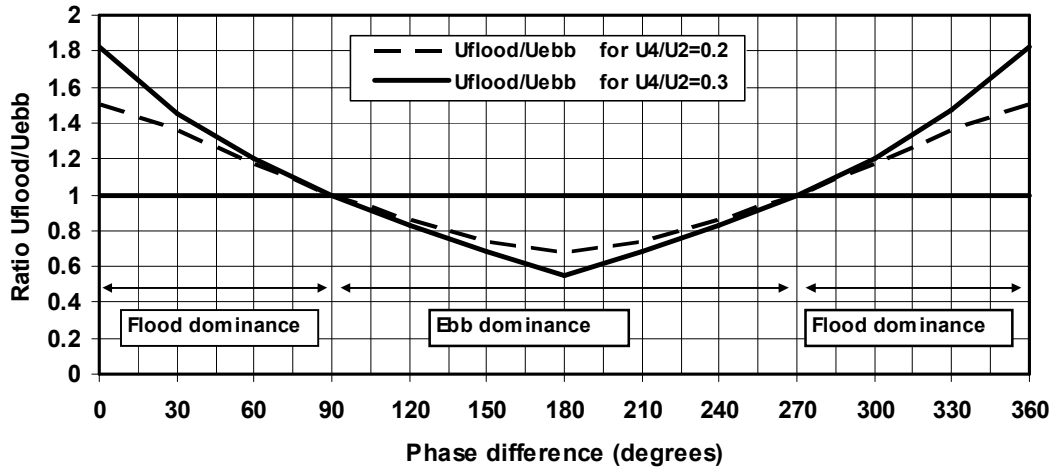

Figure E3 *Ratio $\hat{u}_{flood}/\hat{u}_{ebb}$ as function of the phase difference ϕ*

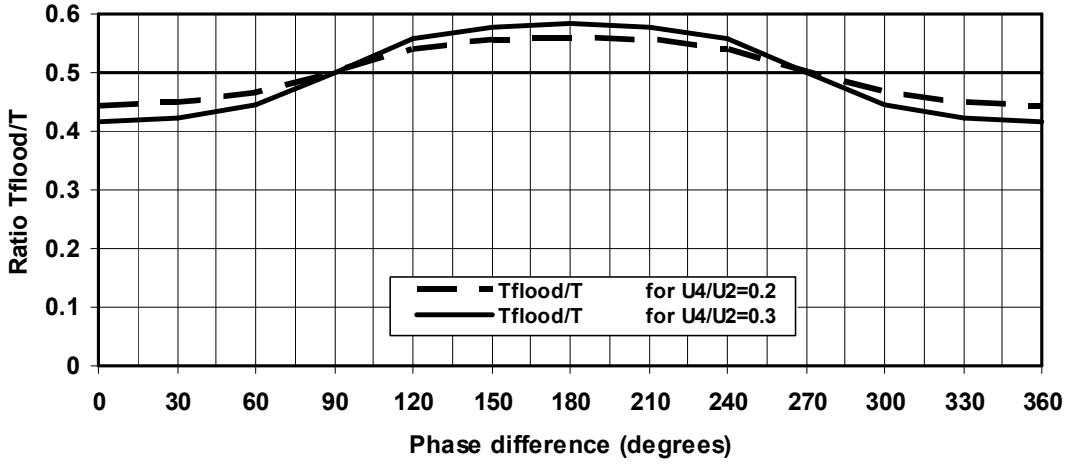

Figure E4 *Ratio T_{flood}/T as function of the phase difference ϕ.*

In practice, the flood duration (T_{flood}) in th entrance section of an estuary often is in the range of 0.4 to 0.5T and thus the velocity ratio $\hat{u}_{flood}/\hat{u}_{ebb}$ is in the range of 1 to 1.8 (see **Figures E3 and E4**).
Using: $\hat{u}_{flood}/\hat{u}_{ebb} = (T-T_{flood})/T_{flood} = T/T_{flood}-1$, it follows that $\hat{u}_{flood}/\hat{u}_{ebb} = 1.5$ for $T_{flood}/T = 0.4$.
Based on both methods, the velocity ratio $\hat{u}_{flood}/\hat{u}_{ebb}$ is in the range of 1 to 1.8.

Defining $\hat{u}_{flood} + \hat{u}_{ebb} = 2\hat{u}_{linear} = 2\hat{u}$ and $\hat{u}_{flood}/\hat{u}_{ebb} = r$ with $\hat{u}$ = peak tidal velcoity based on linearized analytical model, it follows that:

$$\begin{aligned} \hat{u}_{flood} &= [2r/(r+1)]\ \hat{u} \\ \hat{u}_{ebb} &= [2/(r+1)]\ \hat{u} \\ \hat{u}_{flood} - \hat{u}_{ebb} &= [2(r-1)/(r+1)]\ \hat{u} \end{aligned} \qquad \text{(E3)}$$

Using: $\hat{u}_{flood}/\hat{u}_{ebb} = r = 0.7$ to 1.3, it follows that $||\hat{u}_{flood} - \hat{u}_{ebb}| \cong 0.3\hat{u}$

The asymmetry related velocity difference can be in landward or in seaward direction depending on geometrical conditions (channel configuration). Some channels may be flood-dominated, while others are ebb-dominated.

F Analytical solutions of salt intrusion length

F.1 Analytical solutions of salt intrusion length

Introduction

Salt intrusion in tidal estuaries often causes management problems as both the surface water and the groundwater are (partly) saline or brackish over substantial lengths along the estuary obstructing its use for drinking water and agricultural purposes (irrigation). These problems are enhanced when channel depths are increased by dredging to accommodate large vessels to nearby ports. To be able to quantify these effects on salt intrusion, it is necessary to know the basic relationships between salt intrusion and the hydraulic and geometric parameters involved.

The most important parameters influencing the maximum salt intrusion length at the end of the flood flow period in a tidal channel are the tidal characteristics (water level amplitude and peak tidal velocity at the mouth), the river parameters (discharge and cross-section averaged velocity) and the geometrical parameters (depth, width at mouth and width convergence length scale). The tidal parameters vary slightly on the neap-spring time scale of 14 days. The river discharge varies on the seasonal time scale (months) at most locations. The geometrical parameters generally do not vary much in time. Given these relatively large time scales involved, the salt intrusion process generally is in quasi-equilibrium on the tide-averaged time scale of 12 hours. Hence, it is often allowed to use a tide-averaged approach to determine the salt intrusion length, as has been done by many authors (**Ippen and Harleman, 1961; Ippen, 1966; Prandle, 1981, 1985, 2004, 2009; Savenije, 1986, 1989, 2005**). **Ippen and Harleman (1961)** introduced an elegant solution of the time-dependent salt continuity equation in a prismatic channel with partially–mixed flow by splitting this equation in a time-dependent part and a steady-state part. Their steady-state solution described the salinity distribution at low tide (LW). The salinity distribution at high tide (HW) was obtained from the time-dependent solution. Their approach involved two calibration parameters: the dispersion coefficient D_o at the mouth and the distance x_b seaward of the mouth where the salinity is equal to the maximum salinity at sea (S_o). Using laboratory flume data, the x_b-value was found to be about 100 to 150 times the water depth at the mouth. They also showed that the migration distance of the saline front over the flood tide is approximately equal to the tidal excursion length (horizontal shifting of the salinity distribution).

Herein, the attention is focused on the maximum salt intrusion length occurring at High Water Slack (HWS) which is most relevant for management purposes. While tidal propagation in estuaries can be reasonably well described by linearized one-dimensional equations, the physical and mathematical representation of saline intrusion tends to be much more complex.

Adopting a tide-averaged approach, the one-dimensional salt continuity equation can be expressed as a balance between the seaward-directed advective salt transport and the landward-directed dispersive or mixing-type transport. On a tide-averaged time scale the advective transport is caused by the fresh water discharge-related velocity (from the river), whereas the horizontal dispersive-type transport is caused by tide-driven, density-driven and circulation-driven processes. The effective dispersion coefficient reduces with the salinity gradient until it becomes zero near the toe of the salt front. Beyond the toe the dispersion is dominated by small-scale turbulent mixing. Information on the relative importance of the various tide-averaged dispersion processes can be obtained by decomposing the velocity and salt concentration profiles taking residual flows over the depth and width into account.

Using this approach, **Fischer (1972)** and **Fischer et al. (1979)** show that four dispersive terms can be distinguished: dispersive transport due to residual flow over the depth and over the width and shear flow effects (velocity gradient effects) over the depth and over the width. Scale analysis shows that the residual flows over the width yield by far the largest contribution. A major problem in the one-dimensional approach is that all dispersive processes must be represented by a single longitudinal dispersion coefficient *D*, which is hardly feasible (**Prandle, 1981**). Recent developments in estuarine dispersive-type fluxes have been reviewed by **Jay et al. (1997)**, concluding that there is a great lack of knowledge of dispersive processes in real estuaries and stressing that there is a need for additional research using controlled field experiments in combination with mathematical models.

So far, most studies have addressed the salt intrusion problem in prismatic channels. Salt intrusion in a tideless prismatic channel leads to an arrested salt wedge. This phenomenon has been studied extensively (**Schijf and Schönfeld, 1948; Keulegan, 1966** and others). Salt intrusion in partially or well-mixed prismatic channels with tidal action has been studied experimentally and theoretically. Experimental research in long laboratory flumes has been done at Waterways Experimental Station in Vicksburg, USA (**Ippen, 1966)** and at Delft Hydraulics in Delft, The Netherlands (**Rigter, 1973; Van Os, 1993**). Field data sets of salt intrusion have been collected at many sites, see summaries of **Prandle (1985, 2004 and 2009)** and **Savenije (1992, 1993a and 2005)**. Based on the laboratory data of Delft Hydraulics and field data of the Rotterdam Waterway, The Netherlands and the Chao Phya, Thailand, a relatively simple expression for the minimum salt intrusion length for prismatic channels has been proposed (**Van Os, 1993**). This expression has been verified by **Prandle (1985)** by determining the tide-averaged length scale of a salt wedge based on the momentum equation. This latter approach represents the mean salt intrusion length rather than the minimum length. According to **Prandle (2004, 2009)** these expressions for the salt intrusion length in prismatic channels can also be used for convergent channels when the parameters involved (water depth, peak tidal velocity and fresh water velocity) are applied in the centre of the salt intrusion length. This requires, however, iterative computations, as the salt intrusion length is not known a priori.

Analytical salinity distributions for a prismatic tidal channel have been given by various authors (**Ippen and Harleman, 1961; Ippen, 1966; Chatwin, 1976; Prandle, 1985, 2004, 2009 and Savenije, 1992, 2005**). These analytical expressions always involve calibration coefficients related to the dispersive processes (dispersion coefficient in the mouth D_o and other coefficients; Van der Burgh-coefficient *K,* 1972).
Savenije proposed predictive expressions for the dispersion coefficient in the mouth (D_o) and the Van der Burgh-coefficient *K* (the latter supposed to vary between 0 and 1).

Basic considerations

Averaging the salt transport terms over the cross-section and over time yields the balance equation for advective seaward salt transport and dispersive landward salt transport in stationary conditions as follows (river discharge should be constant for some time, say 10 days):

$$\left|\overline{\overline{u}}_r\right|\left\langle \overline{\overline{S}} \right\rangle + D\left\langle \partial\overline{\overline{S}} / \partial x \right\rangle = 0 \quad \text{or}$$

$$\left|Q_r\right|\left\langle \overline{\overline{S}} \right\rangle + AD\left\langle \partial\overline{\overline{S}} / \partial x \right\rangle = 0 \qquad \text{(F1)}$$

with $\left|\overline{\overline{u}}_r\right|$ the cross-section averaged velocity based on river discharge (= $|Q_r|/A$), $\overline{\overline{S}}$ the cross-section averaged salt concentration, D the dispersion coefficient, Q_r the river discharge (fresh water), $A = b\,h$ the area of cross-section, b the average width of cross-section, $h = h_o$ the average water depth to mean water level (assumed to be constant), <...> the time-averaged value (averaged over the tidal period T). The boundary condition is $< \overline{\overline{S}} > = S_o$ at the mouth.

Figure F1 shows various types of time-averaged and cross-section averaged salt concentration distributions in a tidal estuary. The lower, exponential distribution (— —) is a concave distribution (rounded inward) and mainly occurs in prismatic estuaries. The upper distribution (— . —) is a convex-type of distribution (rounded outward) and occurs in large estuaries with a small river at the landward side (Scheldt estuary, The Netherlands; Thames estuary, England).

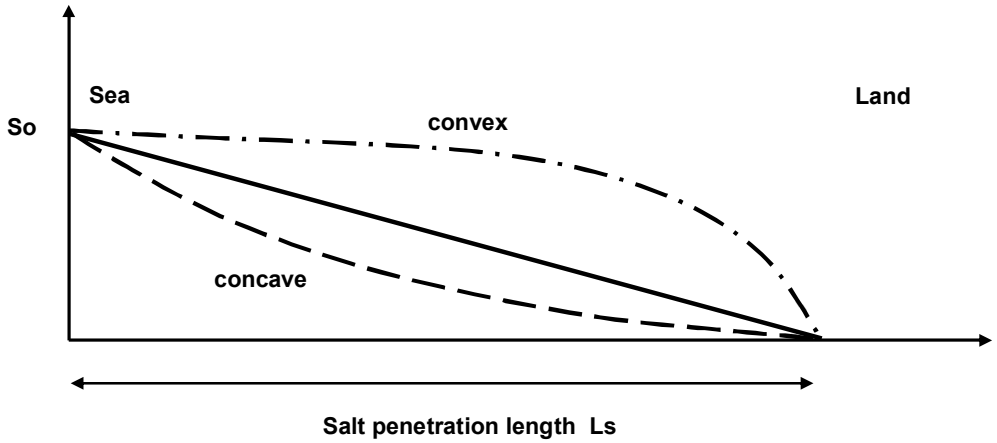

Figure F1 *Various types of tide-averaged salt concentration distributions in a tidal estuary*

In the following the attention is focused on the salinity distribution at high water slack HWS (most landward salinity profile), which is of major importance for management purposes. Similar to the tide-averaged salinity, it can be described by (**Savenije, 1989b**):

$$\left|Q_r\right| \overline{\overline{S}}_x^{HWS} = - A_x\, D_x^{HWS} \frac{d\overline{\overline{S}}_x^{HWS}}{dx} \qquad \text{(F2)}$$

with Q_r the river discharge [m^3/s], S^{HWS} the salinity at high water slack, A the cross-sectional area [m^2], D^{HWS} the dispersion coefficient at high water slack [m^2/s] and x and Q_r as defined before. It is assumed that the salinity of the river water can be neglected.

The salinity in an estuary channel can only be represented by the cross-section-averaged salinity if the lateral mixing proceeds relatively fast within the tidal cycle, which means that the channel width should be small compared with the tidal excursion length and width variations should be gradual.

A tidal channel is herein assumed to be converging if the convergence length scale ($A = A_o e^{-x/L_a}$) of the cross-section is smaller than 10 times the tidal excursion length (L_e): $L_a < 10\ L_e$.

The convergence length scale for the cross-sectional area is approximately equal to the convergence length scale for the width (L_b), as the depth in the entrance of most estuaries is approximately constant.
A converging or funnel-shaped estuary (Delaware Estuary, USA; Western Scheldt Estuary, The Netherlands) has a relatively small salinity gradient near the mouth due to strong tidal mixing. More landward the density-driven processes become important through residual circulation effects resulting in larger salinity gradients.

Savenije (2005) has derived an expression for the longitudinal dispersion coefficient at HWS ($D_{HWS,o}$) based on measured salinity distributions in 13 estuaries focussing on data at HWS, when the salinity intrusion is largest ($L_{s,max}$). The $D_{HWS,o}$ was fitted to the data for each individual case. All $D_{HWS,o}$-values can be represented by the following relationship:

$$D_{HWS,o} = 1400\, \hat{\bar{u}}_o\, h_o\, (L_{e,o}/L_a)\, (N_R)^{0.5} \qquad \text{(F3)}$$

or

$$D_{HWS,o} = 2500\, (L_{e,o}/L_a)\, (v_\Delta/\hat{\bar{u}}_o)\, (\bar{\bar{u}}_{r,o}/\hat{\bar{u}}_o)^{0.5}\, \hat{\bar{u}}_o\, h_o \qquad \text{(F4)}$$

with:

$L_{e,o}$ = tidal excursion length scale at mouth= $(T/\pi)\, \hat{\bar{u}}_o$;
L_a = convergence length scale based on $A = A_o\, e^{-x/L_a}$;
A = area of cross-section;
N_R = $(\Delta\rho_o/\rho_o)\, (g h_o)/(\hat{\bar{u}}_o)^2\, (Q_r T/V_{fl}) = \pi\, (v_\Delta/\hat{\bar{u}}_o)^2\, (\bar{\bar{u}}_{r,o}/\hat{\bar{u}}_o)$= Estuarine Richardson number,
v_Δ = $[(\Delta\rho_o/\rho_o)\, g\, h_o]^{0.5}$= density-related wave speed = velocity of saline front,
$\Delta\rho_o$ = salinity-related density difference between sea water (x = 0) and river water at end of estuary,
ρ_o = fluid density at mouth (x = 0),
Q_r = $\bar{\bar{u}}_{r,o}\, b_o\, h_o$ = fresh water discharge,
V_{fl} = $\hat{Q}\, T/\pi = (\hat{\bar{u}}_o\, b_o\, h_o) T/\pi$ = tidal flood volume,
T = tidal period,
$\hat{\bar{u}}_o$ = peak tidal velocity,
b_o = width of mouth,
h_o = depth of mouth,
L_o = $c_o\, T = (g h_o)^{0.5}\, T$ = tidal wave length related to mouth.

Equation (B3) is only valid for converging estuaries, because L_a goes to infinity for prismatic type of channels resulting in D_o approaching zero.

Kuijper (2011) has re-analyzed the data of Savenije (tide-averaged salinity distributions at HWS). Based on his results, the HWS-dispersion coefficient at the mouth for converging channels can be approximated by (see also **Kuijper and Van Rijn, 2011**):

$$D_{HWS,o} = \alpha_D \pi^{0.5} \ (C/g^{0.5}) \ (v_{\Delta,o}/\hat{\bar{u}}_o) \ (\bar{\bar{u}}_{r,o}/\hat{\bar{u}}_o)^{0.5} \ (\hat{\bar{u}}_o h_o) \quad \text{for } L_a/L_{e,o} < 10 \qquad \text{(F5)}$$

with: $\alpha_D = 60\alpha_c L_{e,o}/L_a$= coefficient (variation range of about ±50%, see **Figure F2**),
α_c= additional calibration coefficient (range of 0.5 to 1.5; default= 1),
C = Chézy-coefficient,
$v_{\Delta,o} = [(\Delta\rho_o/\rho_o)\ (gh_o)]^{0.5}$= density-related wave speed at mouth,
$\Delta\rho_o/\rho_o = \alpha_S < \bar{\bar{S}}_{HWS,x} > /\rho_o$.

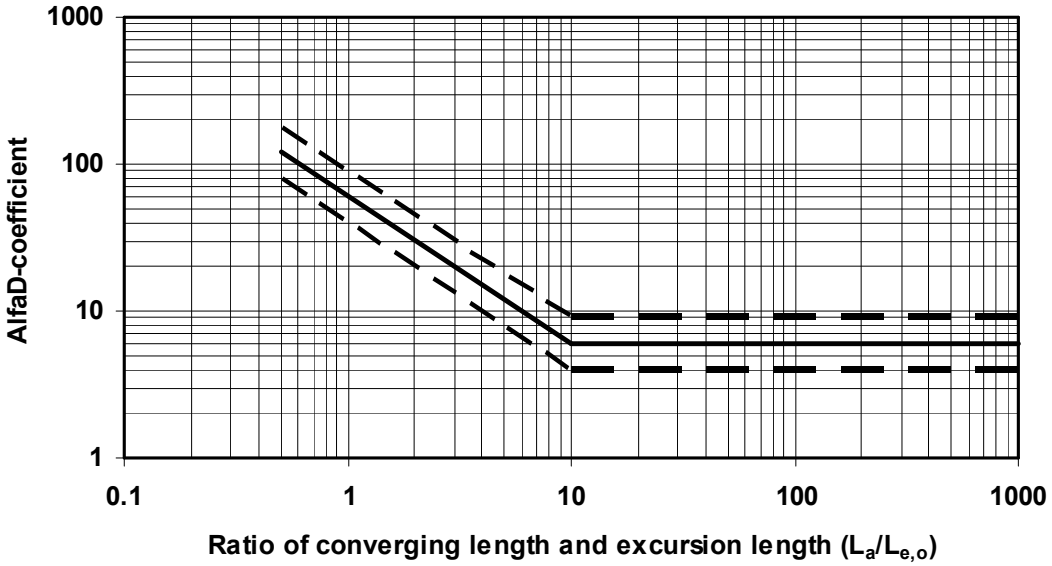

Figure F2 *α_D-coefficient as function of $L_a/L_{e,o}$*

The range $L_a/L_{e,o} < 10$ represents strongly converging estuaries, while the range $L_a/L_{e,o} \geq 10$ represents very weakly converging and prismatic type estuaries.

The best results are obtained if converging channels are schematized into two converging sections and a weighted L_a-value, as follows: $L_a = [L_{a1}\ L_1 + L_{a2}\ (L_{s,max} - L_1)]/L_{s,max}$, with: L_{a1}= converging length scale of mouth section, L_{a2}= converging length scale of saline channel section, $L_{s,max}$ = salt penetration length, L_1= length of mouth section.
This approach requires iterative computations as $L_{s,max}$ is not a priori known (**Kuijper, 2011**).
If only one convergence length scale ($L_{a,1}$) is used to represent the width convergence, then Equation (B5) may overpredict somewhat. This can be corrected by taking $\alpha_c < 1$.

The α_D-coefficient (with $\alpha_c = 1$) is shown in **Figure F2.** The α_c-coefficient can be used to express the variation range; α_c= 1.5 yields a high value of the dispersion coefficient and α_c= 0.7 yields a low value.

Using appropriate values, the $D_{HWS,o}$-parameter is in the range of 10 to 1000 ($\hat{\bar{u}}_o h_o$).

Kuijper and Van Rijn (2011) assume that the D-parameter is valid at all points along the channel, as follows:

$$D_{HWS,o} = \alpha_D \pi^{0.5} (C/g^{0.5}) (\Delta\rho_x/\rho_o)^{0.5} (c_x/\hat{u}_x) (\overline{\overline{u}}_{r,x}/\hat{u}_x) (\hat{u}_x h_x) \quad \text{for } L_a/L_{e,o} < 10 \quad \text{(F6)}$$

$$A_x = A_o \exp(-x/L_a) \quad \text{(F7)}$$

$$b_x = b_o \exp(-x/L_b)$$
$$h_x = h_o \exp(-\gamma x)$$
$$L_e = L_{e,o} \exp(-\alpha_U x) \text{ as the excursion length } L_{e,x} \approx \hat{u}_x$$
$$\Delta\rho_x/\rho_o = \alpha_S < \overline{\overline{s}}_{HWS,x} > /\rho_o$$

with:

γ = $(1/L_b) - (1/L_a)$,
α_U = $0.5\beta - \mu$= tidal damping or amplification coefficient,
x = horizontal coordinate (positive in landward direction),
α_S = coefficient (constant= 0.78) along channel,
$< \overline{\overline{s}}_{HWS,x} >$ = time-averaged and cross-section averaged salinity (in promille) at x,
C = Chézy-coefficient (constant).

Similar to the method for prismatic channels, the salinity distribution for convergent channels is found to be (**Kuijper, 2011**):

$$< \overline{\overline{s}}_{HWS,x} > / \overline{\overline{s}}_o = [1 - \{(0.5 \zeta L_a Q_r)/(A_o D_{HWS,o})\} \{-1 + \exp(x/(\zeta L_a))\}]^2 \quad \text{for } L_a/L_{e,x} < 10 \quad \text{(F8)}$$

with:

$\zeta = 1/(1 - \Psi L_a)$,
$\Psi = 0.5 \alpha_U + 1.5 \gamma + 0.5/L_a$,
$\gamma = 1/L_b - 1/L_a$,
$\alpha_U = 0.5\beta - \mu$,
$\beta = 1/L_b$,
$Q_r/A_o = \overline{\overline{u}}_{r,o}$
x = horizontal coordinate, positive in landward direction.

Two cases can be distinguished: $\alpha_U = 0$ (ideal estuary with constant peak tidal velocity) and $\alpha_U \neq 0$.

Case I: $\alpha_U = 0$, then: $\Psi = 1.5 \gamma + 0.5/L_a$, and $\zeta = 2/(4 - 3L_a/L_b)$,

Ia: $L_a = L_b$ and thus h= constant, $\gamma = 0$, $\Psi = 0.5/L_a$ resulting in: $\zeta = 2$,

Ib: $L_a/L_b = 4/3$ and thus: $\zeta = \infty$ resulting in: $< \overline{\overline{s}}_{HWS,x} > / \overline{\overline{s}}_o = (1 - x/L_s)^2$
with $L_s = 2D_{HWS,o}/\overline{\overline{u}}_{r,o}$
which is similar to the salt penetration length for prismatic channels,

Case II: $\alpha_U \neq 0$, then: $\alpha_U = 0.5\beta - \mu = 0.5/L_b - \mu$,

IIa: $L_a = L_b$ and thus h= constant, $\gamma = 0$ resulting in: $\zeta = 4/(1+ 2\mu L_a)$,
μL_a is in the range of 0.5 to 3 and thus ζ in the range of 0.5 to 2,

IIb: $\mu L_a = 1.5$ then $\zeta = 1$ resulting in:
$< \overline{\overline{s}}_{HWS,x} > / \overline{\overline{s}}_o = [1 - \{0.5\, L_a\, \overline{\overline{u}}_{r,o}/D_{HWS,o}\}\{-1+\exp(x/L_a)\}]^2$

The **maximum** salt penetration length can be determined by assuming: $< \overline{\overline{s}}_{HWS,x} >= 0$ at $x = L_{s,max}$ resulting in (only for $L_a/L_{e,o}<10$):

$$L_{s,max} = \zeta\, L_a\, \ln[\{2D_{HWS,o}/(\overline{\overline{u}}_{r,o}\, \zeta\, L_a)\} + 1] \qquad \text{(F9)}$$

Assuming: $L_a \cong L_b$ and $\gamma = 0$ and μL_a in the range of 0.5 to 3 and ζ in the range of 0.5 to 2 (Case IIa):

a) $\zeta = 0.5$ $L_s \cong 0.5\, L_a\, \ln[\{4D_{HWS,o}/(\overline{\overline{u}}_{r,o}\, L_a)\} + 1]$
$D_{HWS,o}$= 500 m^2/s and $\overline{\overline{u}}_{r,o}$ = 0.01 m/s, L_a= 10000 m then: $L_{s,max} \cong$ 15000 m,
$D_{HWS,o}$= 100 m^2/s and $\overline{\overline{u}}_{r,o}$ = 0.1 m/s, L_a= 10000 m then: $L_{s,max} \cong$ 1500 m,

b) $\zeta = 2.0$ $L_{s,max} \cong 2\, L_a\, \ln[\{D_o/(\overline{\overline{u}}_{r,o}\, L_a)\} + 1]$
$D_{HWS,o}$= 500 m^2/s and $\overline{\overline{u}}_{r,o}$ = 0.01 m/s, L_a= 10000 m then: $L_{s,max} \cong$ 35000 m,
$D_{HWS,o}$= 100 m^2/s and $\overline{\overline{u}}_{r,o}$ = 0.1 m/s, L_a= 10000 m then: $L_{s,max} \cong$ 2000 m.

Focussing on the tide-averaged salinity distribution at LWS, yields:

$$< \overline{\overline{s}}_{LWS,x} > / \overline{\overline{s}}_o = [1 - \{(0.5\, \zeta\, L_a\, Q_r)/(A_o\, D_{LWS,o})\}\{-1 + \exp(x/(\zeta\, L_a))\}]^2 \qquad \text{for } L_a/L_{e,o} <10 \qquad \text{(F10)}$$

with: $\zeta = 1/(1- \phi L_a)$, $\phi = 1.5\gamma + 0.5\alpha_U + 0.5/L_a$, $\gamma = (1/L_b) - (1/L_a)$, $\alpha_U = 0.5\beta - \mu$, $\beta = 1/L_b$,

The **minimum** salt intrusion length **at LWS** can be found from $< \overline{\overline{s}}_{LWS,x} > / \overline{\overline{s}}_o = 0$, yielding:

$$L_{s,min} = \zeta\, L_a\, \ln[1+ 2D_{LWS,o}/(\overline{\overline{u}}_{r,o}\, \zeta\, L_a)] \qquad \text{(F11)}$$

The dispersion coefficient at the mouth (x= 0) **at LWS** can be described by (**Kuijper, 2011**):

$$D_{LWS,o} = \alpha_{D,LWS}\, (C^2/g)\, (v_{\Delta,o}/\hat{\overline{u}}_o)\, (\overline{\overline{u}}_{r,o}/\hat{\overline{u}}_o)^{0.5}\, (\hat{\overline{u}}_o\, h_o) \qquad \text{(F12)}$$

with:

$\alpha_{D,LWS} = 0.4\alpha_c$ for $L_a/L_{e,o} \geq 10$ (prismatic channels),

$\alpha_{D,LWS} = 4\alpha_c/(L_a/L_{e,o})$ for $L_a/L_{e,o} < 10$ (converging channels),

α_c = additional calibration coefficient (range of 0.5 to 1.5; default= 1).

F.2 Analytical solutions of net tide-averaged velocity due to salinity gradient

Due to gravitational circulation a residual flow is generated in a tidal channel with fresh water inflow. The residual flow is landward near the bottom and seaward near the water surface. The point where the tide-averaged flow velocity near the bottom is approximately zero is known as the **null point**.
Residual density-induced flow in a prismatic channel with tidal conditions can be determined by using the tide-averaged momentum equation (**Chatwin, 1976; Prandle, 1985, 2004**).
There are two main contributions: the free convection contribution arising from the density difference between salt water and fresh water and the fresh water discharge contribution.
Assuming well-mixed conditions and relatively small inertial terms (after averaging over the tidal cycle), the tide-averaged continuity and momentum equations for two-dimensional vertical flow in a prismatic channel with rectangular cross-section (width>>depth) can be easily formulated (see also **Chatwin, 1976** and **Prandle, 1985, 2004**):

Well-mixed conditions (ρ constant over depth)
Neglecting the convective acceleration term, the momentum equation reads as:

$$\rho\, \partial u/\partial t + \partial p/\partial x - \partial \tau/\partial z = 0 \qquad \text{(F13)}$$

with:
u= fluid velocity, h= h_o+ h'_o + η= water depth, h_o= water depth to MSL, h_o'= tide-averaged elevation of mean water surface, η= tidal water surface elevation, ρ= fluid density (constant over depth), $\tau = \rho\, \varepsilon\, \partial u/\partial z$, ε = vertical mixing coefficient, x= longitudinal coordinate (positive in seaward direction and negative in landward direction).
The pressure and pressure gradient are:

$$p = \rho\, g\, (h - z)$$
$$\partial p/\partial x = g(h-z)\, \partial \rho/\partial x + \rho g\, \partial h/\partial x$$

After tide-averaging (u and η are periodic functions; $\partial \langle u \rangle/\partial t \cong 0$ and $\partial \langle \eta \rangle/\partial t \cong 0$), it follows that:

$$g(h-z)\, \partial \langle \rho \rangle/\partial x + \langle \rho \rangle g\, \partial h'_o/\partial x - \langle \rho \rangle \langle \varepsilon \rangle \partial^2 \langle u \rangle/\partial z^2 = 0 \qquad \text{(F14)}$$

This can be simplified to

$$g(h_o-z)\, \partial \rho_{sa}/\partial x + \rho_o g\, \partial h'_o/\partial x - \rho_o\, E\, \partial^2 u_{sa}/\partial z^2 = 0 \qquad \text{(F15)}$$

with: ρ_{sa}= tide-averaged fluid density (constant over depth), h'_o= tide-averaged mean sea level elevation, E= tide-averaged mixing coefficient, u_{sa}= tide-averaged residual velocity due to density effects and river flow effects.
The tide-averaged net vertical fluid velocity <w> can be derived from the tide-averaged continuity equation, as follows: $\partial \langle u \rangle/\partial x + \partial \langle w \rangle/\partial z = 0$

The term $\partial \rho_{sa}/\partial x$ represents the density gradient due to decreasing salinity in the (negative) landward direction; and thus the term $\partial \rho_{sa}/\partial x$ is a positive term.
The term $\partial h'_o/\partial x$ represents the water surface slope gradient related to the freshwater river flow; the h'_o value increases in the negative landward direction and thus the term $\partial\, h'_o/\partial x$ is a negative term.

The terms $\partial\rho_{sa}/\partial x$ and $\partial\, h'_o/\partial x$ are constant in vertical direction.
Equation (F15) can be expressed as:

$$\partial^2 u_{sa}/\partial z^2 = [g(h_o - z)/(\rho_o E)]\, \partial\rho_{sa}/\partial x + (g/E)\, \partial h'_o/\partial x$$
$$\partial^2 u_{sa}/\partial z^2 = [gh_o/(\rho_o E)]\, \partial\rho_{sa}/\partial x - [gh_o/(\rho_o E)]\, (z/h_o)\, \partial\rho_{sa}/\partial x + (g/E)\, \partial h'_o/\partial x$$
$$\partial^2 u_{sa}/\partial z^2 = M - M\,(z/h_o) + N \qquad \text{(F16)}$$

with: $M = [gh_o/(\rho_o E)]\, (\partial\rho_{sa}/\partial x)$ and $N = (g/E)\, \partial h'_o/\partial x$; both with dimension 1/(ms).

Focussing on the ***river flow effects*** only (N-term), Equation (F16) can be integrated twice to obtain:

$$\partial^2 u_{r,z}/\partial z^2 = N$$
$$\partial u_{r,z}/\partial z = N\, z + C_4$$
$$u_{r,z} = N\, (1/2)\, z^2 + C_4 z + C_5$$

Applying the boundary constions: $u_{sa} = 0$ at $z = 0$ and $\int u_{sa}\, dz = q_r$, it follows that $C_5 = 0$ and

$$\int_0^h [N\, (1/2)\, z^2 + C_4 z]\, dz = q_r$$
$$[N\, (1/6)\, z^3 + (1/2)\, C_4 z^2 + C_6]_0^h = q_r$$
$$N\, (1/6)\, h_o^3 + (1/2)\, C_4 h_o^2 + C_6 - C_6 = q_r$$
$$N\, (1/6)\, h_o^3 + (1/2)\, C_4 h_o^2 = q_r$$
$$C_4 = 2q_r/h_o^2 - (1/3)\, N\, h_o = 2\,\overline{u}_r/h_o - (1/3)\, N\, h_o$$

with $\overline{u}_r = q_r/h_o$= depth-averaged river velocity

Thus:

$$u_{r,z} = N\, (1/2)\, z^2 + C_4 z = N\, (1/2)\, z^2 + [2\,\overline{u}_r/h_o - (1/3)\, N\, h_o]z$$
$$u_{r,z} = Nh_o^2\, [(1/2)\, (z/h_o)^2 - (1/3)\, (z/h_o)] + 2\,\overline{u}_r\, (z/h_o) \qquad \text{(F17)}$$

The N-parameter is: $N = (g/E)\, \partial h'_o/\partial x$.
Using: $\partial h'_o/\partial x = -I = -\overline{u}_r^{\,2}/(C^2 h_o)$ based on the Chézy-equation and
$E = \gamma\, u_* h_o = \gamma\, (g^{0.5}/C)\, (|\hat{\overline{u}}| + |\overline{u}_r|)\, h_o$ with γ in the range of 0.001 to 0.005,
yields: $N = -g^{0.5}\, \overline{u}_r/\{\gamma(1 + \hat{\overline{u}}/\overline{u}_r) C\, h_o^2\}$

The river flow-related velocity distribution can be expressed as:

$$u_{r,z} = [K\{-(1/2)\, (z/h_o)^2 + (1/3)\, (z/h_o)\} + 2\, (z/h_o)]\, \overline{u}_r \qquad \text{(F18)}$$

with $K = -g^{0.5}/\{\gamma(1 + \hat{\overline{u}}/\overline{u}_r) C\}$.

In the mouth of the estuary the ratio $\hat{\overline{u}}/\overline{u}_r \cong 100$ and the K-value is about 0.1 resulting in an almost linear velocity profile as the first term $\{-(1/2)\, (z/h_o)^2 + (1/3)\, (z/h_o)\}$ of Equation (F18) is very small.
The velocity profile at the mouth is dominated by tidal flow-related mixing. At the landward river section the ratio $\hat{\overline{u}}/\overline{u}_r \cong 0.1$ and the K-value is about 10 resulting in a more parabolic velocity profile. In this latter section the velocity profile is dominated by river flow-related mixing.

Figures F3 (top and middle) show river flow-related velocity profiles based on Equation (B18) for γ= 0.001 and γ= 0.005 and h_o= 10 m, C= 50 $m^{0.5}$/s, $\hat{\bar{u}}$ = 1 m/s, $\bar{u}_r$= 0.1 m/s.

A very simple approach is given by **Chatwin (1976).** He assumes that: $\partial^2 u_{r,z}/\partial z^2$ = constant, yielding:
$u_{r,z}$= 0.5 C_1 z^2+C_2 z + C_3. The three constants can be determined from three boundary conditions: $u_{r,z}$= 0 at z= 0, $\partial u_{r,z}/\partial z$ = 0 at z= h_o and $\int_0^h u_{r,z}\, dz = \bar{u}_r\, h_o$ resulting in: $u_{r,z}= 3\bar{u}_r [0.5(z/h_o)^2 - (z/h_o)]$.

Another approach for the river flow-related velocity profile is just to apply a logarithmic function as given by:

$$u_{r,z} = \bar{u}_r/[(z_o/h_o)-1+\ln(h_o/z_o)]\, [\ln(z/z_o)]$$

with: $z_o= k_s/30$ for hydraulic rough flow conditions.

Focussing on the ***salinity effects*** only (M-terms), Equation (B16) can be integrated twice to obtain:

$$\partial^2 u_{sa}/\partial z^2 = M - M\,(z/h_o)$$
$$\partial u_{sa}/\partial z = M\,z - M\,(1/2)(z^2/h_o) + C_1$$
$$u_{sa,z} = M\,(1/2)\,z^2 - M\,(1/6)\,(z^3/h_o) + C_1 z + C_2$$

Applying the boundary constions: u_{sa}= 0 at z= 0 and $\int u_{sa}\, dz = 0$, it follows that C_2= 0 and

$$\int_0^h [M\,(1/2)\,z^2 - M\,(1/6)\,(z^3/h_o) + C_1 z]\, dz = 0$$
$$[M\,(1/6)\,z^3 - M\,(1/24)\,(z^4/h_o) + (1/2)\,C_1 z^2 + C_3]^h_0 = 0$$
$$M\,(1/6)\,h_o^3 - M\,(1/24)\,(h_o^4/h_o) + (1/2)\,C_1 h_o^2 + C_3 - C_3 = 0$$
$$M\,(1/6)\,h_o^3 - M\,(1/24)\,(h_o^4/h_o) + (1/2)\,C_1 h_o^2 = 0$$
$$C_1 = -(1/4)\,M\,h_o$$

Thus: $u_{sa,z} = M h_o^2\,[-(1/6)\,(z/h_o)^3 + (1/2)\,(z/h_o)^2 - (1/4)\,(z/h_o)]$ (F19)

The maximum residual velocity is approximately: $u_{sa,max} = -0.035 M h_o^2$ about z/h_o= 0.3.

Using: $E= \gamma\, u_*\, h_o = \gamma\, (g^{0.5}/C)\, (|\hat{\bar{u}}|+|\bar{u}_r|)\, h_o$ with γ in the range of 0.005 to 0.01,
$\hat{\bar{u}}$ = peak tidal velocity, $\bar{u}_r$= depth-averged river flow, the M-parameter can be expressed as:

$$M= [g h_o/(\rho_o E)]\, (\partial\rho_{sa}/\partial x) = g^{0.5}\, C/\{\gamma\, (|\hat{\bar{u}}|+|\bar{u}_r|)\, h_o\}\, (h_o/\rho_o)\, (\partial\rho_{sa}/\partial x) \quad \text{(F20)}$$

Figure F3 (top) shows Equation (B19) for h_o= 16 m, $\hat{\bar{u}}$ = 1 m/s, $\bar{u}_r$= 0.2 m/s, C= 50 $m^{0.5}$/s, ρ_o= 1000 kg/m^3, $\partial\rho_{sa}/\partial x$= 0.001 (approximately 10 kg/m^3 per 10 km) and $\partial\rho_{sa}/\partial x$= 0.0001 (1 kg/$m^3$ per 10 km). A relatively large landward density gradient yields a relatively large landward velocity near the bottom of about 0.3 m/s for γ= 0.005 and a relatively small landward velocity of about 0.1 m/s for γ= 0.01. Measured tide-averaged velocities during spring tide (10 September 1975, see **Table F1**) and a river discharge of 1000 m^3/s near Hoek van Holland (about 4 km from the Sea) along the New Rotterdam Waterway are also shown. The measured data reflect the salinity-induced net velocities due to density gradient of about 0.001.

Measured values are about 0.4 m/s near the bottom and the water surface (river flow velocities have been subtracted). The computed data based on Equation (B19) are somewhat too small.
Figure F3 (middle) shows results for a much smaller density gradient of 0.0001 resulting in much smaller net velocities in the range of 0.01 to 0.05 m/s.

Using a similar tide-averaged approach, (**Chatwin, 1976**) has proposed:

$$u_{sa,z} = [\alpha g/(48\, h^3 E)]\, [\partial \langle s \rangle / \partial x][8(z/h)^3 - 15(z/h)^2 + 6(z/h)] + 3\,\overline{u}_r\, [0.5(z/h)^2 - (z/h)] \quad \text{(F21)}$$

The first term arises from the density gradient but makes no contribution to the discharge since the net flow from the sea towards the river in the bottom part of the water column is exactly balanced by the net flow from the river towards the sea in the upper part of the water column. The second term contributes to the total fresh water discharge and is towards the sea at all depths. The value of the gradient $\partial \langle s \rangle / \partial x$ is, so far, unknown. Qualitatively, the salinity gradient is about zero at the mouth, increases in landward direction and reaches its maximum value in the middle of the salt intrusion length and then decreases to become zero at the end of the salt intrusion length. Hence, the residual flow is largest in the middle of the salt intrusion length from the mouth.
The functions $F_1 = [8(z/h)^3 - 15(z/h)^2 + 6(z/h)]$ and $F_2 = [(z/h)^2 - 2(z/h)]$ are shown in **Figure F3 (bottom).**
Using the continuity equation, the tide-averaged vertical velocity can be derived, as follows:

$$\langle w \rangle = [\alpha g/(48\, h^4 E)]\, [\partial^2 \langle s \rangle / \partial x^2][2(z/h)^4 - 5(z/h)^3 + 6(z/h)^2] \quad \text{(F22)}$$

The vertical velocity has the same sign (of the term $[\partial^2 \langle s \rangle / \partial x^2]$) at all depths at a fixed location x.

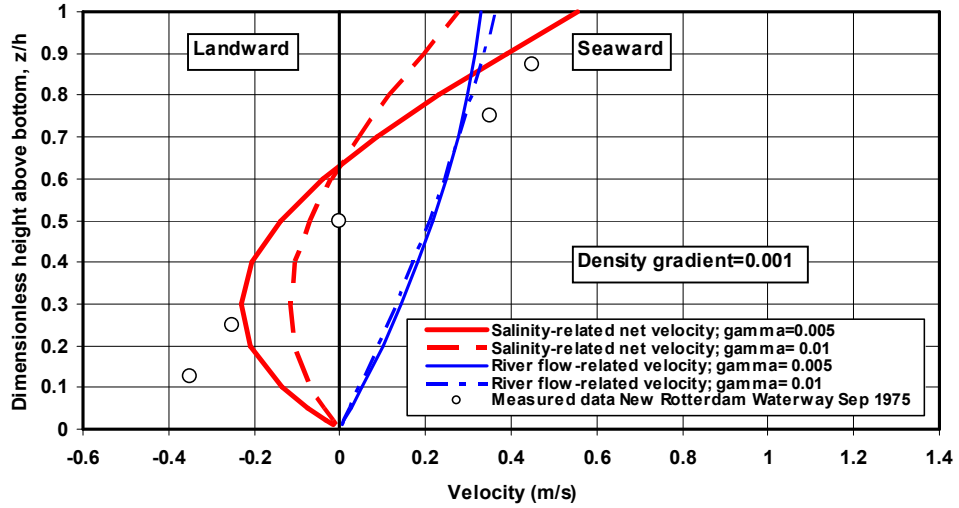

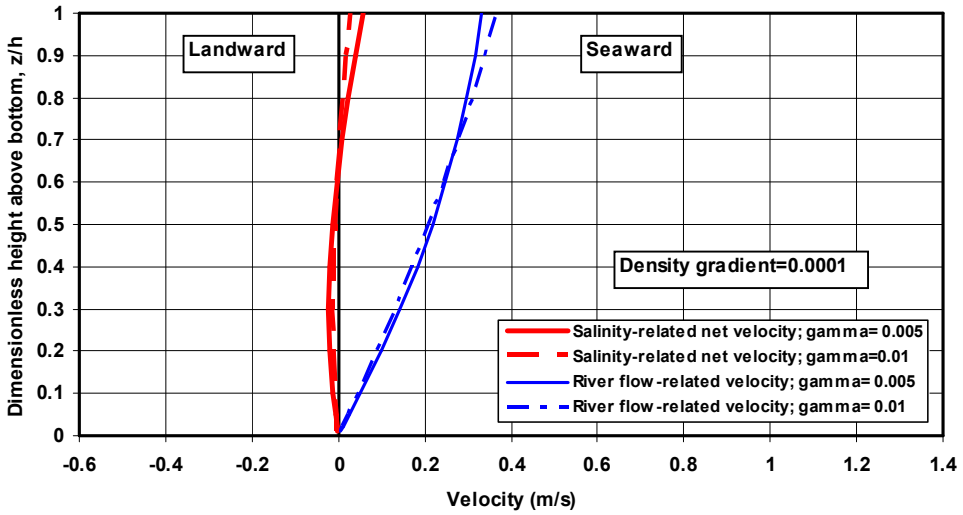

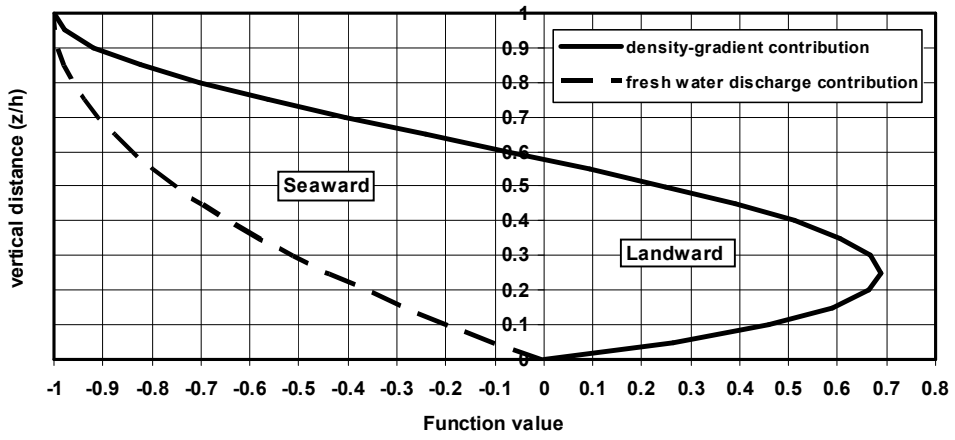

Figure F3 *Net velocity due to salinity gradient and due to river flow*
Top and Middle: Net velocity profiles according to Van Rijn
Bottom: Net velocity profiles according to Chatwin (1976)

Prandle (1985, 2004, 2009) has examined the various circulation processes in narrow estuaries subject to predominant tidal forcing. Residual velocity structures are derived for well-mixed longitudinal density gradients and for fully stratified saline wedges. Representative velocities are:

Well-mixed:	$<u_{surface}> = 0.036\ (S/F)\ \bar{u}_r$ in seaward direction,	(F23)
	$<u_{bottom}> = -0.029\ (S/F)\ \bar{u}_r$ in landward direction,	
Stratified:	$<u_{surface}> = 1.26\ \bar{u}_r/(1-h_s/h)$ in seaward direction,	
	$<u_{bottom}> = -0.18\ \bar{u}_r/(1-h_s/h)$ in landward direction.	

with: <u>= tide-averaged velocity, $S = (h/\rho)\partial\rho/\partial x$ (positive in seaward direction; x is positive in seaward direction), $F = (k\,\bar{u}_r\,\hat{\bar{u}})/(g\,h)$, $\bar{u}_r = Q_r/h$, $\hat{\bar{u}}$ = peak tidal velocity, Q_r = river discharge, h_s = thickness of salt wedge, h= mean water depth, k= friction coefficient (= g/C^2; **Prandle** uses k= 0.0025).

Measured values of tide-averaged net velocities in partially mixed to well-mixed conditions are given below in **Table F1**. Generally, the net velocities in the lower half of the depth are in the range of 0.05 to 0.5 m/s strongly depending on the value of the density gradient. Salinity intrusion is relatively small in stratified conditions with high river discharges (high density gradient and large net velocities). Salinity intrusion is relatively large in well-mixed conditions with low river discharges.

Table F1 *Measured data of tide-averaged net velocities due to salinity gradients*

Location	Water depth (m)	Width (m)	Tidal range (m) and peak velocities (m/s)	Fresh water discharge (m^3/s) and velocities (m/s)	Density gradient (kg/m^3 per m)	Net velocities near bed and near surface (m/s)
New Rotterdam Water way 10 Sep 1975 (partially mixed to stratified) (Delft Hydraulics 1984)	15	400	1 0.5 - 1	1000 0.15 - 0.2	0.001 (30 kg/m^3 over 30 km)	0.3-0.4 (landward) 0.3-0.5 (seaward)
James River, Chesapeake Bay, Virginia, USA partially mixed (Dyer, 1973)	7	1000	0.5 - 1 0.5	150 0.02	0.0005 (15 kg/m^3 over 30 km	0.1 – 0.15 (landward) 0.1 (seaward)
Mersey Narrows Partially to well-mixed (Dyer, 1973)	20 - 25	1000	9 1.5 – 2.2	25 – 200 0.001 – 0.01	0.0002 2 kg/m^3 per 10 km	0.1 (landward) 0.1 (seaward)
Carquinez Strait, 1991, San Francisco Bay, USA Partially mixed (Monismith 1996)	15	1000	2.5 0.5-2	300	0.00033	0.05 – 0.1 (landward) 0.1 (seaward)

Stratified conditions

The fluid pressure and pressure gradient are:

$$p = \rho g (h - \delta) + (\rho + \Delta\rho)g(\delta - z)$$

$$\partial p/\partial x = g(h_o - \delta)\, \partial\rho/\partial x + \rho g\, \partial h'_o/\partial x$$

After tide-averaging and simplifying, it follows that:

$$\partial^2 u_{sa}/\partial z^2 = (\Delta\rho/\rho_o)\, (g/E)\, \partial\delta/\partial x + (g/E)\, \partial h'_o/\partial x$$

$$\partial^2 u_{sa}/\partial z^2 = F$$

with: $F = (\Delta\rho/\rho_o)\, (g/E)\, \partial\delta/\partial x + (g/E)\, \partial h'_o/\partial x$

The term $\partial\delta/\partial x$ represents the saline wedge decrease in the (negative) landward direction; and thus the term $\partial\delta/\partial x$ is a positive term. The term $\partial h'_o/\partial x$ represents the water surface slope gradient related to the freshwater river flow; the h'_o value increases in the negative

landward direction and thus the term $\partial h'_o/\partial x$ is a negative term.The terms $\partial\delta/\partial x$ and $\partial h'_o/\partial x$ are constant in vertical direction.

The momentum equation can be integrated twice to obtain:

$\partial^2 u_{sa}/\partial z^2 = F$

$\partial u_{sa}/\partial z = F\, z + C_1$

$u_{sa,z} = F\,(1/2)\, z^2 + C_1 z + C_2$

Applying the boundary constions: $u_{sa}= 0$ at $z= 0$ and $u_{sa}= 0$ at $z= \delta$, it follows:

$$u_{sa,z} = 0.5F\, \delta^2\, [(z/\delta)^2 - (z/\delta)] \qquad \text{(F24)}$$

The maximum residual velocity is: $u_{sa,max} = -0.125\, F\, \delta^2$ about $z/\delta= 0.5$.

Using: $E= \gamma\, u_*\, h_o = \gamma\, (g^{0.5}/C)\, (|\hat{\overline{u}}|+|\overline{u}_r|)\, h_o$ with γ in the range of 0.005 to 0.01, $\hat{\overline{u}}$ =peak tidal velocity, $\overline{u}_r$= depth-averged river flow, the F-parameter can be expressed as:

$$F= (g^{0.5}C)/\{\gamma(|\hat{\overline{u}}|+|\overline{u}_r|)h_o\}(\Delta\rho/\rho_o)(\partial\delta/\partial x) + (g^{0.5}\, C)/\{\gamma(|\hat{\overline{u}}|+|\overline{u}_r|)h_o\}(\partial h'_o/\partial x) \qquad \text{(F25)}$$

Using data from the Rotterdam Waterway: $\gamma= 0.005$, $C= 60\ m^{0.5}/s$, $h_o= 15$ m, $\delta= 7.5$ m ($= 0.5h_o$), $\hat{\overline{u}} = 0.8$ m/s, $\overline{u}_r= 0.2$ m/s, $\Delta\rho/\rho_o= 30/1000= 0.03$, $\partial\delta/\partial x= 0.0003$ (0.3 m per 1000 m) and $\partial h'_o/\partial x = 0$, it follows that: $F= 0.023$ (1/ms) and $u_{sa,max} = -0.125\, F\, \delta^2 = -0.15$ m/s in landward direction

G References

Chatwin, P.C. 1976. Some remarks on the maintenance of the salinity distribution in estuaries. Estuarine and Coastal Marine Science, Vol. 4, p. 555-566

Davies, L.J., 1964. A morphogenic approach to the worlds' shorelines. Zeitschrift für Geomorphologie, Vol. 8, p. 127-142

Deltares, 2010. LTV O & M Safety (draft report): Data analysis and hypothesis Western Scheldt, Project 1202019, Delft, The Netherlands

De Kramer. J., 2002. Water movement in Western Scheldt Estuary (in Dutch). Dep. of Physical Geography, Report ICG 02/6. University of Utrecht, Utrecht, The Netherlands

Dronkers, J.J., 1964. Tidal computation sin rivers and coastal waters. p. 518. North-Holland, New York

Dronkers, J., 2005. Dynamics of Coastal Systems. World Scientific

Dyer, K.R., 1997. Estuaries: a physical introduction. Wiley and Sons, Aberdeen, U.K.

Falconer, R.A. and Lin, B., 1997. Three-dimensional modelling of water quality in the Humber Estuary. Water resources, Vol. 31, No. 5, p. 1092-1102

Fischer, H.B., 1972. Mass transport mechanisms in partially stratified estuaries. Journal of Fluid Mechanics, Vol. 53, Part 4, p. 671-687

Fischer, H.B., List, E.J., Koh, R.C.Y., Imberger, J. and Brooks, N.H., 1979. Mixing in inland and coastal waters. Academic Press.

Friedrichs, C.T., 1993. Hydrodynamics and morphodynamics of shallow tidal channels and intertidal flats. Ph.D. Thesis, Mass. Inst. of Technology, Woods Hole Oceanographic Inst., Woods Hole, Massachusetts, USA

Friedrichs, C.T. and Aubrey, D.G., 1988. Non-linear tidal distortion in shallow well-mixed estuaries: a synthesis. Estuarine, Coastal and Shelf Science, Vol. 27, p. 521-545

Friedrichs, C.T. and Aubrey, D.G., 1994. Tidal propagation in strongly convergent channels. Journal of Geophysical Research, Vol. 99, No. C2, p. 3321-3336

GfL,Bioconsult, KÜFOG, 2006. Fahrrinnenanpassung der Unter- und Aussenweser an die Entwicklungen im Schiffsverkehr mit Tiefenanpassung der hafenbezogenen Wendestelle, Umweltverträglichkeits-untersuchung, Beschreibung und Bewertung des Ist-Zustandes.

Godin, G., 1988. Tides. Centro de investigacion cientifica y de educacion superior de ensenada. Baja California, Mexico.

Green, G., 1837. On the motion of waves in a variable canal of small depth and width. Trans. Cambridge Philos. Soc., 6, p. 457-462

Harleman, D.R.F., 1966. Tidal dynamics in estuaries, Part II: Real estuaries. In: Estuaries and Coastline Hydrodynamics, edited by A.T. Ippen et al., Mc Graw-Hill, New York.

Hunt, J.N., 1964. Tidal oscillations in estuaries. Geophysical Journal of the Royal Astronomical Society, Vol.8, p. 440-455

Ippen, A., 1966. Tidal dynamics in estuaries, Part I: Estuaries of rectangular cross-section. In: Estuaries and Coastline Hydrodynamics, edited by A.T. Ippen et al., Mc Graw-Hill, New York.

Ippen, A.T. and Harleman, D.R.F., 1961. One-dimensional analysis of salinity intrusion in estuaries. Technical Bulletin No. 5. Committe on Tidal Hydraulics, Corps of Engineers, U.S. Army, USA

Jay, D.A. 1991. Greens's law revisited: tidal long-wave propagation in channels with strong topography. Journal of Geophysical Research, Vol. 96, No. C11, p. 20585-20598

Jay, D.A., Geyer, W.R., Uncles, R.J., Vallino, J., Largier, J. and Boynton, W.R., 1997. A review of recent developments in estuarine scalar flux estimation. Estuaries, Vol. 20, No. 2, p. 262-280.

Keulegan, G.H., 1966. The mechanism of an arrested saline wedge. In: Estuaries and Coastline Hydrodynamics, edited by A.T. Ippen et al., Mc Graw-Hill, New York.

Kuijper, C., 2011. Analytical model for salinity intrusion (in preparation). Report 1002366, Deltares, Delft, The Netherlands

Kuijper, C. and Van Rijn, L.C., 2011. Analytical and numerical analysis of tides and salinities in estuaries; Part II, Salinity distributions in prismatic and convergent channels. Submitted to Ocean Dynamics

Lanzoni, S. and Seminara, G., 1998. On tide propagation in convergent estuaries. Journal of Physical Research, Vol. 103, p. 30793-30812.

Le Floch, J.F., 1961. Propagation de la marée dans l'estuaire de la Seine et en Seine-Maritieme. Centre de Recherches et d'études Océanographiques. Paris, France.

Lorentz, H.A., 1922. Including resistance in tidal flow equations (in Dutch). De Ingenieur, p. 695, The Netherlands (in Dutch)

Lorentz, H.A., 1926. Report Commission Zuiderzee 1918-1926 (in Dutch). Alg. Landsdrukkerij, Den Haag, The Netherlands (in Dutch)

Mazumder, N.C. and Bose, S., 1995. Formation and propagation of tidal bore. Journal of Waterway, Port, Coastal and Ocean Engineering, ASCE, Vol. 121, No. 3

McDowell, D.M. and O'Connor, B.A., 1977. Hydraulic behaviour of estuaries. MacMillan Press, London, U.K.

Nasner, H., 1974. Über das Verhalten von Transportköpern im Tidegebiet. Mitteilungen Franzius Institut, Heft 40, T.U. Hannover, Germany

Parker, B.B., 1984. Frictional effects on the tidal dynamics of a shallow estuary. Doctoral Thesis. John Hopkins University, Baltimore, Maryland, USA

Parker, B.B., 1991. The relative importance of the various nonlinear mechanisms in a wide range of tidal interactions (review). In: Tidal Hydrodynamics by B.B. Parker, John Wiley and Sons, p. 237-268

Pieters, T., 2002. The tide in the Western Scheldt Estuary (in Dutch). Document BGW-0102. Consultancy Tidal Waters, Vlissingen, The Netherlands

Prandle, D, 1981. Salinity intrusion in estuaries. Journal of Physical Oceanography, Vol. 11, p. 1311-1324.

Prandle, D, 1985. On salinity regimes and the vertical structure of residual flows in narrow estuaries. Estuarine, Coastal and Shelf Science, Vol. 20, p. 615-635

Prandle, D, 2003. Relationships between tidal dynamics and bathymetry in strongly convergent estuaries. Journal Physical Oceanography, Vol. 33, p. 2738-2750.

Prandle, D., 2004a. How tides and river flows determine estuarine bathymetries. Progress in Oceanography, Vol. 61, p. 1-26

Prandle, D, 2004b. Salinity intrusion in partially mixed estuaries. Estuarine, Coastal and Shelf Science, Vol. 54, p. 385-397

Prandle, D., 2004c. Saline intrusion in partially mixed estuaries. Estuarine, Coastal and Shelf Science, Vol. 59, p. 385-397

Prandle, D, 2009. Estuaries. Cambridge University Press

Prandle, D. and Rahman, M., 1980. Tidal response in estuaries. Journal Physical Oceanography, Vol. 10, p. 1552-1573

Rigter, B.P., 1973. Minimum length of salt intrusion in estuaries. Journal of the Hydraulics Division, ASCE, Vol. 99, No. HY9, p. 1475

Savenije, H.H.G., 1986. A one-dimensional model for salinity intrusion in alluvial estuaries, Journal of Hydrology, 85, p. 87-109.

Savenije, H.H.G., 1989. Salt intrusion model for high-water slack, low-water slack, and mean tide on spread sheet. Journal of Hydrology, 107, p. 9-18.

Savenije, H. H.G., 1992. Rapid Assessment Technique for Salt Intrusion in Alluvial Estuaries, Ph.D. Thesis, IHE report series, no. 27, International Institute for Infrastructure, Hydraulics and Environment, Delft, The Netherlands.

Savenije, H. H.G., 1993a. Predictive model fors alt intrusion in estuaries. Journal of Hydr., 148, p. 203-218.

Savenije, H.H.G., 1993b. Composition and driving mechanisms of longitudinal tidal average salinity dispersion in estuaries, Journal of hydrology, 144, p. 127-141.

Savenije, H.H.G, 2005. Salinity and tides in alluvial estuaries. Elsevier

Savenije, H.H.G., Toffolon, M., Haas, J. and Veling, E.J.M., 2008. Analytical description of tidal dynamics in convergent estuaries. Journal of Geophysical Research, Vol. 113, C10025, doi:10,1029/2007JC004408

Schijf, J.B. and Schönfeld, J.C., 1948. Theoretical considerations on the motion of salt and fresh water. Proc. Minnesota Int. Hydr. Convention, IAHR and Hydraulics Division ASCE, p. 321-333

Speer, P.E. and Aubrey, D.G., 1985. A study of non-linear tidal propagation in shallow inlet/estuarine systems, part II: theory. Estuarine, Coastal and Shelf Science, Vol. 21, p. 207-224

Stehr, E., 1975. Grenzsdchicht-Theoretische Studie über die Gesetze der Strombank und Riffelbildung. Hamburger Küstenforschung, Vol. 34

Van der Burgh, P., 1972. Development of method for prediction of salinity distributions in estuaries, channels and seas (in Dutch). Rijkswaterstaat-Deltadienst, The Hague, The Netherlands

Van Os, A.G., 1993. Density currents and salt intrusion. Lecture notes IHE, Delft, The Netherlands

Van Rijn, L.C., 1993, 2011. Principles of fluid flow in rivers, estuaries and coastal seas. Aqua Puclications (www.aquapublications.nl)

Verspuy, C., 1985. Lecture Notes: Long waves (in Dutch). Delft University of Technology, Delft, The Netherlands